Does cerebellar cortex function as a forward internal model for motor control?

A DISSERTATION
SUBMITTED TO THE FACULTY OF
UNIVERSITY OF MINNESOTA
BY

Angela L. Hewitt

IN PARTIAL FULFILLMENT OF THE REQUIREMENTS
FOR THE DEGREE OF
DOCTOR OF PHILOSOPHY

Timothy J. Ebner, adviser

June 2013

Acknowledgements

It has been a privilege to be part of the Ebner laboratory. Dr. Timothy Ebner gave me opportunities to pursue my own questions and ideas even as a graduate student. I will always appreciate the numerous times that he rearranged his schedule to help me troubleshoot a recording experiment, teach me the finer points of recording Purkinje cells, or provide feedback to improve my writing and presentation skills. Even my tastes in food and wine have improved under his mentorship, and I will miss being a part of lab celebrations.

Drs. Siavash Pasalar and Claudia Hendrix taught me how to work with the monkeys and the basics of electrophysiology. Dr. Pasalar developed the random tracking task and we recorded the first half of the random tracking data together. Claudia, I will be forever grateful that you gave me the "smarter" monkeys for my projects and that your door was always open when I needed statistics help.

Mike McPhee's help with keeping the lab equipment working, especially when the robot broke down, was invaluable. He also provided graphic assistance for all the figures in this dissertation and moral support during my less successful experimentation periods.

Kris Bettin assisted with manuscript preparation and was always willing to help in any way needed. She, along with Susan Shurson, Nick Berg, and John Paton, was one of the invaluable people who could always answer questions about the paperwork and logistics that accompany research.

Laurentiu Pasalar did all of the firing analyses for the random tracking experiments and often provided Matlab expertise. We had many thoughtful conversations about internal models, but I also appreciated that he was always ready to talk about anything and everything not related to our dissertation topics.

Dr. Gang Chen helped with many of the more difficult monkey chamber surgeries. Lijuan Zhuo also assisted with monkey surgeries and animal training. Sam Cramer, Piradeep Suntharalingam, Justin Barnes, and Wangcai Gao provided feedback about the experiments.

Several students also contributed significantly to the experiments. Yashwant Vijayakumar programmed the robot for the mechanical perturbations task. Bethany Kummer, Gabriel Rodriguez, and Brian Doherty assisted with monkey training and/or data processing.

Unfortunately, it is impossible to name everyone from the Graduate Program in Neuroscience and Medical Scientist Training Program who have supported me as I completed my studies. My committee members Drs. James Ashe, Khalaf Bushara, and Alvin Beitz were always willing to discuss my project and provide useful feedback. For all of the classmates who endured this training with me—especially those of you who edited my dissertation, brought my family and me food, watched my kids, or listened to my practice talks—thank you.

Dedication

My family has been an amazing support during this academic journey. First, I owe my husband Chad much thanks for encouraging me to apply to MD/PhD programs. Thank you for always being supportive and making numerous sacrifices so that I could accomplish this. Mom, thank you for being a role model of how to balance work and family, and for your full-time help managing our home and kids as I wrote this dissertation. Finally, thank you Papa for pushing me to excel in Math and often reminding me that my hard work would someday accomplish great things.

Abstract

Motor control theorists have postulated that to produce rapid, finely tuned movements, a component of the control circuitry must bypass long sensory feedback delays by providing an estimate of the consequences resulting from a motor command. This control element, termed a forward internal model, receives an efferent copy of the motor command and information about the current state in order to predict the future state (i.e. kinematic variables like position, velocity) of the limb. Previous psychophysical, imaging, and patient case studies suggest that the cerebellum is a possible location for implementation of an internal model.

However, very few electrophysiological studies have investigated whether the firing discharge from cerebellar neurons is consistent with the output of a forward internal model. To specifically evaluate the simple spike firing from Purkinje cells in lobules IV-VI, we trained rhesus macaques to perform different hand movement tasks using a 2 joint robotic manipulandum. Two electrophysiology experiments tested several aspects of a forward internal model. First, we hypothesize that Purkinje cell simple spike firing predicts future hand kinematics, even when the task is highly unpredictable. Second, the encoding is invariant, so that the model output can generalize to other tasks. A third hypothesis is that the simple spike discharge will show evidence of learning when animals adapt to a predictable mechanical perturbation, as expected from a forward internal model.

Experimental results found many theoretical components of a forward internal model present in the Purkinje cell simple spike discharge. Simple spikes encode both feedforward and feedback representations of movement kinematics, with position and velocity signals explaining the most firing variability. These representations supply the predictive kinematic signals used downstream and the feedback information potentially used locally to construct predictions, calculate errors, and update the model. Many Purkinje cells exhibit dual encoding for a single kinematic parameter, so that these

separate feedforward and feedback mechanisms may take place within individual cells. For most cells, model coefficients generated from random tracking data accurately estimate simple spike firing in either circular tracking or center-out reach. Adaptation to a predictable perturbation initiates steady, progressive changes in the parameter sensitivity (βs) of both the feedforward and feedback signals. The timing sensitivity (τ) also demonstrates significant shifts, with time encoding in the simple spikes often changing sign during adaptation (e.g. feedback to feedforward). Population analyses suggest that large changes in parameter sensitivity first occur in the feedback signals, then transfer to the feedforward representations. This may reflect use of the simple spike feedback to update model predictions. These results conclude that kinematic encoding from the cerebellar cortex uses a forward internal model that can generalize between tasks, but is also highly plastic and adaptable.

Table of Contents

List of Figures

Chapter 2

Purkinje Cell Simple Spike Discharge Is Conserved Across Multiple Tasks

Chapter 3

Purkinje Cell Simple Spike Discharge Adapts to a Mechanical Perturbation

CHAPTER 1: INTERNAL MODELS AND MOTOR LEARNING IN THE CEREBELLUM

The cerebellum is essential for the production of smooth, continuous movements. However, the cerebellum's specific contributions to motor control remain controversial. Numerous hypotheses have been formulated regarding cerebellar function including motor learning (Gilbert and Thach, 1977;Marr, 1969;Ito, 2002), providing internal models (Wolpert et al., 1998;Kawato, 1999;Lisberger, 2009), movement timing (Braitenberg and Atwood, 1958;Welsh et al., 1995;Keele and Ivry, 1990;O'Reilly et al., 2008;Liu et al., 2008;Wu et al., 2011), and error detection and correction (Oscarsson, 1980). These hypotheses are not necessarily exclusive of one another. For example, motor learning may represent the updating or formation of accurate internal models and likely requires information about movement timing and errors. Testing the validity of these or future hypotheses requires identification of the movement and non-movement information signaled by cerebellar neurons and understanding how this information is processed. Ideally, we need to understand the signals encoded in the inputs of the mossy and climbing fibers and the transformations occurring in the cerebellar cortex. Critical are the parameters carried by the Purkinje cells, the sole output of the cerebellar cortex to the cerebellar nuclei. Finally, we need to understand the representations in the cerebellar nuclei, the final output of the cerebellum.

Inverse dynamics vs. forward internal models

Humans possess extraordinary abilities to execute graceful, precise movements despite changing environmental dynamics. Motor control theorists have accounted for adaptive, precise control by proposing that neuronal networks act as internal models that mimic the input and output properties of the motor apparatus (Kawato, 1999). Two types of internal models may work together to execute accurate, well-timed movements in a feedforward manner (Bhushan and Shadmehr, 1999). An inverse dynamics internal model inputs the desired trajectory (movement path) and computes the motor commands necessary to execute the movement (Wolpert et al., 1998). The output neurons of an inverse dynamics

model must signal kinetic variables, such as joint torques or muscle forces (Schweighofer et al., 1998). Conversely, a forward internal model of the hand utilizes an efferent copy of the motor command and information about the current hand state to predict the future state of the hand (Wolpert et al., 1998). Forward internal model output would provide an estimate of the consequences arising from the motor command, and might express the future state in terms of kinematic variables (i.e., position and velocity). These predictions would have multiple purposes, such as coordinating movements between multiple limbs (Miall et al., 2000), overcoming delays in sensory feedback (Kawato, 1999;Wolpert et al., 1998), and predicting sensorimotor errors (Wolpert et al., 1995;Kawato and Wolpert, 1998).

Numerous studies have provided evidence that the central nervous system utilizes both forward and inverse dynamics internal models to produce movements requiring predictive, feedforward control. Most prevalent are psychophysical studies that have examined adaptation during arm reaching movements. For example, several studies used a robotic two-joint manipulandum to generate novel force fields that altered subjects' hand/arm dynamics during reaching movements in a horizontal plane (Thoroughman and Shadmehr, 1999;Scheidt et al., 2000;Scheidt et al., 2001;Hwang et al., 2006;Shadmehr and Mussa-Ivaldi, 1994). In these studies, force field adaptation was measured by hand kinematic changes that led to an efficient reaching movement. Catch-trials, in which the force field was suddenly removed, resulted in wayward hand trajectories that reflected the kinematic errors observed when the subject was first exposed to the novel force field. Furthermore, adaptation transferred to new areas of the workspace, demonstrating that subjects developed internal representations of the force field dynamic elements.

These adaptive reaching studies could not dissociate whether learning takes place in the inverse dynamics or forward internal model. To address this, tasks must separate force production and kinematics. Probe trials and an "error clamp" were added to the adaptive reaching task in the viscous force field to examine whether an inverse dynamics model could respond appropriately to novel conditions (Wagner and Smith, 2008). On probe

trials, unpredictable pulsed perturbations altered hand velocities to conditions that had never been practiced in the viscous force field. The "error clamp" constrained movements to one direction to prevent undesirable learning from the kinematic errors that would otherwise arise from the pulsed perturbations (Scheidt et al., 2000;Scheidt et al., 2001). Subjects responded to the novel hand velocities with lateral force profiles that nearly perfectly compensated viscous field effects in real time. These results showed that the inverse dynamics model controlling hand forces must receive input from a forward internal model of hand kinematics about future hand velocity. Otherwise, after the perturbation began, it would not have been able to internally represent dynamic elements of the viscous field and compensate in real-time time. The findings also illustrate the need for kinematic predictions and demonstrate that an inverse dynamics and forward internal model work together to produce accurate movements.

Coordination between an inverse dynamics model and a forward internal model is also required for precision grip force, in which the forces exerted must be just large enough to prevent an object from slipping without crushing it. In one such task, subjects grasped a manipulandum between their thumbs and index fingers and pushed or pulled it towards their body (Flanagan and Wing, 1997). This coupled object load forces with arm kinematics, and required prediction of the different inertial, viscous, and composite loads acting on the manipulandum in order to grip it precisely. Grip force paralleled the changes in load force without delays, indicating that the grip force controller did not rely upon proprioceptive feedback and instead had access to a forward internal model of arm kinematics.

Where might a forward internal model be located?

In normal human subjects, changes in cerebellar activation following motor learning have strongly implicated the cerebellum in the acquisition and storage of internal models (Imamizu et al., 2000;Shadmehr and Holcomb, 1997;Diedrichsen et al., 2005;Imamizu and Kawato, 2008;Nezafat et al., 2001). However, not all functional imaging studies concluded that motor adaptation takes place in the cerebellum (Seidler et al.,

2002;Flament et al., 1996). Most of the imaging studies also did not distinguish between an inverse dynamics or forward internal model. One fMRI study of precision grip force, in which predictable arm movements caused the load forces on a hand-held ball to change, found increased activation in the contralateral cerebellum. Contralateral activation distinguished the novel activity from ispsilateral motor activity (Kawato et al., 2003). This contralateral activity was interpreted to represent a forward model that predicts the arm kinematics required for predictive, coordinated grip force. Other studies provide support that this cerebellar activation depicts a forward internal model rather than an inverse dynamics model. In a monkey trained to grasp and lift objects that were predictably perturbed, muscimol injections into the anterior interpositus nucleus resulted in absent anticipatory grip forces (Monzee et al., 2004). Similarly, numerous patient studies also indicate that grip force does not match the load forces with cerebellar injury or disease (Rost et al., 2005;Muller and Dichgans, 1994;Nowak et al., 2002).

Psychophysical studies indicate that control loops identified in the cerebellum act as a forward model to provide the kinematic predictions needed to coordinate eye and hand movements. Smooth pursuit eye movement accuracy increases when the eyes track a target directly attached to the subject's hand, compared to when the target moves independently across a computer screen (Vercher et al., 1997). The difference in performance further increases when the target is subjected to predictable perturbations, but completely disappears when applied arm vibrations eliminate proprioceptive feedback (Vercher et al., 2003). This behavior can be explained if the oculomotor system utilizes a forward model of hand kinematics to predict hand movements. Similarly, saccadic eye movements reliably forecast hand position during predictable hand perturbations (Ariff et al., 2002), but cannot adjust to unpredictable perturbations (Nanayakkara and Shadmehr, 2003). If proprioceptive feedback and a model of inverse limb dynamics were sufficient for state estimation, the eye movements should remain robust even during the unpredictable perturbations.

Building upon these results, another study used transcranial magnetic stimulation (TMS) to demonstrate the cerebellum's contribution to estimating the state of the hand (Miall et al., 2007). On baseline trials, subjects made reaching movements to virtual 3D targets displayed on a screen with relatively small errors even in the absence of visual feedback. In a number of randomized trials, TMS disrupted the function of the ipsilateral cerebellum just prior to reach initiation. For these trials, initial direction and end point errors significantly increased. The final reaches were consistent with having planned the movement for a kinematic state of the arm or hand that occurred ~140 ms previously. These results add weight to hypotheses that a functioning cerebellum is required for accurate state estimation (Miall et al., 2007;Paulin, 2005).

Patients with cerebellar injury or disease often lack motor predictions required for learning new motor tasks. These patients can react, but cannot adapt, to predictable task perturbations (Maschke et al., 2004;Smith and Shadmehr, 2005;Bastian, 2006;Nowak et al., 2007;Morton and Bastian, 2006). One particular study also examined how sensory errors might affect adaptation to a visuomotor rotation in hereditary cerebellar ataxia patients (Tseng et al., 2007). Unlike controls, patients often made motor corrections at compensatory angles that would have been appropriate at earlier time points in the movement, but were incorrect for the current arm kinematics. This resulted in multiple, inefficient corrections and slow adaptation to the task. The authors proposed that these inappropriate corrections occurred because the patients did not have intact forward models of arm kinematics to facilitate fast error detection, and instead relied upon delayed sensory feedback.

Cerebellar anatomy can support predicted forward model physiology

Although only circumstantial evidence, inputs to cerebellar cortex are consistent with those predicted for a forward internal model. Inputs to a forward model are hypothesized to include information about the current state and the motor command. In primates, spinal cord afferents relay proprioceptive and exteroceptive information about the current state (Bloedel and Courville, 1981). For example, the dorsal spinocerebellar tract

(DSCT) conveys proprioceptive information from muscle spindles and golgi tendon organs as well as exteroceptive inputs from slowly adapting receptors and mechanoreceptors that can be used to assess the current state of the lower limb. The ventral spinocerebellar tract (VSCT) also relays proprioceptive information, but is additionally modulated by flexor reflex afferents that may provide an efference copy of the lower limb motor command to the cerebellar cortex. Similarly, secondary projections from primary motor cortex (via pontocerebellar fibers) can be interpreted to convey the motor command (Li et al., 2001;Kalaska et al., 1989). All of these inputs come via mossy fibers, which converge onto granule cells that bifurcate to form parallel fibers that synapse onto Purkinje cell dendrites. The vast dendritic arbors and large cell bodies characteristic of Purkinje cells may enable them to quickly integrate large amounts of incoming information about the motor command and current state, as required of a forward model. Moreover, as reviewed below, the cerebellar cortex has tremendous capacity for plastic changes that would be required to implement a forward internal model.

As a final piece of anatomical evidence, cerebellar-like structures (Bell, 2002) in advanced bony fish act as forward models to predict sensory consequences resulting from information about the current state and motor command (Bell et al., 2008). Fish with electrosensory organs identify predators and prey by measuring the weak electric fields other fish produce. In order to accurately estimate the external world, their cerebellar-like structures must generate a sensory prediction of the electric field arising from its own movement and subtract the prediction from the actual measured field. This is analogous to a forward model that predicts the sensory consequences of a motor command and compares it to current sensory feedback to minimize delays in correcting movement errors.

Do cerebellar Purkinje cells specify the motor command?

Although numerous studies conclude that a forward internal model is found in the cerebellar cortex, many arguments have been made that it is actually an inverse dynamics

model that encodes force parameters. However, the evidence for Purkinje cell discharge encoding the motor command needed to execute hand movements is limited. Early electrophysiology studies demonstrate that Purkinje cell simple spikes exhibit reciprocal activity with single joint movement timing and muscle activity, but the muscle activity was not dissociated from the movement kinematics (Thach, 1968;Thach, 1970;Gilbert and Thach, 1977;Smith, 1981;Frysinger et al., 1984). In visuomotor tracking, the simple spike firing exhibits stronger correlations with arm kinematics than with the EMG activity (Coltz et al., 1999a;Roitman et al., 2005), and the spatial tuning functions of individual arm muscles differ from those of the Purkinje cells (Roitman et al., 2005). Likewise, during grasp and lift of objects with different weights and textures, only a small percentage of Purkinje cells exhibit spimple spike firing that significantly correlates with the grasp force or rate of force production (Smith and Bourbonnais, 1981;Frysinger et al., 1984;Frysinger et al., 1984). The simple spike discharge often lags forearm muscle contraction and does not persist for the duration of the grasp (Smith and Bourbonnais, 1981). Several other studies interpreted modest changes in cerebellar neuron firing prior to muscle activation as encoding force production. The changes in force-correlated Purkinje cell activity occurred well in advance of muscle activity (Mason et al., 2006;Dugas and Smith, 1992), while increased firing from interpositus neurons ended prematurely to force cessation (Monzee and Smith, 2004).

More recent studies further addressed Purkinje cell encoding of force and muscle activity. In one, monkeys produced invariant movement kinematics while performing elbow rotation movements under assistive or resistive force fields (Yamamoto et al., 2007). Although brief changes in simple spike discharge occurred when switching between resistive and assistive forces, the magnitude of the loads was not systematically varied nor was a null field used. Consequently, the encoding strength for the loads and/or EMG activity was not evaluated, and it was not determined if the simple spike firing encodes the specific joint torques and/or muscle forces expected from the output of an inverse dynamics model of the arm. Another study trained monkeys to push a series of buttons in response to a light cue. Cross-correlation analyses were used to evaluate the relationship

between Purkinje cell simple spike firing and arm muscle activity (Holdefer and Miller, 2009). On average, only 6-7% of the firing variability was explained by the muscle activity. Moreover, movement kinematics were not explicitly controlled or included in the analyses, and therefore not disentangled from the muscle activity. Strong evidence for Purkinje cell encoding of force-related or motor command-like signals is still lacking.

Multi-joint movement studies that unambiguously dissociate force production from the movement kinematics while varying the forces required by the task have not been done until recently. To fill this gap, monkeys were trained to track a target moving in a circular path under varying force fields and loads (Pasalar et al., 2006). Hand forces and arm EMG activity changed appropriately with the applied force fields and loads. In contrast, hand position and speed remained constant, allowing dissociation between hand forces/arm EMG activity and kinematic parameters. For the vast majority of Purkinje cells, simple spike firing was neither modulated by the type (e.g. viscous or elastic) nor amplitude of the force field or by changes in EMG activity. These results are inconsistent with hypotheses postulating that Purkinje cell firing encodes muscle activity, interaction torques, or the motor command (Schweighofer et al., 1998;Wolpert et al., 1998;Kawato, 1999;Bastian et al., 1996;Miller and Houk, 1995;Smith, 1981). Therefore, there is compelling evidence that Purkinje cell simple spike firing from cerebellar cortex does not represent the output of an inverse dynamics model.

Do cerebellar Purkinje cells encode kinematics?

Psychophysical studies imply that the predictions from a forward internal model might be expressed in terms of kinematic variables (Wagner and Smith, 2008;Flanagan and Wing, 1997;Vercher et al., 1997;Vercher et al., 2003;Ariff et al., 2002). Although the motor command must eventually be expressed in terms of forces or joint torques, a vast literature shows that the central nervous system explicitly plans movements in kinematic reference frames. Point-to-point reaching movements are executed with little variability in the trajectory or velocity profile, despite changes to load forces or movement speeds (Atkeson and Hollerbach, 1985;Lacquaniti et al., 1986;Abend et al., 1982;Georgopoulos

et al., 1981). Errors made during reaching movements depend on the direction and distance to the target, as well as the initial position of the hand (Soechting and Flanders, 2008;Soechting and Flanders, 1989;Vindras and Viviani, 1998). Consequently, visually-guided movements, in which the cerebellum is thought to play a crucial role (Stein and Glickstein, 1992), require the representation and processing of kinematic signals. The output of a forward internal model may predict sensory feedback or the resultant kinematic state of the limb, both which could be used to estimate errors without long delays in sensory feedback, permitting rapid, yet, finely-tuned movements (Wolpert et al., 1995;Kawato, 1999).

Electrophysiological evidence for encoding movement kinematics is found at all levels of the cerebellum. Global kinematic parameters such as position, direction, and velocity of limb movements are encoded as early as the dorsal spinocerebellar tract and the cuneate nucleus during passive limb manipulations in anesthetized cats (Bosco et al., 1996;Bosco and Poppele, 1997) and rats (Garifoli et al., 2002;Giaquinta et al., 1999). Cerebellar inputs conveyed by the mossy fibers encode position, direction, and velocity of single joints in behaving monkeys (van Kan et al., 1993). Mossy fiber signals appear conserved in the granule cell activity, the first level of integration in the cerebellar cortex (Kolb et al., 1987;Bengtsson and Jorntell, 2009).

Numerous electrophysiology studies have documented that Purkinje cell simple spike firing signals kinematic variables in the cerebellar cortex. Simple spike firing from Purkinje cells in lobules IV-VI of the intermediate zone is correlated with movement position, amplitude, direction, velocity, and speed (Roitman et al., 2005;Pasalar et al., 2006;Coltz et al., 1999a;Fu et al., 1997a;Fortier et al., 1989;Marple-Horvat and Stein, 1987;Mano and Yamamoto, 1980;Harvey et al., 1977;Thach, 1970), kinematic variables that might convey predictions about the future state of the arm/hand. Recordings from floccular Purkinje cells during various eye movements show strong correlations between simple spike discharge and eye position, velocity, and acceleration. The firing also precedes the actual movements (Shidara et al., 1993;Stone and Lisberger, 1990;Medina

and Lisberger, 2008;Medina and Lisberger, 2009;Gomi et al., 1998). Another study examined smooth pursuit eye movements while tracking targets that predictably changed direction. Eye velocity and simple-spike firing learned to anticipate the directional change and respond 50-100 ms before it occurred (Medina and Lisberger, 2008). During passive limb movements, position and velocity are signaled in the simple spike firing of anesthetized or decerebrate cats and rats (Valle et al., 2000;Kolb et al., 1987;Giaquinta et al., 2000;Rubia and Kolb, 1978). Therefore, for both arm and eye movements there is considerable evidence that Purkinje cell simple spike firing is consistent with output from a forward model, as firing correlates with and leads the movement kinematics.

Whether these kinematic signals in the cerebellum are leading or lagging the movements is fundamental to interpreting how they are used for motor control. If the firing discharge lags kinematics, this is consistent with a role in error detection or monitoring feedback. Conversely, firing leading the actual kinematics would support feed-forward control, the output of a forward model, or encoding of task-related signals. Simple spike firing often leads hand kinematics by approximately 100 ms during arm tracking movements (Roitman et al., 2005;Coltz et al., 1999a) or center-out reaching tasks (Fu et al., 1997a;Marple-Horvat and Stein, 1987). A confound in these results is that the tasks are highly predictable. In circular tracking, the cyclic movements can co-vary with the firing discharge at multiple points in time (Roitman et al., 2005). Some findings suggest that timing sensitivity may be hard-wired within the cerebellar circuitry. The latencies of Purkinje cell simple spike responses to passive limb movements are greater in cells recorded medially that project to the fastigial or lateral vestibular nuclei compared to those recorded more laterally that likely project to the interpositus nucleus (Gray et al., 1993). Likewise, during intentional arm movements, Purkinje cells with the greatest "leads" tend to be recorded more laterally (Marple-Horvat and Stein, 1987), suggesting that timing relationships between firing discharge and movement kinematics may segregate in the different corticonuclear zones.

Motor learning in the cerebellum

Critical to the forward internal model hypothesis is the model's ability to adapt to changes in the environment. Otherwise, model predictions would quickly become inaccurate. The concept that the cerebellum is a main site of motor learning is based on two theoretical studies proposed by Marr (Marr, 1969) and Albus (Albus, 1971). Although a large number of experimental studies followed, the cerebellum's exact role in motor adaptation, skill learning, and classical conditioning has been highly debated over the past 40 years. This debate has included many ardent denials that the cerebellum has any role in any type of learning or adaptation (Llinas and Welsh, 1993;Kelly et al., 1990). However, the prevalence of evidence from human and animal behavioral studies with lesions or disease has firmly established that the cerebellum is critical for motor learning and adaptation. In visuomotor control, lesion and patient studies have demonstrated involvement in saccadic adaptation (Golla et al., 2008;Xu-Wilson et al., 2009;Takagi et al., 1998). The oculomotor vermis, including lobules VI and VII, is a critical lesion location providing a dissociation between motor adaptation and pure motor deficits (Golla et al., 2008;Takagi et al., 1998;Barash et al., 1999). Adaptation of smooth pursuit and vestibulo-ocular reflex (VOR) eye movements both depend upon the floccular complex and oculomotor vermis (Takagi et al., 2000;Robinson, 1976;Rambold et al., 2002). For human limb movements, adaptation to novel dynamics is disrupted by cerebellar degeneration or lesions (Maschke et al., 2004;Smith et al., 2000). This includes patients with spinocerebellar ataxia type 6 in which the pathology is largely limited to Purkinje cells (Maschke et al., 2004). Learning visuomotor transformations is cerebellar-dependent (Martin et al., 1996;Tseng et al., 2007;Martin et al., 1996), as is adaptation to speed changes in split treadmill walking (Morton and Bastian, 2007). Finally, there is an extensive literature on the role of the cerebellum in classical conditioning, most studies focusing on eye-blink conditioning (Bao et al., 2002;Mauk, 1997;Koekkoek et al., 2003;McCormick and Thompson, 1984;Yeo et al., 1985a;Yeo et al., 1985b). Therefore, the role of the cerebellum in motor learning and adaptation is unequivocal.

Cellular and molecular mechanisms of cerebellar learning

The neurobiological basis for cerebellar adaptation has focused on synaptic plasticity at parallel fiber-Purkinje cell synapses. Inspired by the Marr (Marr, 1969) and Albus (Albus, 1971) theoretical models, Ito and others provided the first demonstrations of long-term depression (LTD) at the parallel fiber-Purkinje cell synapse (Ito and Kano, 1982;Ekerot and Kano, 1985;Sakurai, 1987). Induction of parallel fiber-Purkinje cell LTD requires repetitive conjunction activation of climbing fiber and parallel fiber input at low frequencies (~1 Hz). Following the conjunction stimulation, the excitatory, post-synaptic potentials (EPSP) generated by parallel fibers are reduced. The requirement for climbing fiber activation was conceptualized as an error signal that provided the feedback to change synaptic weights (Albus, 1971;Ekerot and Kano, 1989;Ito, 1982).

The molecular and cellular mechanisms for parallel fiber-Purkinje cell LTD have been studied extensively *in vitro*. Expressed postsynaptically in Purkinje cells, LTD requires activation of metabotropic glutamate receptors (Ichise et al., 2000;Conquet et al., 1994) and protein kinase C (PKC) (Crepel and Krupa, 1988;Linden and Connor, 1991). PKC activation leads to internalization of postsynaptic AMPA receptors (Wang and Linden, 2000). High levels of intracellular calcium are needed, consistent with requirements for both parallel fiber and climbing fiber activation (Coesmans et al., 2004). Although limited, studies have also confirmed similar processes *in vivo* (Gao et al., 2003).

The exact role parallel fiber-Purkinje cell LTD plays in cerebellar adaptation has a long and controversial history. Classical eye-blink conditioning (Yeo, 1988;Koekkoek et al., 2003;Thompson and Krupa, 1994), adaptation to perturbation of reaching movements (Gilbert and Thach, 1977), smooth pursuit learning (Li et al., 2011;Medina and Lisberger, 2009;Medina and Lisberger, 2008), and many other forms of motor learning have been ascribed to LTD at the parallel fiber-Purkinje cell synapse. Initially, this mechanism was strongly implicated in VOR adaptation (Raymond and Lisberger, 1998;Lisberger et al., 1994), culminating in development of a transgenic mouse with Purkinje cell-specific inhibition of PKC, loss of parallel fiber-Purkinje cell LTD, and loss of VOR adaptation

(De Zeeuw et al., 1998). One of the most compelling studies recorded Purkinje cell discharge before and after learning in the monkey flocculus. During smooth pursuit adaptation, increases in complex spike activity were linked to a decrease in simple spike firing in the subsequent trial (Medina and Lisberger, 2008). Further, this study documented behavioral changes in smooth pursuit coupled to the reduction in simple spike activity (Medina and Lisberger, 2009;Medina and Lisberger, 2008).

However, a large number of studies have challenged the view that parallel fiber-Purkinje cell LTD underlies cerebellar dependent learning. These include failure to find the required Purkinje cell signals during visuomotor reach adaptation (Ojakangas and Ebner, 1992) and demonstrations of VOR adaptation without climbing fiber activation (Raymond and Lisberger, 1997). During saccadic adaptation, there is strong evidence that the complex spike activation does not provide the hypothesized error signals (Dash et al., 2010). Potentially, the most damaging evidence comes from a recent study in a transgenic mouse that disrupted the final steps of the signaling pathway in the internalization of AMPA receptors in Purkinje cells (Schonewille et al., 2011). Although parallel fiber-Purkinje cell LTD was blocked, these mice adapted normally in a battery of visuomotor tests. At a minimum, these challenges demonstrate that all cerebellar-dependent motor learning is not due to a single mechanism. Even more importantly, it is unlikely that any one form of learning relies solely on synaptic depression at a single synapse in the circuit.

Subsequent to the discovery of parallel fiber-Purkinje cell LTD, there have been many demonstrations of different types of synaptic plasticity throughout the cerebellar cortex and nuclei. At the parallel fiber-Purkinje cell synapse, there are both pre-synaptic (Hirano, 1991;Kano et al., 1992;Linden and Ahn, 1999;Salin et al., 1996) and post-synaptic forms of long-term potentiation (LTP). LTP occurs at the input stage of the cerebellar cortex, at the mossy fiber-granule cell synapses (D'Angelo et al., 1999;Armano et al., 2000). The synapses between parallel fibers and cerebellar cortical interneurons are plastic (Linden, 1998). Purkinje cells also have homeostatic plasticity (Belmeguenai

et al., 2010). Finally, there is synaptic plasticity in the cerebellar nuclei (Aizenman and Linden, 2000). While there is little if any information on these forms of plasticity in specific behaviors, they provide a host of mechanisms to potentially change cerebellar network properties.

Electrophysiological evidence for cerebellar learning

Electrophysiological evidence supporting the Marr-Albus-Ito theory of cerebellar learning has been controversial. Numerous studies examining adaptation of wrist/arm movements (Gilbert and Thach, 1977;Ojakangas and Ebner, 1992), smooth pursuit eye movements (Medina and Lisberger, 2008;Li et al., 2011), or saccades (Catz et al., 2005;Prsa and Thier, 2011) recorded increased complex spike activity in relation to learning. Often, as predicted by the Marr-Albus-Ito theory, the complex spike discharge was coupled to decreases in simple spike firing that mirrored behavioral learning (Medina and Lisberger, 2008;Gilbert and Thach, 1977). However, many studies also reported mismatches between complex spike firing and learning-related changes in the behavior and/or simple spike firing rates. Significant simple spike firing changes occurred even in the absence of complex spike modulation (Ojakangas and Ebner, 1990;Medina and Lisberger, 2009;Medina and Lisberger, 2008;Raymond and Lisberger, 1997), reaffirming that other mechanisms significantly contribute to plasticity at parallel fiber- Purkinje cell synapses. In the oculomotor vermis, Thier and colleagues documented that the greatest complex spike modulation in Purkinje cells occurs late in both saccadic and smooth pursuit adaptation. It even persists after the animals have fully mastered the task (Catz et al., 2005;Dash et al., 2010). Late changes in complex spike discharge were also common during reach adaptation to a visuomotor gain change (Ojakangas and Ebner, 1990).

Only two studies have quantified how the simple spike encoding of movement parameters changes with voluntary motor learning. This would be analogous to hypotheses that a forward internal model updates, or tunes, its input-output properties with learning (Wolpert et al., 1995;Desmurget and Grafton, 2000). Both studies examined Purkinje cell firing during smooth pursuit adaptation (Medina and Lisberger,

2009;Dash et al., 2013). One study involved adaptation to a change in the direction of tracking (Medina and Lisberger, 2009), while the other utilized a change in tracking speed (Dash et al., 2013). Although the models differed in form, both studies regressed simple spike firing against linear combinations of eye position, velocity, and acceleration. Medina and Lisberger (Medina and Lisberger, 2009) argued that the velocity and acceleration sensitivities changed, with both increases and decreases observed in 60.4% of individual Purkinje cells recorded from the flocculus. The study by Dash et al. (Dash et al., 2013) recorded Purkinje cells in the oculomotor vermis and found enhanced velocity sensitivity for gain increase adaptation, although changes in the regression coefficients were small. Velocity representations did not change with gain decrease adaptation. Changes in position or acceleration sensitivity were not reported. The study also made no attempt to determine if the simple spike discharge changed sensitivity within individual cells (i.e. did the regression βs increase or decrease). The authors stated that the changes in simple spike firing of individual Purkinje cells cannot provide a "reliable explanation" of the behavior (Dash et al., 2013;Prsa and Thier, 2011). Instead, only group results from a population analysis were reported. Clearly, if some Purkinje cells increased while others decreased their velocity sensitivity, the net effect across the population would cancel.

Changes in the timing sensitivity of parameter specific encoding have not been addressed. Although regression models in the smooth pursuit study described above accounted for time leads or lags between the neural firing and eye kinematics, learning-related changes in simple spike timing sensitivity were not reported (Medina and Lisberger, 2009). Another smooth pursuit learning study found that simple spike firing changes did not occur at the same time as changes in the behavioral response for a significant subset of the recorded Purkinje cells (Li et al., 2011). Similarly, in a task where saccade duration was critical to successful adaptation, simple spike firing changes were often transient despite robust, progressive changes in the behavior (Catz et al., 2008). However, at a population level, saccade duration (and thus learning) could be modeled by shifts towards bursts of activity from early firing vs. late firing Purkinje cells

(Catz et al., 2008;Prsa and Thier, 2011). Therefore, timing sensitivity likely plays an important role in motor adaptation, as would be expected from a forward internal model.

Are kinematics encoded invariantly?

If a forward internal model can adapt its predictions to the changing environment, the same plasticity mechanisms should allow models to generalize across movements. Instead, an fMRI study suggests that multiple internal models exist (Imamizu et al., 2003). In this study, subjects learned to use two different visuomotor representations of a mouse controlled cursor projected onto a screen. The rotations were either position or velocity dependent. After learning, two areas of activation persisted in the lateral and posterior cerebellum, corresponding to the two different tasks. The locations of activation were significantly different, with <10% overlap. The authors concluded that the areas of activation provided evidence for two different competing internal models. However, one might argue that a single model that can undergo small modifications by changing the weights (i.e. βs) of the model parameters is a more efficient implementation for learning, especially since limb movements can be broken into submovements that are similar across a wide range of tasks (Roitman et al., 2004;Pasalar et al., 2005;Miall et al., 1986). Evidence from one study showed that regression coefficients calculated from kinematic and Purkinje cell firing data during circular manual tracking could reconstruct the cell firing during the non-tracking, intercept epoch of the task (Roitman et al., 2005). However, invariant encoding must be tested more rigorously using movement paradigms with different control strategies and properties.

Hypotheses and rationale

Several lines of evidence suggest that cerebellar cortex is an appropriate candidate for a forward internal model. Moreover, the hypothesis helps explain how the varied motor control functions attributed to the cerebellum may arise from a simple, stereotypic architecture. For instance, psychophysical studies of grip force (Flanagan and Wing, 1997;Muller and Dichgans, 1994), predictive eye movements (Ariff et al., 2002;Nanayakkara and Shadmehr, 2003;Medina and Lisberger, 2008), and coordinated

reaching (Wagner and Smith, 2008) have demonstrated that kinematic output from a forward model is an essential control component needed to learn new movement dynamics and generate coordinated movements in real time. These functions match the cerebellum's known roles in the timing, learning, and coordination of movements. Yet despite the abundance of circumstantial evidence, no mammalian studies have explicitly tested whether Purkinje cell firing corresponds with forward internal model output. Therefore, we tested three properties of a forward internal model by recording the simple spike discharge from cerebellar Purkinje cells in lobules IV-VI of the intermediate/lateral cerebellar zones. The experiments and results are described in Chapters 2 and 3.

First, feedforward encoding of kinematic signals would be consistent with the predictions from a forward internal model. Some evidence suggests that Purkinje cell simple spikes encode hand kinematics in a feedforward manner, but the cells were recorded during highly predictable tasks (Roitman et al., 2005;Coltz et al., 1999a;Fu et al., 1997a;Marple-Horvat and Stein, 1987). Therefore, timing relationships between Purkinje cell simple spike firing and hand movements must still be evaluated.

Hypothesis 1: Purkinje cell simple spike firing predicts future hand kinematics, even when the task is highly unpredictable.

Secondly, it is unknown whether a single internal model can generalize to other tasks by modestly changing the weightings of the model parameters, or if multiple internal models exist for different movement tasks (Imamizu et al., 2003).

Hypothesis 2: Kinematic parameter encoding from individual Purkinje cells is by and large invariant across tasks, with modest changes occurring in the parameter and timing sensitivity for different tasks.

Third, a forward internal model must adapt to changes in the environment in order to maintain accurate predictions. Only two electrophysiological studies have quantified

changes in the simple spike firing with learning (Medina and Lisberger, 2009;Dash et al., 2013). These studies were both of eye movements, and only Medina and Lisberger (Medina and Lisberger, 2009) evaluated changes within individual cells. Changes in timing sensitivity were not reported.

Hypothesis 3: Purkinje cell simple spike discharge will exhibit progressive changes with kinematic adaptation. This will be reflected by changes in the parameter sensitivity (i.e. increases or decreases in the βs), timing sensitivity (i.e. time changes in τ), or both.

CHAPTER 2: PURKINJE CELL SIMPLE SPIKE DISCHARGE IS CONSERVED ACROSS MULTIPLE TASKS

Introduction

Many theories have been proposed to explain how the cerebellum might use representations of movement kinematics to produce accurate, coordinated movements. One prominent hypothesis is that the cerebellum acts as a forward internal model, transforming the motor command and the current state of the limb into a prediction about the future state of the limb, such as the upcoming movements or errors (Kawato and Wolpert, 1998;Wolpert et al., 1998;Kawato, 1999). These predictions of the upcoming movements would likely be expressed in terms of sensory consequences and kinematic variables (Wolpert et al., 1995).

A forward internal model by definition would require feedfoward and predictive control (Bastian, 2006;Ebner and Pasalar, 2008). Many previous studies used highly predictable tasks in which the monkeys were given cues about upcoming task parameters and the trajectory paths were relatively fixed, allowing the animals to easily anticipate and plan subsequent movements (Coltz et al., 1999a;Roitman et al., 2005;Marple-Horvat and Stein, 1987;Fu et al., 1997a;Fortier et al., 1989). These paradigms result in highly stereotypical movements with relatively few task-related errors in which Purkinje cell simple spike discharge largely leads arm/hand kinematics (Roitman et al., 2005;Marple-Horvat and Stein, 1987;Fu et al., 1997a). However, the predictable movements and relatively few task errors make it difficult to determine whether the observed leads reflect the subject's anticipation and planning for the upcoming trial, or direct control of the current movement trajectory. A task with minimal predictability is necessary to answer this question.

Another important issue is the degree to which a single Purkinje cell invariantly signals the same information for different movements. This question is central to the hypothesis that the cerebellar cortex is the site of multiple internal models (Kawato and Wolpert,

1998;Imamizu et al., 2003;Wolpert et al., 1998). If signals in the simple spike discharge differ greatly for different tasks, this would reflect a non-parametric representation consistent with the concept of multiple internal models for specific movements. Conversely, if the signals present in a particular type of movement can be used to predict the firing in different tasks, this would suggest that Purkinje cells have a parametric representation of limb kinematics that can generalize over a wide range of behaviors. Our previous study showed that estimates of the kinematic signals obtained during circular tracking were able to predict with modest accuracy the simple spike firing during the target intercept period (Roitman et al., 2005). However, circular tracking and other previously tested behavioral tasks provide only limited coverage of the kinematic workspace, which limits the robustness of any firing models created from the data sets. Rigorous testing of invariant encoding requires firing models built from data that extensively explores the kinematic workspace, so that model bias is minimized when applied to different movements.

Previous studies also typically relied on substantial data averaging, both across trials and time, to assess the signals present in the simple spike firing (Roitman et al., 2005;Fu et al., 1997a;Pasalar et al., 2006;Marple-Horvat and Stein, 1987;Shidara et al., 1993;Coltz et al., 1999a;Medina and Lisberger, 2009). While providing significant insights into the parameters signaled, averaging firing data discards information in the data set, leading to regression coefficients that are likely biased (Zar, 1999;Freund, 1971). Conclusions about the nature of the signals encoded in the firing cannot be assured to generalize to other movements or tasks. Furthermore, averaging is guaranteed to increase the R^2 value by removing variability in the sample. The increase is deceptive because models based on averaged data (also called aggregate models) describe the grouped behavior rather than the effects of individual time points or trials (Kenny, 1979). Therefore, the goal should be to understand the nature and the strength of the signals carried in the instantaneous firing rate, rather than striving to simply maximize the variance that a model can account for (O'Grady, 1982).

In this study, we developed a behavioral paradigm in which monkeys were trained to manually track a target that moved pseudo-randomly at unpredictable speeds and directions. Although used to study the encoding of information in the motor cortex (Paninski et al., 2004a;Paninski et al., 2004b), deficits in cerebellar stroke (Boyd and Winstein, 2004), and cerebellar activation during neuroimaging (Imamizu et al., 2000), a random tracking paradigm has not been utilized in an electrophysiology study targeting the cerebellum. Random tracking has several advantages. The task provides excellent coverage of the position, velocity, and speed workspaces (Paninski et al., 2004a) and eliminates the confound of predictability. Random tracking also reduces the statistical dependencies among the kinematic parameters and requires continuous control of the movement throughout the task (Paninski et al., 2004a). Purkinje cell simple spike firing recorded during a random tracking task was evaluated for position, velocity, and speed encoding. Timing relationships between the firing and these parameters were also characterized. We compared regression model results using averaged vs. non-averaged data to determine whether these kinematic variables are reliably encoded in the firing at the level of individual trials. Finally, Purkinje cell firing was evaluated in two additional tasks, to determine whether the signals present in random tracking generalize to either circular tracking or center-out reach.

The content of this chapter has been published in the *Journal of Neurophysiology* (Hewitt A, Popa L, Pasalar S, Hendrix CM, Ebner TJ (2011) Representation of limb kinematics in Purkinje cell simple spike discharge is conserved across multiple tasks. J Neurophysiol 106:2232-2247.)

Methods

The experimental protocol was approved and monitored by the University of Minnesota Institutional Animal Care and Use Committee and conformed to the "Guiding Principles in the Care and Use of Animals" of the American Physiological Society.

Behavioral paradigms

Two rhesus monkeys (*Macaca mulatta*; female "N" 6.3 kg; male "I" 6.2 kg) were trained, with their heads fixed, to perform three different movement paradigms (Figure 1). Each monkey used a two-joint robot manipulandum (In Motion 2, Interactive Motion Inc., Boston, MA) in the horizontal plane to control a cursor and track targets displayed on a vertically oriented video screen placed 50 cm in front of the animal. The animal received an automated juice reward after successful trial completions. During each recording session, a monkey performed the random tracking paradigm and at least one of the other two tasks (circular tracking or center-out reach) so that each cell's firing was evaluated in multiple tasks requiring different movement strategies. The animals typically executed 100-200 trials of the random tracking task and 80-150 trials of circular tracking or center-out reach tasks during a 4 hour recording session.

All tasks began with an initial hold period requiring the monkeys to move to and hold a "+" style cursor (0.5 x 0.5 cm) within a red "start" target for a randomized time (1000-2000 ms). All targets for center-out reach and circular tracking were 2.5 cm diameter circles, and the start target was always located at the center of the workspace. In random tracking, target size was enlarged to 3.0 cm due to the increased task difficulty, and the start target was positioned randomly within the 12 cm x 12 cm workspace viewed on the screen.

Random tracking (Figure 1A): After the initial hold period, the target began moving pseudo-randomly so that the monkey had no knowledge of the upcoming trajectory. To ensure the task was achievable (i.e., no abrupt changes in curvature or speed), target trajectories were generated a priori using sum of sine waves (Imamizu et al., 2000;Paninski et al., 2004a) and smoothed with a low-pass filter. Trajectories with a sharp turn (i.e., angle greater than 75^{o} between adjacent 50 ms segments of the binned trajectory) were discarded. Speed was controlled along the entire target path using the equation speed = $cK^{-1/3}$, where K is the curvature of the current path and the constant c was chosen to yield an average speed of 4 cm/s. This is an implementation of the two-

thirds power law found to govern natural arm movements (Viviani and Terzuolo, 1982;Lacquaniti et al., 1983). Additional filtering was used to prevent rapid speed increases at the onset of tracking. At the end of each trajectory, the target ceased moving and the animal was required to maintain the cursor within the target for a "final" hold period (1000 ms). Due to the difficulty of the task, brief excursions (< 500 ms) outside of the target were permitted. Longer excursions during any trial period automatically aborted the trial. A set of 100 trajectories, 6-10 s in duration, were predefined and randomly presented at each recording session.

Circular tracking (Figure 1B): As described previously (Roitman et al., 2005;Pasalar et al., 2006), after the initial hold a yellow cue target appeared at one of 4 initial angles (0, 90, 180, or 270^{o}) and moved at constant speed along a 5.0 cm radius circular path at 60^{o}/s (5.2 cm/s) or 80^{o}/s (7.0 cm/s) in either the clockwise (CW) or counter-clockwise (CCW) direction. After 180^{o} of travel, the cue target changed color (yellow to red) signaling the onset of interception. The monkey had 65^{o} of target travel to intercept the moving target, and then continued tracking the target for an additional 360^{o}. A "final" hold period required that the animal maintain the cursor within the unmoving target for a brief time (1000 ms). To be comparable to the random tracking task, trials were again aborted if at any time the cursor deviated from the target for more than 500 ms.

Center-out reach (Figure 1C): This paradigm was also described in prior studies (Georgopoulos et al., 1982;Fortier et al., 1989;Fu et al., 1997a). After the initial hold, a red cue target appeared in one of eight directions spaced at 45^{o} intervals and 5.0 cm from the workspace center. The animal had 1500 ms to intercept the cue target with the cursor, and then maintained cursor position inside the target for an additional 500 ms "final" hold period.

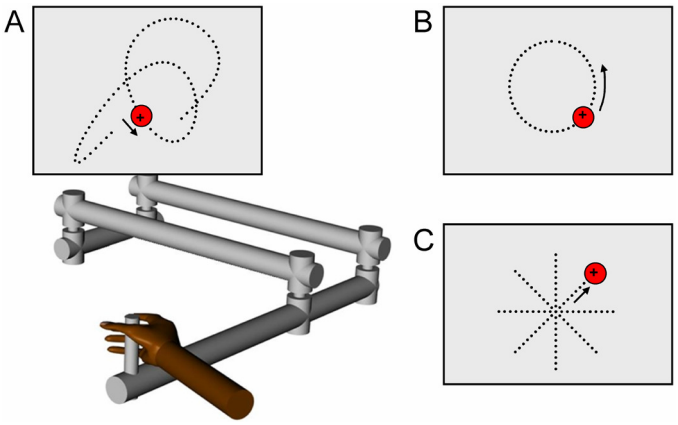

Figure 1: *Random tracking, circular tracking, and center-out reach paradigms*. Monkeys used a two-joint manipulandum to control a "+" style cursor viewed on a video screen. All three tasks begin when the animal holds the cursor within a circular "start" target (located at screen center for circular tracking and center-out reach, or randomly positioned for random tracking) for a variable time period (1-2 s). A) *Random tracking*: the cursor is maintained within the target as it moves at pseudo-randomized directions and speeds across the workspace; brief excursions (<500 ms) outside of the target are permitted to make the task achievable. B) *Circular tracking*: a moving yellow "cue" target (not shown) first indicates target direction and speed (±60 or 80 ^{o}/s) as it moves along a circular path (5 cm radius) for 180^{o}. When the cue target turns red, animals move the cursor to intercept and track the target for 360^{o}. Brief excursions are again permitted to match random tracking constraints. C) *Center-out reach*: A red target appears at one of eight randomized locations spaced 5 cm from the workspace center. Targets can be intercepted immediately, without further cues or constraints on movement speed. All three tasks end with maintaining the cursor inside a motionless "final hold" target for 1 s. Note that the dotted lines and arrows are only shown to illustrate typical target paths and are not normally visible.

Surgical procedures

Head restraint hardware and a recording chamber were chronically implanted in each animal using aseptic techniques and full surgical anesthesia (Pasalar et al., 2006;Roitman et al., 2005;Coltz et al., 1999a). The head was restrained during training and recording experiments using a circular stainless steel halo attached to the skull with 3-4 surgical steel posts and screws. The recording chamber was placed over the right parietal cortex (both animals were trained to use their right hands for movement tasks), and stereotaxically positioned over a 2.0 cm diameter craniotomy to target recordings from lobules IV-VI of the intermediate and lateral cerebellar zones (Pasalar et al., 2006;Roitman et al., 2005;Coltz et al., 1999a) where hand and arm related Purkinje cells have been described (Thach, 1968;Mano and Yamamoto, 1980;Fortier et al., 1989;Ojakangas and Ebner, 1992;Fu et al., 1997a;Roitman et al., 2005;Pasalar et al.,

2006;Yamamoto et al., 2007). The two monkeys used in this study have not been euthanized and are subjects in another experiment.

Anatomical modeling

Microelectrode recording positions were reconstructed for each monkey (Figure 2) based upon electrode penetration coordinates and individual CT scans obtained post-recording. It was not possible to acquire MRI data from either monkey because the metal recording hardware created large artifacts and both animals are still being studied in another experiment. Instead, whole brain MRI images (T1-weighted with a voxel size of 0.5 x 0.5 x 0.5 mm^3) were collected from a similarly-sized monkey using a custom-built monkey coil and a 7T MR scanner (Siemens) equipped with a head gradient coil (80mT/m G-maximum, 200mT/m/ms). Using the software Monkey Cicerone v1.2 (Miocinovic et al., 2007), each monkey's CT scan was co-registered with the MRI images using the eye sockets, mandible, skull, nasal turbines, and teeth as landmarks (Figure 2A). A custom anatomical model of the rhesus monkey cerebellum and primary fissure was created from the whole brain MRI data using 3D volume rendering (AVIZO software, Visualization Sciences Group, Burlington, MA). The anterior and posterior commissures were also modeled as landmarks for aligning the cerebellum model with each monkey's co-registered imaging data. Having aligned the anatomical data, a virtual recording chamber was placed on the skull using the stereotaxic surgery coordinates. Model microelectrodes were inserted through the chamber at the angle, positions, and depths at which the Purkinje cell recordings were obtained. The virtual microelectrode penetrations were exported along with the cerebellum model to visualize the recording locations.

Electrophysiological recordings and data collection

After full recovery of the animal, Purkinje cells were recorded extracellularly using quartz-platinum/tungsten single microelectrodes (1-2 MΩ impedance; Thomas Recording, Germany) that were inserted through the dura using a guide tube (22 gauge), and then advanced using a hydraulic microdrive (Narishige, Japan) to depths of 22.5-33.8

mm. Purkinje cells were identified by the presence of complex spikes (Thach, 1968;Ojakangas and Ebner, 1992;Fu et al., 1997a;Roitman et al., 2005;Pasalar et al., 2006). Conventional techniques were used to amplify and filter (30 Hz-3 kHz band pass, 60 Hz notch) the spike waveforms prior to the discrimination of simple spikes. Because of the long duration of the experiments (3-5 hours), recordings focused on optimizing the discrimination of the simple spikes. Discrimination was performed online using the Multiple Spike Detector system (Alpha-Omega Engineering, Israel), and the resulting spike trains were digitized and stored at 1 kHz. The raw electrophysiological data were also digitized at 32 kHz and stored to disk. The spike trains were transformed to a continuous firing rate using fractional intervals with down sampling to 50 Hz and low pass filtering (12^{th} order Butterworth with a 12 Hz cut-off). All data channels (kinematic and firing) were then merged and aligned on movement onset for each trial. For regression analyses, the mean firing rate for each trial was subtracted from the instantaneous firing rate.

Hand position was acquired by optical encoders at each robot joint and used to display cursor position in real time on the vertical screen. Hand position and target position data were both written to disk at 200 Hz. Velocity, speed, direction of movements, and other kinematic variables were calculated from the stored position data (Roitman et al., 2005;Pasalar et al., 2006).

Kinematic data analyses

Stored kinematic data were down sampled to 50 Hz and low pass filtered (12^{th} order Butterworth with a 12 Hz cut-off). The filtered data were used to calculate instantaneous kinematic error (e) measures (see Figure 5A) that included the differences in movement direction ($Direction_e = |\theta_h - \theta_{tgt}|$) and speed ($Speed_e = |\mathbf{V_h}| - |\mathbf{V_{tgt}}|$; bold type denotes vectors) between the hand (h) and target (tgt). Radial position errors were assessed by calculating the distance from target center (r), which was normalized by target radius (r_{tgt}) to account for the different target sizes between random and circular tracking (Radial $Position_e = r / r_{tgt}$). Hold periods and the circular tracking intercept period were excluded

from the analyses, so that only tracking movements were evaluated. The probability of each error measure was determined, and Chi-square tests assessed whether an association exists between the error counts and the tracking task (e.g. random or circular). These results were also averaged for each recording session to obtain a mean direction and speed error for each recording session. One-way within subjects ANOVAs ($\alpha = 0.05$) were conducted to compare the effects of the behavioral paradigm (e.g. random or circular tracking) on error.

Cross-correlation analyses were used to calculate time leads or lags (kinematic τ values) that describe the timing relationships between hand and target trajectories over a complete trial for both random and circular tracking. For position, τ values were determined as the time corresponding to the maximum cross-correlation between the hand and target position (X_h vs. X_{tgt} and Y_h vs. Y_{tgt}) from -500 to 500 ms with 20 ms resolution. The τ values describing the timing relationships between target $\mathbf{V_{tgt}}$ (Vx_{tgt}, Vy_{tgt}) and hand $\mathbf{V_h}$ velocity (Vx_h, Vy_h) trajectories were calculated in the same way. Negative τ values imply that the hand leads the target. Chi-square tests evaluated if an association exists between the τ value counts and the task (e.g. random or circular).

Models of simple spike firing

Based on qualitative analyses of the averaged simple spike firing data and previous studies (Pasalar et al., 2006;Fu et al., 1997a;Coltz et al., 1999a;Roitman et al., 2005;Marple-Horvat and Stein, 1987;Mano and Yamamoto, 1980), the simple spike firing was fit to a multiple linear regression model including terms for hand position ($\mathbf{P_h}$), velocity ($\mathbf{V_h}$), and speed (S_h). We refer to this as the PVS regression model (eqn. 1). An additional model parameter, τ, was incorporated to estimate the lead or lag between simple spike firing (f) and the kinematics. Parameters b_o and ε, respectively, depict baseline firing and the residual error.

Eqn. (1) $$f(t) = b_o + \mathbf{b_P}\,\mathbf{P_h}(t-\tau) + \mathbf{b_V}\,\mathbf{V_h}(t-\tau) + b_S\,S_h(t-\tau) + \varepsilon$$

Two similar models were also constructed to evaluate the contributions of direction, speed, and velocity. A PŪS regression model (eqn. 2) used hand position ($\mathbf{P_h}$), unit velocity (i.e. direction, $\mathbf{\bar{U}_h}$), and speed (S_h), while the PV regression model (eqn. 3) simplified the PVS model by eliminating the speed term.

Eqn. (2) $$f(t) = b_o + \mathbf{b_P}\,\mathbf{P_h}(t-\tau) + \mathbf{b_U}\,\mathbf{\bar{U}_h}(t-\tau) + b_S\,S_h(t-\tau) + \varepsilon$$

Eqn. (3) $$f(t) = b_o + \mathbf{b_P}\,\mathbf{P_h}(t-\tau) + \mathbf{b_V}\,\mathbf{V_h}(t-\tau) + \varepsilon$$

The firing data from each Purkinje cell were fit to the above models using a five bin partition for each kinematic parameter. This resulted in a 5 x 5 grid of 2.4 x 2.4 cm bins for the position workspace (-6 to 6 cm) and a 5 x 5 grid of 4.8 x 4.8 cm/s bins for the velocity workspace (-12 to 12 cm/s, see Figures 9 and 10). Direction was computed as the unit velocity vector ($\bar{U}x_h$, $\bar{U}y_h$) and again binned in a 5 x 5 grid of 0.4 x 0.4 unit bins (-1 to 1 units) to match the velocity binning. The speed workspace (0 to 12 cm/s) was partitioned into five bins of 2.4 cm/s. Hand kinematics were sorted and averaged within the bins, along with the associated simple spike firing rates, to generate an average kinematic value (i.e., position, velocity, or speed) and firing rate for each bin. For each cell, regressions fitting the averaged data from each bin to the models were performed across multiple τ values (-500 to 500 ms in 20 ms increments). The τ value providing the best fit (i.e., highest R^2_{adj}) for each cell was identified as the optimal τ value and used for modeling. Negative τ values imply that the firing leads hand kinematics. Semi-partial correlation coefficients were also calculated to approximate how much of the firing variance was described by each term in the PVS model at the optimal τ value (Zar, 1999).

Averaged vs. non-averaged regression models

As shown in the results, the PVS regression model provided the best description of the simple spike firing, and cross correlograms of hand position ($\mathbf{P_h}$), velocity ($\mathbf{V_h}$), and speed (S_h) averaged across all trials and sessions confirmed that these parameters were only weakly correlated (see Figure 8) and, therefore, could be used in a multiple linear regression model (Zar, 1999;Freund and Littel, 2000;Belsley et al., 1980). Three

additional analyses were conducted using this PVS model. First, the effects of averaging the data were evaluated. The PVS regression model was computed for each cell using the instantaneous hand kinematics and the instantaneous firing (20 ms bins) instead of the averaged data. Again, the τ value providing the best fit (i.e., highest R^2_{adj}) for each cell was determined. Resulting R^2_{adj}, τ , and coefficient values from the regressions based on the non-averaged data were plotted against those based on the averaged data. The correlation coefficients and slope of these plots were determined to compare the regression results obtained from the averaged and non-averaged data.

The second additional analysis evaluated whether curvature altered the optimal τ value, as previous studies in the motor cortex suggest that firing leads or lags may change relative to the curvature, k (eqn. 4), of the hand movement path (Moran and Schwartz, 1999).

Eqn. (4) $$k = (\dot{x}\ddot{y} - \ddot{x}\dot{y})/(\dot{x}^2 + \dot{y}^2)^{3/2}$$

The instantaneous curvature of the hand movement data (20 ms bins) was determined and divided into ten bins ranging from -9.9 to 9.9 cm^{-1} or five bins ranging from 0 to 9.9 cm^{-1} for unsigned curvature (absolute value of k) so that each bin included a similar number of data points. The non-averaged kinematic and firing data in each bin were fit to the PVS model and the optimal τ value was identified. An ANOVA determined if there were any significant differences across the τ values for each bin.

Individual τ values

The initial PVS regression model (eqn. 1) only evaluates τ as a global time lead or lag for the ensemble of kinematic terms. Therefore, we performed a third additional analysis that determined the optimal τ for each parameter. Ideally, this would be calculated using a single regression model with independent τ values for each parameter, but this approach was computationally prohibitive. Analysis of a single Purkinje cell across all τ values would require 51 iterations of the regression model for each of the 5 model parameters

(51^5= 345,025,251 iterations per cell). Instead, we performed single linear regressions for each of the five PVS model parameters by restricting eqn. 1 to fit one kinematic variable at a time. The same five bin partition described above for the PVS model was used. This resulted in five different R^2_{adj} profiles per cell (one for each model parameter) from τ= -500 to 500 ms. The individual profiles were then summed and compared to the global profile using the Root Mean Square Deviation (RMSD). We then examined a modified version of the PVS model (eqn. 1) that incorporated these individual τ values in place of the global τ. The resulting model R^2_{adj}, beta regression coefficients, and semi-partial correlation coefficients were computed for each cell and compared to the original PVS model.

Invariant encoding across tasks

For each cell, the optimal τ value and PVS model regression coefficients obtained from the non-averaged random tracking data were used to estimate the firing in the circular tracking or center-out reach tasks. The neural activity recorded during circular tracking was sorted and averaged using 10 degree bins (0 to 360^o) corresponding to the angular hand position. Data recorded during the center-out task were averaged across trial direction, smoothed using a 10 point sliding average window, and aligned to the maximum speed with a time window of -600 to 600 ms. The neural data were preprocessed as described for the random tracking task. Correlation coefficients were employed to measure the fit between the estimated and recorded neural activity.

Results

Microelectrode recording locations

Anatomical modeling of the recording chamber and electrode positions shows that an electrode placed in the center of Monkey N's chamber would project to the intermediate zone of the cerebellum (Figure 2A). Sagittal MRI slices illustrate that the center electrode trajectory lies just anterior to the primary fissure (Figure 2B). Very similar electrode positioning was found for Monkey I. All electrode positions from which at least two cells were successfully recorded were plotted on the surface of the 3D

cerebellum model (Figure 2C and D). In both monkeys, penetrations are mostly in lobules IV-V of the intermediate zone and anterior to the primary fissure, a region strongly implicated in the control of the arm (Thach, 1968;Mano and Yamamoto, 1980;Fortier et al., 1989;Ojakangas and Ebner, 1992;Fu et al., 1997a;Roitman et al., 2005;Pasalar et al., 2006).

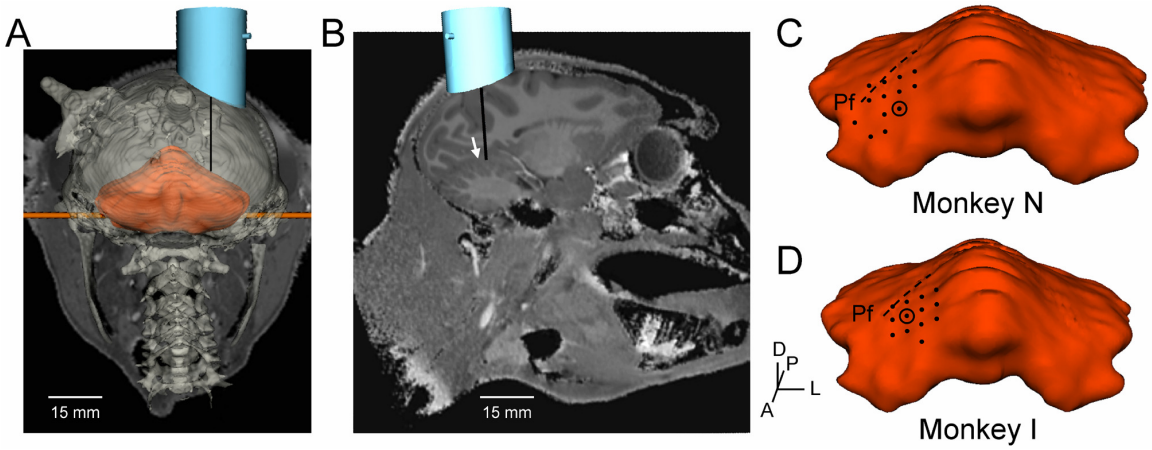

Figure 2: *Microelectrode recording positions*. A) Bony landmarks were identified and used to co-register each monkey's CT images with high resolution MRI data from a similarly-sized rhesus macaque. Virtual microelectrodes were inserted through a recording chamber (positioned using the surgical stereotaxic coordinates and CT landmarks) at the angle, positions, and depths used to record this data set. A posterior view of the coronal images shows an electrode inserted in the chamber center falls in the intermediate zone of the cerebellum model (shown in orange). B) A sagittal MRI slice shows the same center electrode has a trajectory anterior to the primary fissure (white arrow). C, D) All electrode penetrations from which at least two cells were successfully recorded are indicated with dots on the cerebellum surface. The circle denotes the recording chamber center, and a dashed line represents the primary fissue (Pf). Axes illustrate the anterior (A), posterior (P), dorsal (D), and lateral (L) orientations.

Random tracking fully covers kinematic workspace

Hand kinematics from a typical recording session are plotted in Figure 3 and illustrate differences in workspace coverage between the three tasks. Random tracking hand trajectories (X_h vs. Y_h) thoroughly cover the position workspace (Figure 3A). All directions and speeds from 0-12 cm/s are executed across the entire X-position workspace. Additionally, the full range of speeds is applied to all movement directions. Results are similar for the Y-position data (not shown).

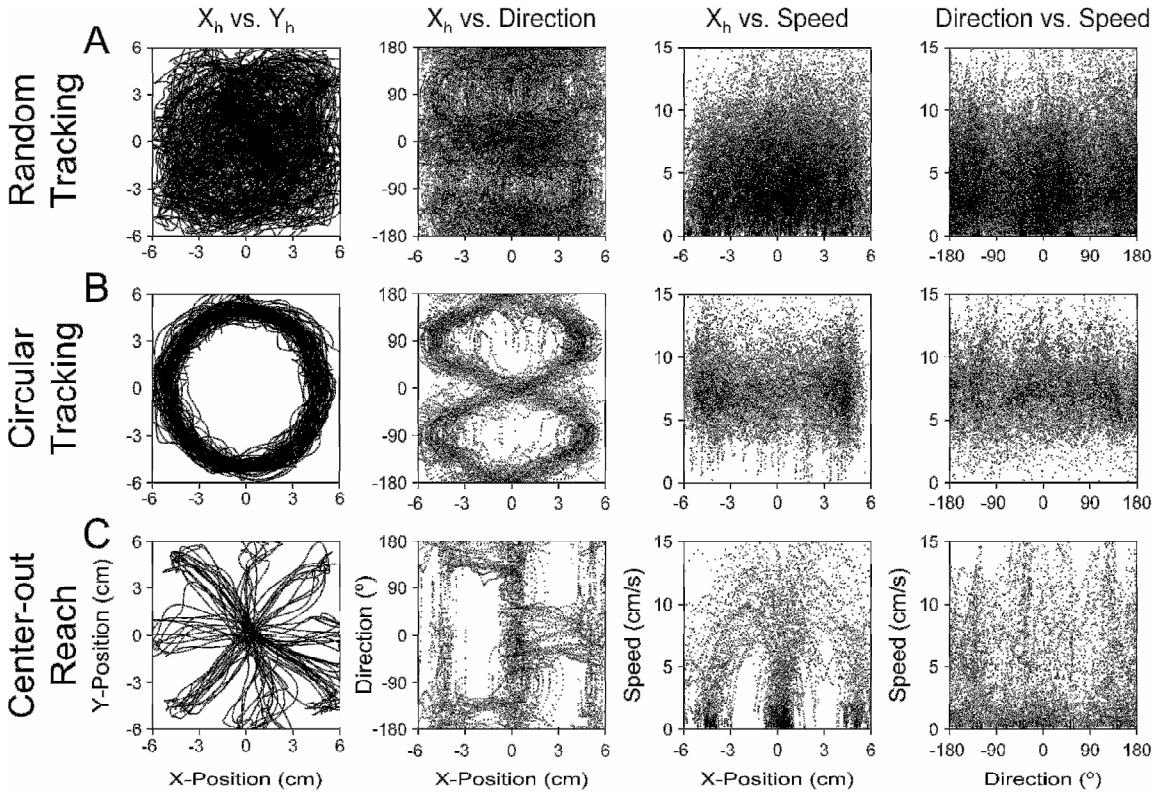

Figure 3: *Coverage of the kinematic workspace*. A) The top row shows an example of hand kinematics collected from a typical 100 trial random tracking recording session. Plotted left to right are: 1) hand position trajectories (X_h vs. Y_h) across the 12 x 12 cm workspace, 2) hand position (X_h, -6 to 6 cm) vs. hand movement direction (-180 to 180°), 3) hand position (X_h) vs. hand speed (S_h, 0 to 12 cm/s), and 4) hand movement direction vs. hand speed (S_h). B) Similar plots for 100 trials of circular tracking are shown in the middle row and include both clockwise and counter-clockwise tracking directions. C) Bottom row depicts 100 trials of center-out reach movements. Comparable results were observed for the Y-position data (not shown) in all three tasks.

In comparison, both the circular tracking (Figure 3B) and center-out reach tasks (Figure 3C) leave large areas of the position workspace untraversed. Plots of hand position (X_h) vs. direction or speed demonstrate coupling between the position and velocity vectors for these two movement paradigms. For circular tracking, movements span the complete range of directions (-180 to 180°), but are mostly limited to a narrow speed range of 5 to 10 cm/s. Similarly, center-out reach covers the low speed range, but is limited to the positions of the cue and intercept targets. Fast movements (i.e., high speed range) are limited to the 8 directions corresponding to the intercept targets. Again, similar findings are observed for direction or speed versus hand Y-position (Y_h). Collectively, these

results reaffirm the limits of previous movement paradigms (Coltz et al., 1999a;Fu et al., 1997a;Roitman et al., 2005;Fortier et al., 1989) and demonstrate that the random tracking task achieves one of its major aims of providing more complete coverage of the kinematic workspace (Paninski et al., 2004a).

Kinematic error measures

Figure 4 depicts Purkinje cell simple and complex spike occurrences and hand kinematics superimposed on the hand path (Figure 4A) or hand velocity (Figures 4B-C) during a single trial of random tracking. Recorded neural activity from the first second of hand movement (Figure 4A, lower left) includes three complex spikes that produced brief pauses in simple spike firing (Bloedel and Roberts, 1971;McDevitt et al., 1982). This one second of example firing is labeled blue for simple spike firing in the corresponding kinematics plots. Comparison of the hand and target paths show that the hand briefly went outside the target three times during this trial, illustrating the task difficulty (Figure 4A). Mismatches between hand and target velocity were also prevalent and suggest that the animals were unable to fully predict future target movement directions or speeds (Figure 4B-C). Qualitative interpretation of the relationship between the raw firing and hand kinematics is challenging because each trial of the random tracking task produced unique target trajectories and different hand kinematics. Additionally, the spacing between kinematic data points (and thus the overlaid simple or complex spike occurrences) is greater during periods of fast movements and smaller during slow movements, potentially giving the misleading perception of differences in simple spike firing with curvature or acceleration.

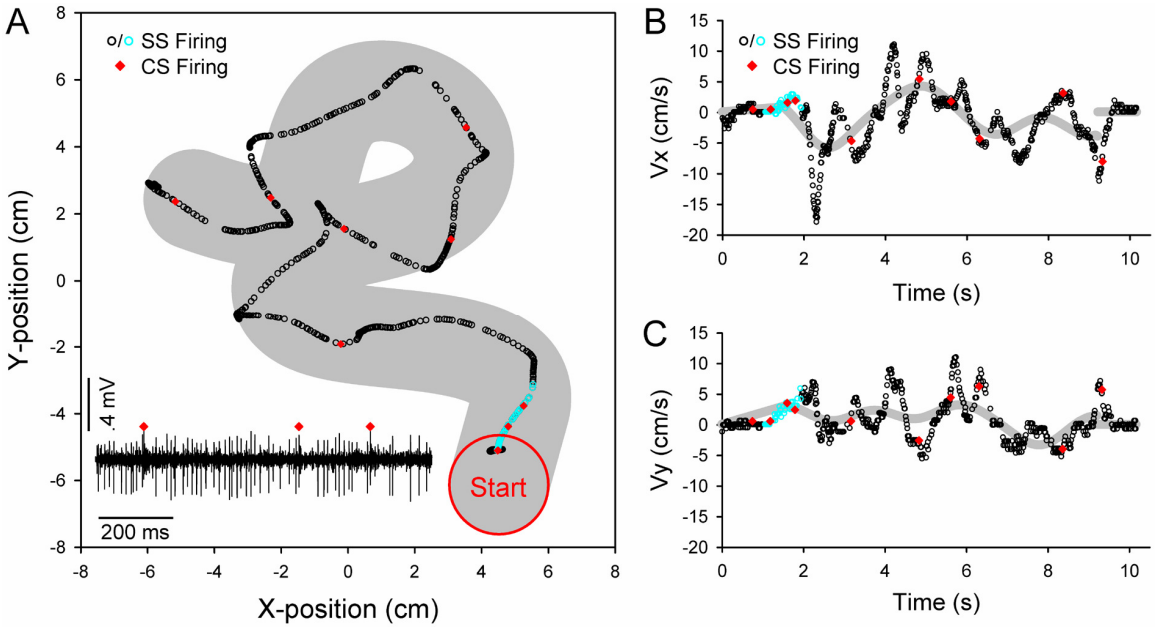

Figure 4: *Tracking performance and electrophysiology data.* A) The red "start" target is drawn at the beginning of the target trajectory, with the target path (X_{tgt}, Y_{tgt}) shown in grey (target diameter= 3 cm). Simple (black o) and complex (red ◊) spikes are superimposed upon the hand position (X_h, Y_h) at the time of occurrence. Blue symbols denote simple spikes (blue o) from the first 1 second of hand movement, and this raw electrophysiology data (shown in the lower left) includes three complex spikes (red ◊). B-C) Similarly, target velocity (grey) in the x-direction (Vx_{tgt}) or y-direction (Vy_{tgt}) was plotted versus time, with the simple and complex spikes superimposed upon the hand velocity (Vx_h or Vy_h).

Instantaneous error measures, including direction, speed, and radial position error, were calculated from hand and target kinematic data of successfully completed circular and random tracking trials across all recording sessions (Figure 5A). Direction errors ($|\theta_h - \theta_{tgt}|$) show that the hand and target mostly move in the same direction (mode = 0.5^o for both tasks, Figure 5B). However, large direction errors (i.e., hand movements opposite the direction of target movement) are more frequent during random tracking (mean = 42.5 ± 40.6^o) than circular tracking (mean = 19.8 ± 22.1^o, $X^2(179, N = 10{,}909{,}856) = 511{,}130.96$, $p < 0.0001$, Figure 5B). Hand speeds overall exceed target speeds ($|\mathbf{V_h}| - |\mathbf{V_{tgt}}|$) for random tracking (mean = 1.3 ± 2.6 cm/s, Figure 5C), which is consistent with observations that both monkeys frequently made quick catch-up movements to compensate for tracking errors (see velocity plots, Figures 4 and 6). In circular tracking, the mean speed error approaches zero (mean = 0.2 ± 2.4 cm/s, Figure 5C), suggesting that

the monkeys are better able to predict and, therefore, match target movements. Conversely, the speed errors for random tracking are larger than in circular tracking (X^2(88, N=10,903,151) = 344,254.18, p < 0.0001). Excursions outside of the target (i.e., radial errors > 100%) occur ~10% of the time in both tasks. These radial position errors (r / r_{tgt}, Figure 5D) are slightly greater for circular tracking (mean = 66.4 ± 50.4% target radius) than random tracking (mean = 64.4 ± 59.1% target radius, X^2(99, N = 10,738,785) = 31,768.87, p < 0.0001). The large radial position errors show that the animals do not attempt to keep the cursor exactly in the target center even during circular tracking when target movement directions and speeds are predictable. Why the animal uses this strategy is not obvious, but there are no specific requirements or training to keep the cursor at the target center. Consequently, direction and speed errors are better performance indicators and provide evidence that random tracking is the less predictable, more difficult task.

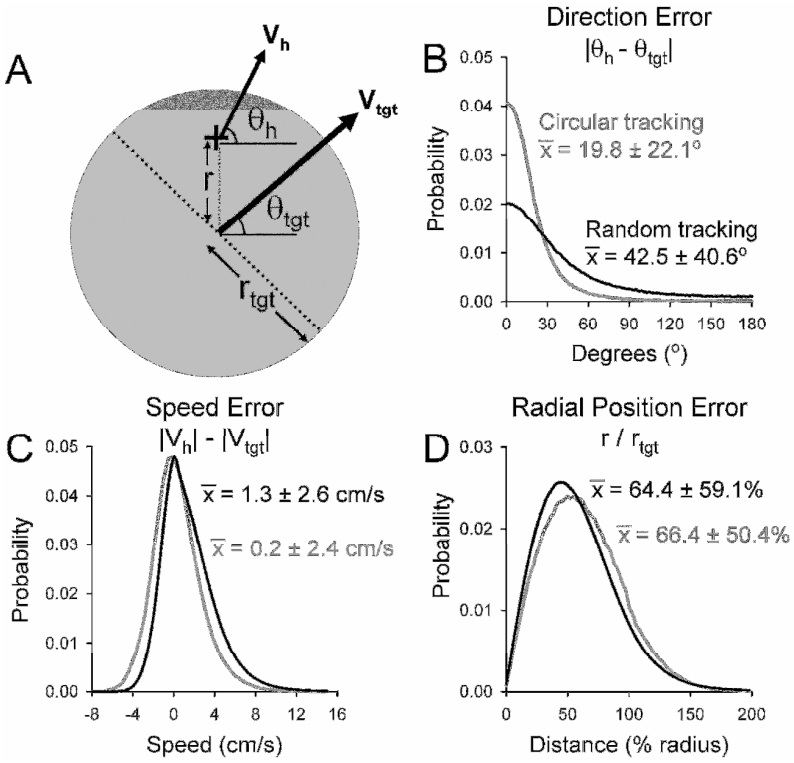

Figure 5: *Kinematic errors*. A) Diagram of the instantaneous hand (h) and target (tgt) kinematics used to calculate the kinematic errors. Grey circle is the target; cursor position is denoted by the "+". B-D) The probability distribution functions of the errors were determined from all successfully completed random (black) and circular (grey) tracking trials (from both animals and all recording sessions). Distributions of the probability of the direction, speed, and radial position errors are plotted. For each plot, the mean ± SD of the error is shown.

To examine hand and target relationships across longer time intervals, the cross-correlation between hand and target position or velocity profiles was evaluated for individual random and circular tracking trials (insets Figure 6). As described in the Methods, the profiles were shifted across multiple τ values (-500 to 500 ms in 20 ms increments) to determine the time lead or lag that results in the maximum correlation coefficient. Hand and target paths are highly correlated in both tracking tasks (mean random $\rho_{Px} = 0.96 \pm 0.13$, $\rho_{Py} = 0.96 \pm 0.12$; mean circular $\rho_{Px} = 0.98 \pm 0.11$, $\rho_{Py} = 0.97 \pm 0.13$). For both random and circular tracking, hand and target position are similar across the entire length of the trial (Figures 6A and 6C). The mean τ values tend towards zero (mean random $\tau_x = -14.9 \pm 71.2$ ms, $\tau_y = -14.1 \pm 68.4$ ms; mean circular $\tau_x = -5.4 \pm 63.8$ ms, $\tau_y = -8.9 \pm 76.8$ ms), although the hand lags the target more in random than in circular tracking (τ_x $X^2(24, N = 26{,}810) = 636.90$, $p < 0.0001$, τ_y X^2 $(20, N = 26{,}786) = 1308.55$, $p < 0.0001$). This is expected, as the task constraints require hand position to closely match target position for successful trials. Hand and target velocity profiles, however, are less closely coupled, especially for the random tracking task (mean random $\rho_{Vx} = 0.65 \pm 0.14$, $\rho_{Vy} = 0.69 \pm 0.14$; mean circular $\rho_{Vx} = 0.87 \pm 0.12$, $\rho_{Vy} = 0.88 \pm 0.13$). The insets in Figures 6B and 6D illustrate the "intermittent" nature and rapid changes that occur in hand velocities (Roitman et al., 2009). Random tracking velocity τ values (Figure 6B) are highly skewed negatively (mean $\tau_{Vx} = -94.9 \pm 112.4$ ms, $\tau_{Vy} = -115.6 \pm 117.4$ ms), indicating that the hand often lags the target considerably during changes in velocity. In contrast, circular tracking velocity τ values are only slightly skewed towards negative values (mean $\tau_{Vx} = -21.1 \pm 74.6$ ms, $\tau_{Vy} = -26.8 \pm 87.5$ ms), and for a large fraction of the trials (57.1%) the τ value is zero. These cross-correlation results further confirm that the random target movements are more difficult to predict, causing more tracking errors to be made during random tracking than circular tracking (τ_{Vx} $X^2(24, N = 26{,}828) = 6284.23$, $p < 0.0001$, τ_{Vy} $X^2(24, N = 26{,}785) = 6346.87$, $p < 0.0001$).

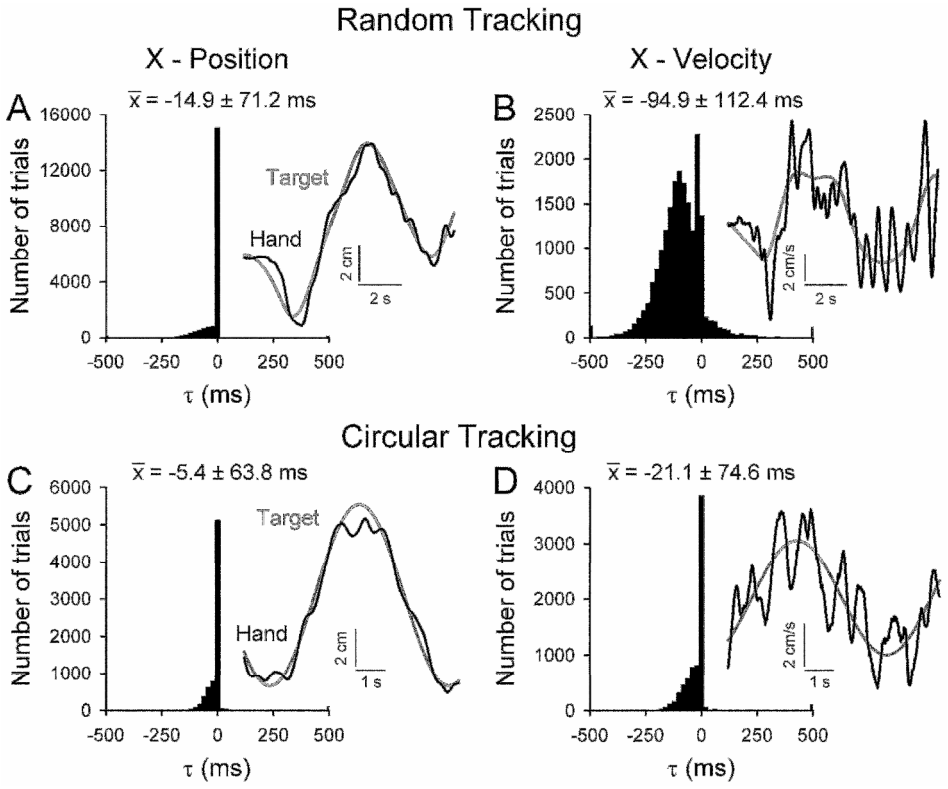

Figure 6: *Timing between hand and target kinematics.* Hand kinematic data were compared with target kinematic data across individual trials using cross-correlation analyses to determine the kinematic τ values that describe the time of maximal correlation between the hand and target movements. A-B) Histograms of τ values for the X-position and X-velocity trajectories during random tracking. Insets show example hand (black) and target (grey) trajectories from one trial. C-D) Similar τ value histograms and insets for the X-position and X-velocity trajectories during circular tracking. Similar results were obtained for position and velocity measures in the Y direction in both tasks (not shown). The histograms represent all successfully completed random and circular tracking trials from both animals and all recording sessions. For each histogram, the mean ± SD of the τ values is shown.

We also evaluated whether there was any evidence for learning or improvement in motor performance during random tracking. The direction and speed errors (Figure 7) were averaged for each recording session, plotted chronologically, and fit to a linear regression to evaluate performance. The mean errors remain fairly constant across days, and nearly all mean error coefficient confidence intervals contain zero for both monkeys (i.e., the slopes are not different from zero). The one exception is that the mean direction error coefficient ($\beta_{direction}$) for monkey N is 0.054 ($R^2 = 0.09$, $F(1,63) = 5.87$, $p = 0.018$), indicating that performance minimally worsened over the course of the recording period.

In comparison, the direction error slope coefficient in monkey I is not significantly different from zero ($R^2 = 0.02$, $F(1,54) = 0.96$, $p = 0.332$). Overall, there is no evidence that the animals improved their performance or learned the target trajectories over time.

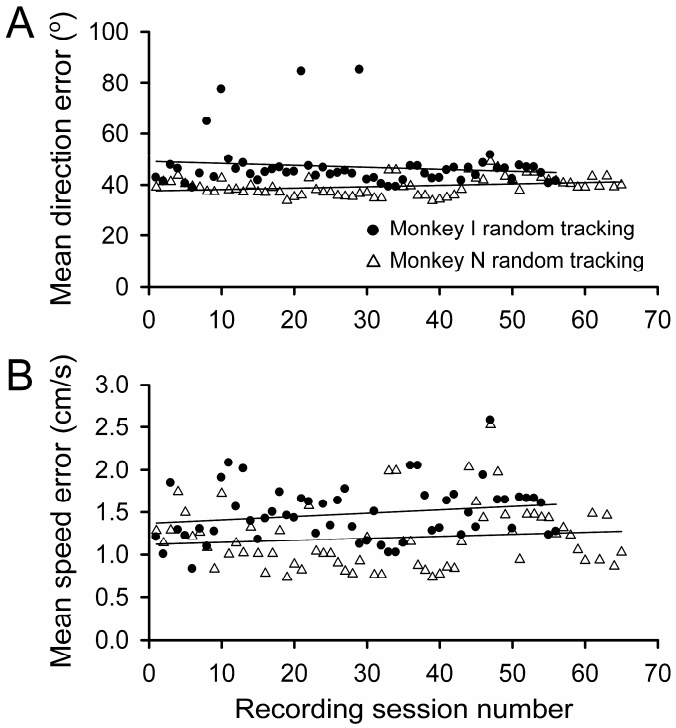

Figure 7: *Movement performance and learning over time*. Direction and speed errors were plotted chronologically by recording session and fit to a linear regression (thin lines) for each monkey during random tracking. A) Mean direction errors for Monkey I (circle) show no significant trend (i.e., confidence intervals for the linear regression slope coefficients contain zero). Monkey N (triangle) slightly increases in direction error over time, that is performance worsens (slope $\beta_{direction}$ coefficient = 0.054, $R^2 = 0.09$, $F(1, 63) = 5.87$, $p = 0.018$). B) Similar plots for mean speed errors show no significant changes with time for either monkey.

Comparison of regression models

The PV model resulted in a higher mean R^2_{adj} than the PŪS model (PV R^2_{adj}=0.33 ± 0.19, PŪS R^2_{adj}= 0.30 ± 0.16, $t(119) = 4.17$, $p < 0.0001$), suggesting that decomposing velocity into direction (i.e. unitary velocity) and speed does not provide as good a description of the simple spike modulation. However, the PV model could not sufficiently describe approximately 10% of Purkinje cells in which the simple spike activity was predominantly modulated by speed (see below and Figure 10). In random tracking

movements, velocity and speed are independent regressors and can be used together in the same linear regression model (see Figure 8). The PVS model had the greatest mean R^2_{adj} (0.35 ± 0.19) and captured speed related modulation. It was therefore judged the best of the three models in describing the simple spike discharge.

Simple spike firing was recorded from 120 Purkinje cells during the random tracking task and additionally from either circular tracking or center-out reach. Qualitative examination (see Figures 9 and 10) of the average simple spike firing binned as described in the Methods revealed modulation with position (**P**), velocity (**V**), and speed (S). Correlation analyses of the hand kinematics across all sessions confirmed these three parameters were not highly correlated. For the PVS model in which a single global τ was used for all kinematic terms, one only needs to assess the correlation at a lead/lag of 0 ms, because all kinematic terms are shifted together in determining the optimal τ. The highest correlation among these variables was between X_h and Y_h ($\rho = 0.08$, Figure 8A), allowing these terms to be incorporated into a multiple linear regression model describing simple spike firing of individual Purkinje cells.

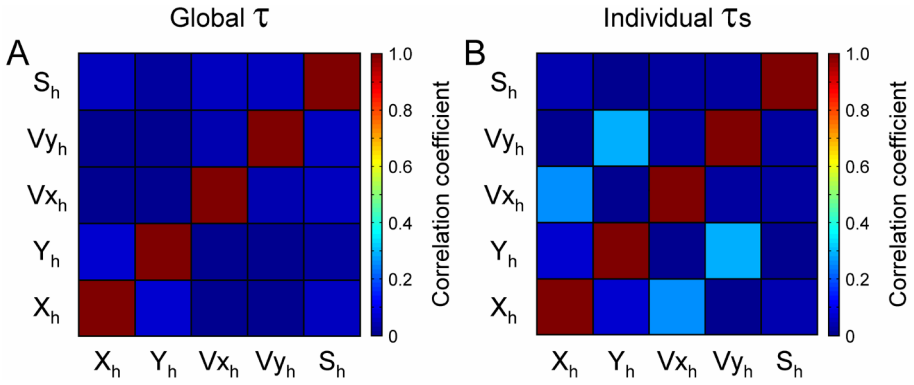

Figure 8: *Relative independence of regression model parameters*. The matrix plots show the average cross correlation coefficient for each of the five kinematic parameters used in the PVS model, based on the hand kinematics across all recording sessions. A) The average correlations among the kinematic parameters at a 0 ms lead/lag were obtained from the PVS regression model and correspond to the single global τ. B) The average correlations among the kinematic parameters were also evaluated at the individual optimal τ values.

PVS regression model

An example Purkinje cell is shown in Figure 9, in which the simple spike firing is simultaneously tuned to both position and velocity. For each position or velocity bin (see Methods), simple spike firing is averaged to obtain a visual representation of position (Figure 9A) and velocity (Figure 9B) encoding. Position modulation is shown by the increases in simple spike firing when the hand moves in the upper left quadrant (negative X and positive Y coordinates) of the workspace, and decreases in the lower right quadrant (Figure 9A). Velocity modulation is evident by the increases in firing for positive Vx_h and Vy_h, with relative decreases for negative Vx_h and Vy_h (Figure 9B). Plots of simple spike firing across positions at different speed levels show almost no modulation with speed (Figure 9C). The time lead or lag between simple spike firing and hand kinematics is calculated using the PVS model (eqn. 1) and regressing across multiple τ values. In this cell, a τ value of -200 ms yields the maximal R^2_{adj} value of 0.63 (Figure 9D), suggesting that simple spike firing leads hand kinematics. In agreement with the visual representations, semi-partial R^2 values (Figure 9E) indicate that the position (55% of R^2_{adj}) and velocity (44% of R^2_{adj}) terms account for nearly all this cell's firing variability, with very little contribution from the speed term (<1% of R^2_{adj}).

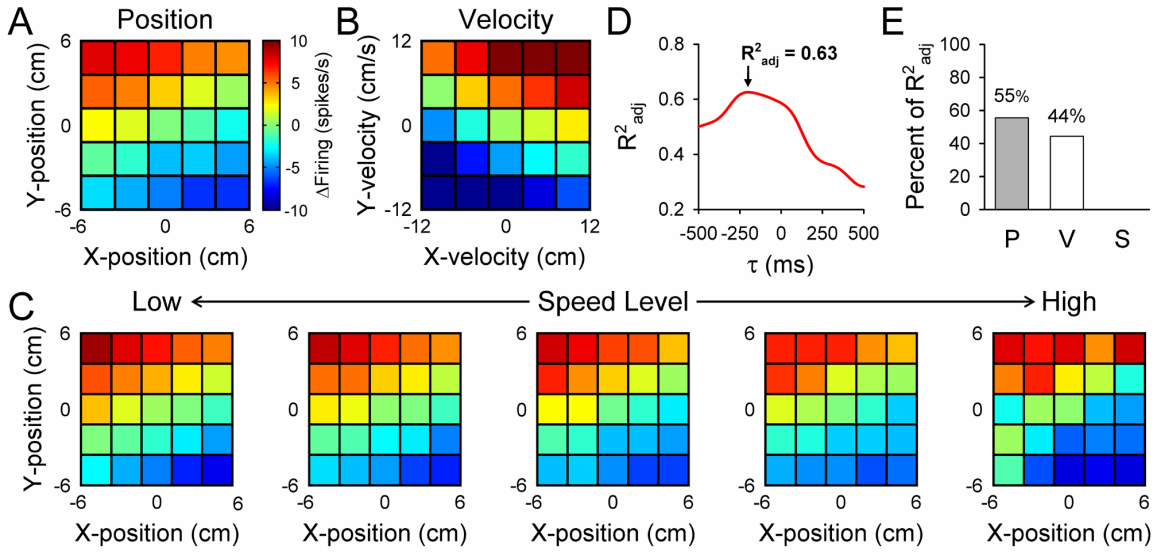

Figure 9: *Example position and velocity Purkinje cell.* Hand kinematics and simple spike firing data were binned and averaged across A) position and B) velocity to create plots of the cell firing. The color code illustrates the deviation from the mean firing, in which dark red represents increased firing and blue decreased firing. Simple spike firing increases when hand position is in the upper left quadrant of the workspace (A) and with higher velocities in both the X and Y directions (B). C) Plots of averaged firing across position at different speed levels (0 – 12 cm/s, binned in increments of 2.4 cm/s) show almost no variance in firing with speed. D) The R^2_{adj} values are plotted versus the time leads or lags (τ values). In this cell, a τ value of -200 ms yields a maximal R^2_{adj} value of 0.63. E) Semi-partial R^2 values indicate that the position (55% of R^2_{adj}) and velocity (44% of R^2_{adj}) terms account for most of this cell's firing variability, with almost no contribution from the speed term.

In several Purkinje cells (11/120), the speed term described greater than 40% of the explained firing variability. Figure 10 shows an example "speed cell". Modulation with hand position is weak (Figure 10A), while the velocity plot (Figure 10B) exhibits a semi-ring pattern of maximal firing along the outer borders that represent the greatest speeds. This demonstrates the presence of speed modulation that cannot be reduced to a linear combination of the velocity terms. Plots of averaged firing across position (Figure 10C) verify that movement speed highly influences the firing rates. The optimal τ value of -180 ms (Figure 10D) suggests that the discharge leads hand kinematics. Semi-partial R^2 values (Figure 10E) verify that this cell is highly speed modulated (61% of R^2_{adj}), with velocity (32% of R^2_{adj}) also describing some of the firing variability. Position (8% of R^2_{adj}) contributes little to changes in simple spike firing.

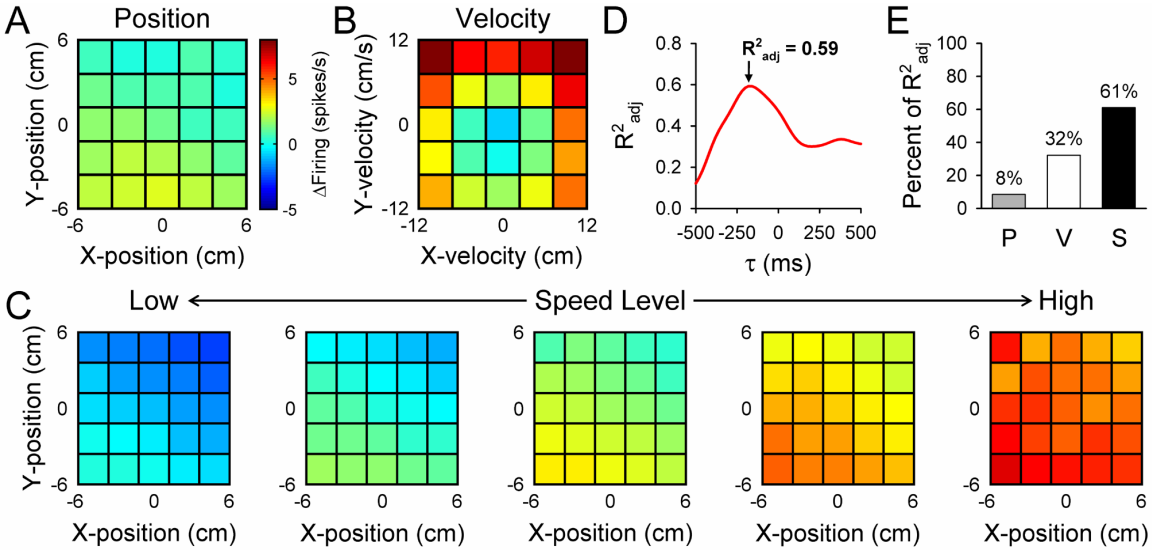

Figure 10: *Example speed cell*. A and B) This cell displays minimal positional preference, while the velocity plot exhibits a ring-like pattern of increased firing rates, suggesting that the simple spike firing is speed modulated. C) Plots of averaged firing across position at different speed levels confirm that firing increases with speed irrespective of movement direction. D) A maximal R^2_{adj} of 0.59 results when τ equals -180 ms. E) Semi-partial R^2 values corroborate that the simple spike firing is highly speed (61% of R^2_{adj}) modulated, while the velocity (32% of R^2_{adj}) term also describes some of the firing variability. Layout and conventions are as in Figure 9.

A wide range of sensitivities to PVS model parameters were observed across the population of Purkinje cells. Optimal τ values (Figure 11A) are skewed towards negative numbers (mean= -35.1 ± 192.8 ms) and confirm that the firing of most cells (72/120) leads hand kinematics. However, 38% (45/120) of the cells have a positive τ value suggesting that simple spike firing also encodes feedback about hand movements. Remaining cells (3/120) lie within the τ= 0 ms bin that neither leads nor lags hand kinematics. The mean R^2_{adj} value shows that the parameters in the PVS model account for approximately 35% of the simple spike firing variability (Figure 11B). Mean semi-partial R^2 values (Figure 11C) indicate that, on average, velocity (63 ± 30% of R^2_{adj}) describes more of the firing variability than position (28 ± 24% of R^2_{adj}) or speed (11 ± 19% of R^2_{adj}). Importantly, τ values were not highly correlated with the model R^2_{adj} (ρ = -0.034), demonstrating that the firing leads and lags obtained from the PVS model explained similar amounts of variability. Similarly, τ values were not highly correlated with the semi-partials (ρ_P= -0.052; ρ_V = 0.066; ρ_S = -0.020) indicating that the tau values

are not biased by a single parameter (e.g. cells with strong velocity signals do not have more negative tau values.)

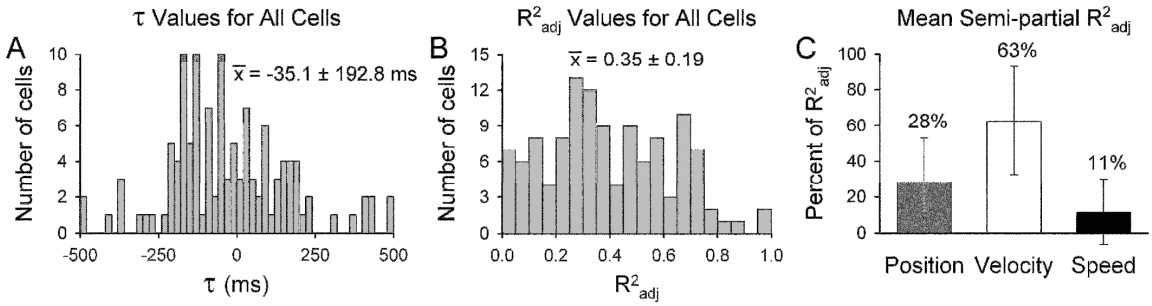

Figure 11: *Population summary of firing data from all 120 cells recorded during random tracking*. A) Distributions of the optimal firing τ values and B) R^2_{adj} values resulting from the PVS linear regression model with averaged kinematic data. C) Bar plots and SD of the mean semi-partial R^2 values for all cells.

Averaged vs. non-averaged regression models

To evaluate whether the same kinematic parameters are reliably encoded in single trial observations, the instantaneous single trial (non-averaged) simple spike firing data for each cell were fit to the same PVS regression model (eqn. 1) across multiple τ values (see Methods). Results from an example Purkinje cell show that R^2_{adj} as a function of the τ has similar profiles for the averaged and non-averaged data (Figure 12A). As expected, maximal R^2_{adj} values are smaller when non-averaged, single trial data are used, but the R^2_{adj} values scale down similarly across all cells (Figure 12B, $\rho = 0.84$, slope = 2.54). Across the population of Purkinje cells, comparisons of regression model coefficients (Figures 12D-F) illustrate that the speed (b_S, $\rho = 0.78$, slope = 0.64), position (b_P, x: $\rho =$ 0.96, slope = 0.98 y: $\rho = 0.98$, slope = 1.02) and velocity (b_V, x: $\rho = 0.95$, slope = 0.93 y: $\rho = 0.95$, slope = 1.00) terms are highly correlated with slopes near 1, confirming that regression models based on non-averaged data capture the same relationships as the models based on averaged data. The optimal τ values are also consistent between averaged vs. non-averaged data (Figure 12C, $\rho = 0.52$, slope = 0.75), but the strength of the correlation is less than for the coefficients, suggesting that averaging can influence the timing relationships.

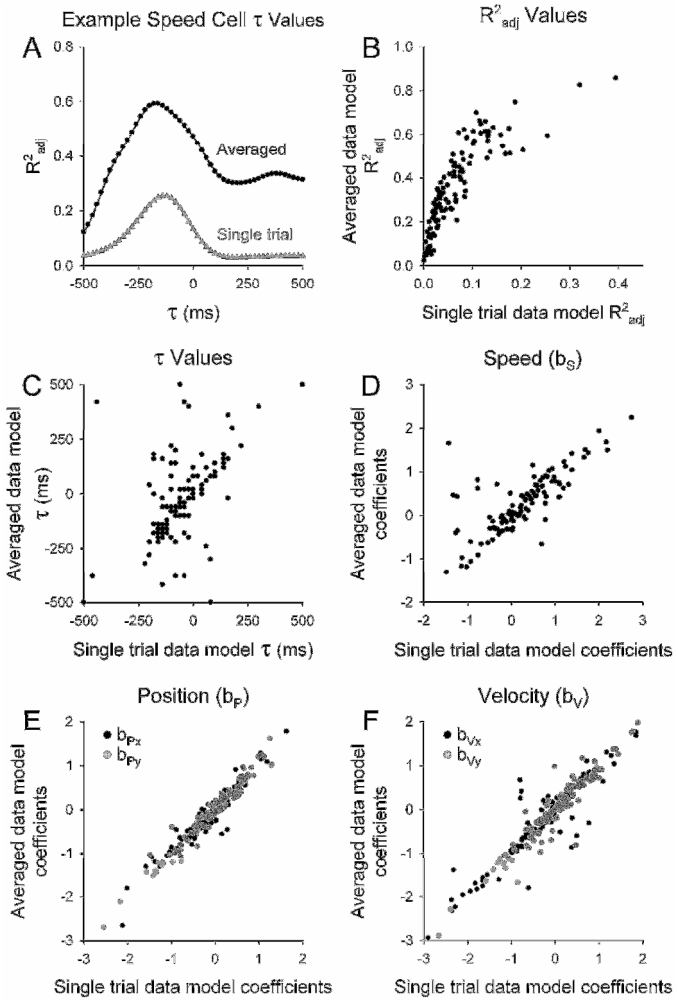

Figure 12: *Averaged versus non-averaged firing models*. A) The R^2_{adj} values arising from different τ values of the PVS regression model are plotted for the example speed cell (Figure 10) using averaged data (black) or non-averaged single trial data (grey). B) Maximal R^2_{adj} values resulting from the averaged data regression model (y-axis) are plotted vs. the non-averaged data regression model (x-axis) for each cell. C) Similar plots show optimal τ values are consistent between averaged vs. single trial data. Plots of the averaged vs. non-averaged regression model coefficients for the speed- b_S (D), position- b_P (E), and velocity- b_V (F) terms also demonstrate tight linear relationships.

Curvature

Prior studies in the motor cortex suggest that firing leads or lags change with the curvature of the hand movement (Schwartz and Moran, 1999), leading us to investigate the influence of trajectory curvature on the optimal tau value. As described in the

Methods, both curvature (-9.9 to 9.9 cm^{-1}) and absolute curvature (0 to to 9.9 cm^{-1}) were calculated for the hand trajectory and divided into ten bins. The data from each bin were fit to the PVS model and the optimal τ was identified for each bin. An ANOVA showed no significant difference across the mean τ for each bin regardless of whether curvature ($F(9,1190) = 0.32$, $p = 0.970$) or absolute curvature ($F(4,595)= 0.49$, $p= 0.745$) was used for the comparison. Therefore, as opposed to the properties of neurons in the motor cortex, the lead or lag of the simple spike firing does not appear to be related to the curvature.

Prediction of simple spike firing in different tasks

For each Purkinje cell, the τ value and regression coefficients calculated from random tracking data were used to estimate the simple spike firing rates for the kinematics recorded during circular tracking or center-out reach. Importantly, we elected to use regression coefficients obtained from the non-averaged data, although the coefficients were mostly equivalent between the two models (Figure 12). Estimates of firing during counter-clockwise (CCW) and clockwise (CW) circular tracking for an example cell are shown in Figure 13. Although the averaged hand paths are similar for both tracking directions (left panels, Figure 13A, B), there is a large shift (~90^0) in the position of maximal firing (right panels, Figure 13A, B) indicating that this neuron encodes both position and direction information (Roitman et al., 2005). Regression coefficients from the PVS linear regression model for random tracking (eqn. 1) provide an accurate estimate of the simple spike firing for both directions of movement (right panels, Figure 13A, B; $\rho_{CCW} = 0.80$, $\rho_{CW} = 0.78$). Correlation coefficients from all 32 circular tracking cells in both tracking directions (mean = 0.49 ± 0.36, Figure 13C) indicate most cells encode hand kinematics invariantly for both random and circular tracking.

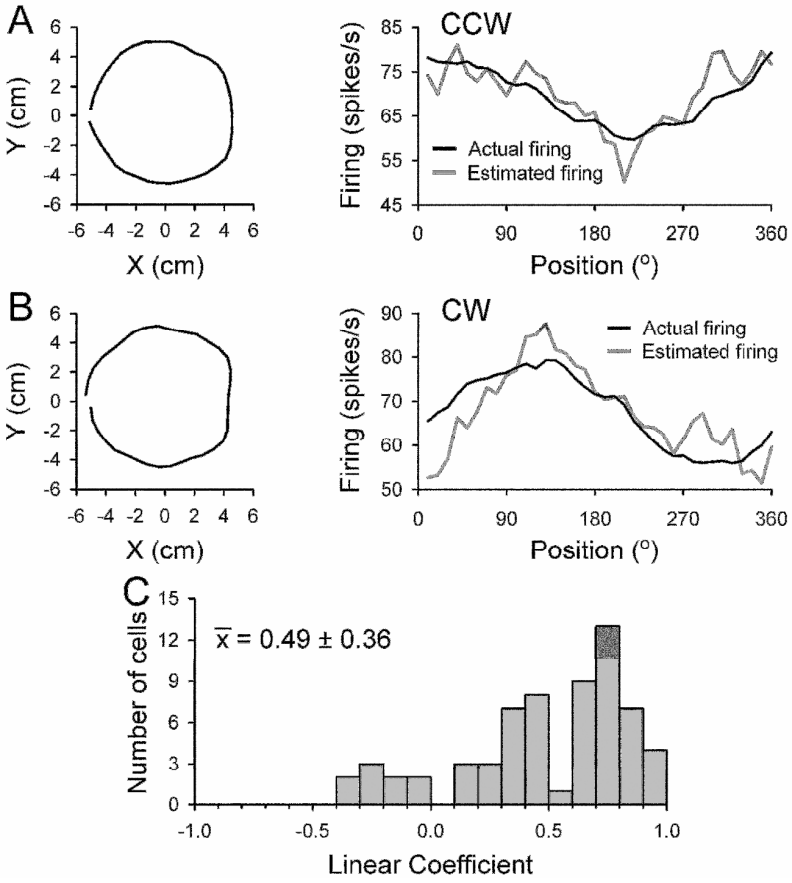

Figure 13: *Estimation of circular tracking firing based on the model using random tracking data.* Left panels show average hand position (X_h, Y_h) traces for 360° of A) counter-clockwise (CCW) or B) clockwise (CW) circular tracking recorded from an example Purkinje cell. Right panels depict the binned and averaged actual recorded simple spike firing rates (black traces) against the estimated firing activity (grey traces). Firing was estimated by applying the τ value and PVS linear regression model coefficients (non-averaged model) computed from the random tracking data to the circular tracking hand kinematics. C) Distribution of the correlation coefficients from the 32 Purkinje cells. The correlation coefficients are plotted for each direction of tracking, resulting in twice the number of coefficients than cells.

Similar accuracy was achieved for estimation of firing during center-out reach, despite vastly different movement strategies and kinematics. Typical center-out reach movements are fast, ballistic, relatively straight trajectories (Figure 14A, center plot) during which the early part of the reach uses feedforward control (Beaubaton et al., 1978;Ojakangas and Ebner, 1991;Keele and Posner, 1968). In contrast, tracking tasks continually utilize error feedback to make numerous, small corrective movements. In the example cell shown, the PVS model coefficients and τ value calculated from the random

tracking data successfully estimate the actual firing for all eight directions of center-out reach (Figure 14A, outer plots). The estimates accurately capture the temporal profile for the 6 reach directions between 180 and 45^0. The average correlation coefficient is 0.88 for all 8 directions. The mean correlation coefficient for the 58 Purkinje cells studied in the center-out task is $\rho = 0.44 \pm 0.21$ (Figure 14B), indicating that many cells encode hand kinematics invariantly for both random tracking and center-out reach. Therefore, the regression model coefficients attained from non-averaged random tracking data can faithfully predict the simple spike firing in other movements for a majority of Purkinje cells.

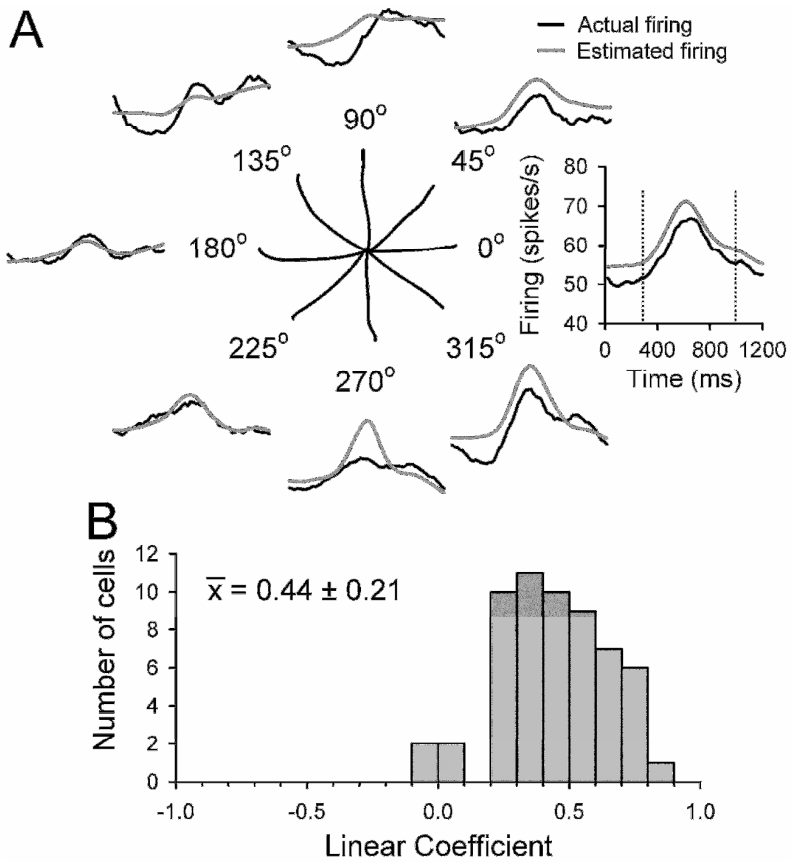

Figure 14: *Estimation of center-out reach firing based on the model using random tracking data*. A) Center plot depicts averaged hand position (X_h, Y_h) traces for the eight directions of center-out reach. The binned and averaged actual recorded firing data (black trace) from an example Purkinje cell are plotted against the estimated firing rate (grey trace) for each direction of reaching. Firing was estimated by applying the τ value and PVS linear regression model coefficients (non-averaged model) computed from the random tracking data to the center-out reach hand kinematics. B) Distributions of the averaged correlation coefficients from all 58 cells.

Global vs. individual τ values

To investigate the influence of individual model parameters on the timing relationship between simple spike firing and hand kinematics, the firing was fit to the five parameters of the PVS model individually (see Methods). Figure 15 shows the R^2_{adj} temporal profiles for each term of the PVS model (A-E, left and middle columns), a single global τ (black traces in F), and the summed individual temporal profiles (grey traces in F) for the two example cells described previously (Figures 9 and 10). For both cells, the temporal profiles and best individual τ values vary greatly between parameters (Figure 15 A-E) and do not necessarily align with the global τ values (Figure 15 F), suggesting that each parameter may be encoded at independent lead/lags. However, note that the global τ is often very close to the individual τ of the parameter with the highest semi-partial R^2_{adj} value (indicated by '*'), and the summed individual profiles (Figure 15 A-E) provide an excellent approximation of the temporal profile for the global τ model (grey traces in Figure 15 F). Similarity between the global τ profile and summation of the individual parameter profiles was quantified by the Root Mean Square Deviation and confirmed that the individual kinematic representations are highly additive for the example cells (position/ velocity cell: RMSD = 0.043; speed cell: RMSD = 0.017).

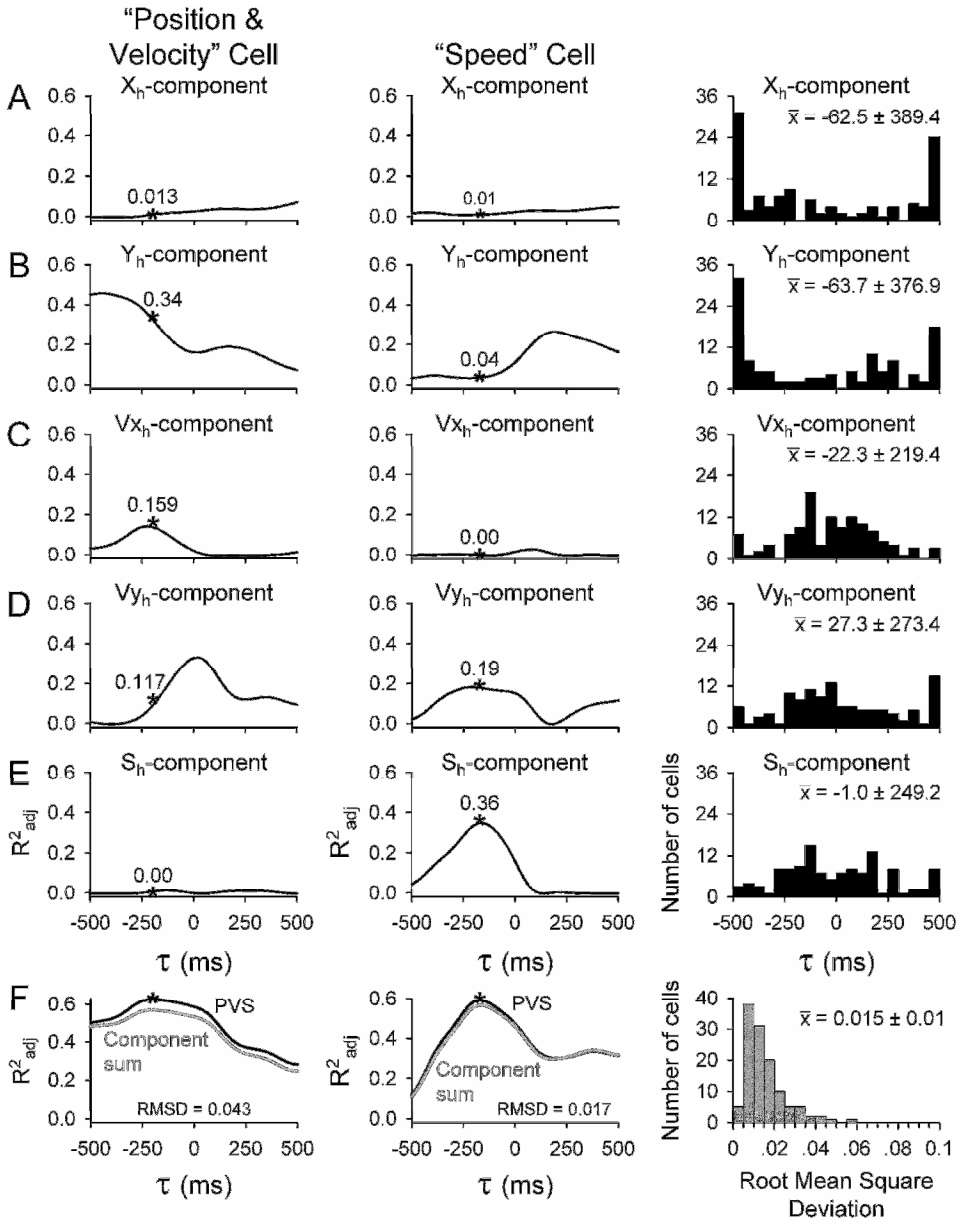

Figure 15: *Optimal τ values for individual PVS model parameters.* A-E) Plots of R^2_{adj} vs. τ arising from X_h, Y_h, Vx_h, Vy_h, and S_h are provided for the two example position/velocity and speed cells (left and middle columns) shown previously in Figures 9 and 10, along with the individual τ value distributions for all 120 cells (right column). The '*' indicates the semi-partial contribution of each variable at the time of the optimal global τ. F) The left and middle columns show the R^2_{adj} vs. τ for the example cells from both a single global τ model (black traces) and summation of the individual parameter profiles (grey traces). The similarity between these two traces was quantified by the RMSD. The distribution of RMSD values for all 120 cells is shown in the right column.

The additive property of the individual profiles is conserved at the population level, as demonstrated by the distribution of RMSD values (Figure 15 F, right column). The mean RMSD for the cell population was 0.015 ± 0.01, supporting the assumption that the kinematic parameters are effectively independent. Furthermore, the distributions of individual parameter optimal τ values (Figure 15 A-E, right column) suggest that the velocity and speed components were comparable to those obtained for the global τ model. That is, there is a mixture of cells with simple spike firing leading and lagging the hand kinematics. Positional lead/lag distributions differ from the velocity and speed distributions, exhibiting clustering at the ± 500 ms limits.

It was necessary to assess whether using individual τ values introduced unacceptable correlations among the regressors. Therefore, the correlations among the hand kinematics were reevaluated using the times of the individual τ values (Figure 8B). The average correlations remained low, with the greatest correlations between Y_h and Vy_h ($\rho = 0.30$) and X_h and Vx_h ($\rho = 0.27$). These values are still consistent with the assumption of independence required by multi-linear regression modeling (Freund and Littel, 2000;Belsley et al., 1980).

This allowed us to evaluate a modified version of the PVS model (eqn. 1) in which the individually calculated τ values replaced the global τ parameter. This modified model assesses how the individual leads/lags alter the contributions of the different parameters. The overall R^2_{adj} values were highly correlated between the two models ($\rho = 0.97$) and the mean R^2_{adj} were nearly identical (global τ: $R^2_{adj} = 0.35 \pm 0.19$, individual τ: $R^2_{adj} = 0.34 \pm 0.19$), further confirming that the contributions of the individual kinematic terms are relatively independent and can sum linearly. Regression model coefficients for the five model parameters remained highly correlated between both models for the position (b_P, x: $\rho = 0.91$, slope = 1.40, y: $\rho = 0.95$, slope = 1.27), velocity (b_V, x: $\rho = 0.98$, slope = 1.06, y: $\rho = 0.97$, slope = 1.20), and speed (b_S, $\rho = 0.94$, slope = 1.13) terms. Further analyses revealed that the individual τ model coefficients were more broadly distributed compared to the global τ model coefficients (i.e., the individual beta coefficients for all 5

parameters no longer peaked around zero and positive model coefficients generally increased in magnitude while negative coefficients decreased), which accounts for the positive slopes when comparing coefficients. Therefore, incorporating the individual τ values captures more of the firing variability, especially in the position and speed terms that need not peak at the global τ value. The mean semi-partial R^2s also validate this, as position increased from 28 ± 24% to 38 ± 26% of R^2_{adj} when the individual τ values were used in the model. The average semi-partial R^2 for speed also increased from 11 ± 19% to 16 ± 19%, while the velocity contribution decreased from 63 ±30% to 44 ± 25%.

Discussion

Random tracking provides a useful paradigm for assessing the motor signals present in the discharge of neurons (Paninski et al., 2004a;Paninski et al., 2004b). As shown, random tracking provides greater coverage of the position, direction, speed, and velocity kinematic workspaces compared to the center-out reach or circular tracking paradigms previously used to characterize the signals in Purkinje cell simple spike discharge (Coltz et al., 1999a;Roitman et al., 2005;Fortier et al., 1989;Marple-Horvat and Stein, 1987;Fu et al., 1997a). Random tracking results in extensive combinations of position, direction, and speed, delivering a robust data set to assess the encoding of kinematic signals. Most importantly, these parameters are minimally correlated during the random tracking movements (see Figure 8), allowing for use of linear regression models without the problems of correlated predictors (Zar, 1999;Belsley et al., 1980;Freund and Littel, 2000).

As expected, random target movements are difficult to predict. Errors in hand movement speeds and directions relative to the target are significantly greater in random tracking than in circular tracking. Comparisons of random tracking kinematic profiles across time show that hand velocity lags target velocity by ~95 ms—a significantly greater lag than with circular tracking (~21 ms). These analyses confirm that the random tracking task is a feedback-dependent, highly unpredictable task.

In random tracking, the monkeys appear to use a strategy of controlling position. This is expected, as the task requires maintaining the cursor within the moving target. Hand and target position are highly correlated and, in a large fraction of the trials, hand position had a zero time lag with target position. Similar results were obtained for circular tracking. Both findings suggest position is highly controlled in these two tracking tasks.

Encoding of kinematics

Analyses of the simple spike firing focused on finding kinematic parameters that are relatively independent. This approach allows for unambiguous statements about the relationships between firing and the specific kinematic variables of position, velocity, and speed. It also differs from our previous studies that allowed interaction terms and did not rigorously assess the degree of correlations between model parameters (Coltz et al., 1999a;Roitman et al., 2005;Fu et al., 1997a). Similar to previous findings, the velocity term explains the greatest amount of the firing variability, with position also contributing considerably (Roitman et al., 2005;Mano and Yamamoto, 1980;Marple-Horvat and Stein, 1987). Psychophysical studies show that humans and monkeys use a combination of velocity and position information to intercept and track targets (Engel and Soechting, 2000;Roitman et al., 2004). These results provide further support that position and velocity are key control parameters during visually-guided tracking tasks.

Global vs. individual τ values

For many Purkinje cells, the global τ analysis found that simple spike firing led hand movements (Figure 11A). This finding is consistent with other electrophysiology studies that have found Purkinje cell simple spike firing mostly leads hand kinematics during manual tracking (Coltz et al., 1999a;Roitman et al., 2005) or center-out reaching (Marple-Horvat and Stein, 1987;Fu et al., 1997a) and supports the concept that Purkinje cells encode feedforward or predictive signals (Wolpert et al., 1998;Bastian, 2006;Ebner and Pasalar, 2008). Unlike prior tasks, monkeys performing random tracking had no knowledge of the upcoming movements. The present results demonstrate that the firing leads are not a function of task predictability and that the simple spike firing from a

majority of Purkinje cells provides feedforward kinematic signals irrespective of the task demands.

We also determined the optimal individual τ values for each PVS model parameter by computing individual regressions for each of the five parameters. The sum of the R^2_{adj} profiles from the individual regressions closely matched the profile obtained using a single global τ, verifying the validity of the model and the independence among the regression parameters. Estimates of the individual leads/lags for the velocity and speed terms demonstrate a mixture of feedforward and feedback signals, similar to the global τ. Distributions of the τ values for the position parameters differ from velocity and speed, with clusters at the limits of the ± 500 ms time window. Position signals vary slowly compared to velocity (Figure 4), limiting the temporal resolution at which changes can be reliably detected. It is yet unclear whether this property has physiological relevance, reflecting longer time relationships between the position signals and their neural representations.

Using the individually determined τ values in the PVS model alters the weighting and variability explained by the individual terms, so that across the cell population, the model is less influenced by the dominant term. Using a global τ tends to exaggerate the contribution of the parameter that has its peak at or near that τ value. The individual τ model increased both the position and speed semi-partial R^2s, suggesting that use of a global τ overemphasizes the velocity contribution. Improved analytical techniques as well as experimental paradigms are needed to further dissect out the timing of the individual parameters.

Like prior studies (Marple-Horvat and Stein, 1987;Fu et al., 1997a;Roitman et al., 2005), the distribution of τ values is wide and includes cells in which firing lags hand kinematics. These findings are consistent with processing sensory feedback. It should not be surprising that Purkinje cells may dually encode both feedforward and feedback signals, as visually-guided tasks, like tracking, rely heavily upon performance feedback.

Imaging studies reveal cerebellar activation is related to feedback signals such as motor errors (Miall and Jenkinson, 2005;Diedrichsen et al., 2005;Grafton et al., 2008;Flament et al., 1996). The cerebellum could potentially support both feedforward and feedback control due to numerous bi-directional connections with the motor cortex (Kelly and Strick, 2003;Ito, 1984) and extensive sensory inputs (Bloedel and Courville, 1981). Factors influencing the timing relationships of the signals are unknown. The task itself appears to have little effect, as the range of τ values are similar between single joint wrist flexion/extension (Mano and Yamamoto, 1980), center-out reach (Marple-Horvat and Stein, 1987;Fu et al., 1997a), manual tracking (Roitman et al., 2005), and reach-to-grasp (Dugas and Smith, 1992). Possibly, the resultant leads or lags reflect hard-wired circuitry. For example, cells with greater lead times tended to be recorded from more lateral locations in the cerebellar cortex during limb movements (Gray et al., 1993;Marple-Horvat and Stein, 1987). However, the information on timing is too limited to make strong inferences.

Generalization of the signals to other tasks

For many Purkinje cells, the kinematic signals extracted from the simple spike firing in random tracking were able to estimate firing rates in either circular tracking or center-out reach. It is worth re-emphasizing that this estimate was based on the PVS model using non-averaged firing and kinematics data. Even model fits with positive τ values (suggesting that the cell processed sensory feedback) were still able to provide good estimates of cell firing for the other tasks. These results further support conclusions that most Purkinje cells provide a parametric representation of movement kinematics in which simple spike activity reflects kinematic parameters irrespective of the movement or task.

For a limited number of Purkinje cells, the results show that model coefficients are not effective in estimating the simple spike discharge in other tasks. For a few cells, the prediction even resulted in a negative correlation. Good fits between the estimated and actual firing do not correlate with model R^2_{adj} or τ values, and low R^2_{adj} values cannot

account for all of the poor predictions. Therefore, some Purkinje cells may change their signaling with different tasks.

Averaged vs. non-averaged data

Overall, the total R^2_{adj} explained by the PVS model is somewhat less than in previous reports. Three major differences contribute to the lower R^2 values. First, as noted above, the PVS model is limited to parameters that are minimally correlated, which was not the case for our two previous manual tracking studies (Coltz et al., 1999a;Roitman et al., 2005). Also, whereas the PVS model is restricted to linear fits, previous models were based on regression analyses that included a number of interactive and non-linear terms (Coltz et al., 1999a;Roitman et al., 2005). In one study, the interaction terms resulted in a complex model with nine predictors (Roitman et al., 2005), whereas only five predictors are used in this PVS model. Second, random tracking covers larger parts of the kinematic workspace compared to other tasks, greatly increasing the variability in the data. The firing model was fit to the entire kinematic data set as opposed to specific segments of the data, as used in some studies (Shidara et al., 1993;Gomi et al., 1998;Medina and Lisberger, 2009).

The third, and potentially most important difference, is the extent of averaging used. It is well established that averaging artificially reduces the inherent variability of the data set (Zar, 1999;Kenny, 1979), so that the model error cannot accommodate expected levels of noise. As a result, linear regression models may be biased and have poor predictive performance (Freund, 1971). Therefore, any conclusions about the nature of the signals encoded in the firing cannot be assured to generalize to other movements or tasks. Averaging may also alter the timing relationships between firing and kinematics, and limit understanding of the signals at the level of single trials. In the present study, the regression analysis based on averaged data divided the position, velocity, and speed workspaces into 3125 (5^5) bins as compared to 32 bins in Coltz, et al. 1999 and 360 bins in Roitman, et al. 2005. A small number of bins was also used in previous center-out reach studies (Fu et al., 1997a;Fortier et al., 1989). The effects of averaging can be

appreciated by using the same model parameters and only changing the bin resolution. The average R^2_{adj} of the PVS model is 0.35 when the workspace is partitioned in 5^5 bins compared with 0.31 or 0.46 when partitioned into 6^5 or 3^5 bins, respectively. Further averaging, by restricting the regression analysis to only velocity (Vx_h, Vy_h), results in a mean R^2_{adj} of 0.70. Similarly, limiting the regression variables to position parameters (X_h, Y_h) inflates the mean R^2_{adj} to 0.64. Therefore, the extent of the bin size and degree of averaging heavily influence the model R^2.

The regression analyses performed without averaging further illustrate this issue. Using the instantaneous simple spike firing and hand kinematics without binning results in smaller R^2 values (Figure 12). However, the regression coefficients and τ values obtained from the non-averaged data were highly correlated to those obtained using the averaged, binned data. No additional physiological information is gained by using averaged data for regression modeling. Instead, models based on non-averaged data provide a better understanding of the real-time signals contained in the firing of individual Purkinje cells.

The use of non-averaged firing data raises questions about the encoding of signals in the simple spike discharge of Purkinje cells. It might be argued that an R^2 value of 0.05 or 0.1 for the PVS model implies a poor fit to the data or that the instantaneous firing is inherently noisy, limiting the encoding. However, the results suggest otherwise and show that explaining even a small fraction of the firing variability is highly relevant. As demonstrated, random tracking model coefficients with modest R^2 values can adequately estimate the simple spike firing in reaching and circular tracking, even though the tasks differ substantially in their properties and workspace coverage. Therefore, the magnitude of the R^2 is not likely to be the most important indicator of model validity, as has been suggested for biological data sets (O'Grady, 1982). Conversely, the small model R^2 and conserved encoding of kinematic signals suggests that Purkinje cell simple spike discharge could encode numerous parameters. This would be consistent with the 100,000 to 200,000 parallel fiber synapses on a single Purkinje cell (Napper and Harvey, 1988) and that only 100 to 200 parallel fiber synapses are needed to generate a simple spike

(Barbour, 1993;Isope and Barbour, 2002). If, as found in this study, each signal does not need to account for a large percentage of the firing variability but only be highly conserved, a single Purkinje cell could provide a wealth of information and participate in a large number of behaviors.

Implications for the forward internal model hypothesis

Several of the findings are consistent with Purkinje cells acting as the output of a forward internal model that predicts upcoming kinematics (Wolpert et al., 1995;Kawato and Wolpert, 1998;Kawato, 1999). The first is that Purkinje cell simple spike firing is highly correlated with movement kinematics. Given the evidence that Purkinje cells do not encode kinetics or muscle activity in other manual tracking tasks (Pasalar et al., 2006;Coltz et al., 1999a;Roitman et al., 2005), the signals undoubtedly represent kinematics. Second, for the majority of Purkinje cells, simple spike firing leads the kinematics as required by a forward model. Third, the future kinematic signals are present in an unpredictable task, in which the monkey is not provided any information about the upcoming target movements; yet, Purkinje cell activity signals future hand kinematics. We argue that this is a strong test of the forward model. If the cerebellum acts as a forward internal model (Wolpert et al., 1998), it will combine the motor command with feedback about the present state of the arm and transform the output into a prediction of the movement consequences, irrespective of whether the task is dominated by feedback or feedforward characteristics. Therefore, finding kinematic signals encoded prior to the actual movements in random tracking is solid support for a forward internal model.

CHAPTER 3: PURKINJE CELL SIMPLE SPIKE DISCHARGE ADAPTS TO A MECHANICAL PERTURBATION

Introduction

Improving movement efficiency and accuracy is essential for learning complex, precision tasks like playing a musical instrument, as well as everyday simple reflexive movements. Our changing bodies and environment force us to continually adapt to new situations and circumstances. The cerebellum has been identified as a key site where motor adaptation takes place. Patients with cerebellar damage can react, but cannot adapt to perturbations that predictably alter arm or hand movements (Muller and Dichgans, 1994;Nowak et al., 2004;Smith and Shadmehr, 2005;Maschke et al., 2004). Cerebellar injury also disrupts motor learning during eye movements including saccades (Golla et al., 2008;Xu-Wilson et al., 2009) and smooth pursuit (Takagi et al., 2000). Additionally, neuroimaging shows unique cerebellum activation that is retained during adaptation to visuomotor tranformations or novel force fields (Imamizu et al., 2000;Nezafat et al., 2001;Kawato et al., 2003;Shadmehr and Holcomb, 1997).

The dominant theory of cerebellar learning proposes that plasticity occurs primarily at synaptic inputs to Purkinje cells, the sole output neurons of the cerebellar cortex (Marr, 1969;Albus, 1971;Ito, 1989;Ito, 2001). Purkinje cells receive two very distinct inputs. First, information from cortical, brainstem, and spinal nuclei is conveyed through hundreds of thousands of parallel fiber synapses onto a Purkinje cell's dendrites (Akhtar et al., 2002;Eccles et al., 1967;Bloedel and Courville, 1981). These synapses produce Na^+/K^+ action potentials called simple spikes that have a baseline firing rate of 50-150 spikes/sec. Second, climbing fibers arise from the contralateral inferior olive (Ito, 1984;Bloedel and Courville, 1981). A single climbing fiber forms 300-500 synapses with Purkinje cell dendrites (Hillman, 1969) to create a powerful, all-or-none postsynaptic response called a complex spike. These primarily Ca^{2+} based action potentials fire at 1-2 spikes/sec and are hypothesized to convey the error signals necessary for motor learning (Sturrock, 1990;Coesmans et al., 2004;Oscarsson, 1980;Ito, 2000;Graf et al.,

1988;Kobayashi et al., 1998;Barmack and Shojaku, 1995;Kitazawa et al., 1998). Numerous studies have confirmed that concurrent activation of climbing fiber and parallel fiber inputs can lead to long-term depression at the parallel fiber-Purkinje cell synapse as detailed in Chapter 1 (for reviews see (Ito, 1989;Ito, 2001)). However, there are numerous other types of synaptic plasticity in the cerebellar cortex that can also alter synaptic strength, including multiple forms of long-term potentiation at the parallel fiber – Purkinje cell synapses. These mechanisms provide the capacity for rapid and extensive circuitry changes and are also reviewed in Chapter 1 (for reviews see (Jorntell and Hansel, 2006;Hansel et al., 2001)).

Electrophysiological evidence supporting the Marr-Albus-Ito theory of cerebellar learning has been controversial. Numerous studies examining adaptation of wrist/arm movements (Gilbert and Thach, 1977;Ojakangas and Ebner, 1992), smooth pursuit eye movements (Medina and Lisberger, 2008;Li et al., 2011;Dash et al., 2010), or saccades (Catz et al., 2005;Prsa and Thier, 2011) recorded increased complex spike activity in relation to learning. Often, as predicted by the Marr-Albus-Ito theory, the complex spike discharge was coupled to decreases in simple spike firing that mirrored behavioral learning (Medina and Lisberger, 2008;Gilbert and Thach, 1977). However, many studies also reported mismatches between complex spike firing and learning-related changes in the behavior and/or simple spike firing rates. Significant simple spike firing changes occurred even in the absence of complex spike modulation (Ojakangas and Ebner, 1990;Medina and Lisberger, 2009;Medina and Lisberger, 2008;Raymond and Lisberger, 1997), reaffirming that other mechanisms significantly contribute to plasticity at parallel fiber- Purkinje cell synapses. In the oculomotor vermis, Thier and colleagues documented that the greatest complex spike modulation in Purkinje cells occurs late in both saccadic and smooth pursuit adaptation. It even persists after the animals have fully mastered the task (Catz et al., 2005;Dash et al., 2010). Late changes in complex spike discharge were also common during reach adaptation to a visuomotor gain change (Ojakangas and Ebner, 1990).

Individual complex spikelets propagate poorly down Purkinje cell axons (Khaliq and Raman, 2005;Monsivais et al., 2005) and are converted into only 1 or 2 conventional spikes at target neurons in the deep cerebellar nuclei (Monsivais et al., 2005). Therefore, it is the simple spike activity, influenced by multiple plasticity mechanisms, which should best reveal the functional signals that refine movements with learning. Understanding the role of the cerebellar cortex in motor learning requires studying how the signals encoded in Purkinje cell simple spike change over the time course of learning. It is well established for different types of non-learning tasks that Purkinje cell simple spike discharge encodes movement kinematics including position, velocity, and acceleration (Hewitt et al., 2011;Coltz et al., 1999a;Mano and Yamamoto, 1980;Pasalar et al., 2006;Roitman et al., 2005;Medina and Lisberger, 2009;Shidara et al., 1993;Fu et al., 1997a;Marple-Horvat and Stein, 1987), in addition to kinematic errors (Popa et al., 2012). The neural signals can lead or lag movement kinematics by up to 500 ms in an individual cell and this timing sensitivity is widely distributed across the cell population (Hewitt et al., 2011;Popa et al., 2012;Coltz et al., 1999b). However, very few studies have quantified how the sensitivity of the simple spike discharge to specific parameters changes during voluntary learning. In fact, the only published study examined floccular complex Purkinje cell responses during smooth pursuit adaptation (Medina and Lisberger, 2009). In this study, velocity and acceleration regression coefficients differed significantly for pre-learning vs. late-learning trials in 60.4% of Purkinje cells during the brief time window of the learned behavioral response (Medina and Lisberger, 2009). Additionally, others have argued that changes in Purkinje cell simple spike activity during saccade adaptation cannot be understood at the single cell level (Prsa and Thier, 2011;Dash et al., 2013).

Changes in the timing of specific parameter encoding have not been addressed. Although regression models used to evaluate floccular Purkinje cell discharge during smooth pursuit adaptation accounted for time leads or lags between the neural firing and eye kinematics, learning-related changes in simple spike timing sensitivity were not reported (Medina and Lisberger, 2009). Another smooth pursuit learning study found that simple

spike firing changes did not occur at the same time as changes in the behavioral response for a significant subset of the recorded Purkinje cells (Li et al., 2011). Similarly, in a task in which saccade duration was critical to successful adaptation, simple spike firing changes were often transient despite robust, progressive changes in the behavior (Catz et al., 2008). However, at a population level, saccade duration (and thus learning) could be modeled by shifts towards bursts of activity from early firing vs. late firing Purkinje cells (Catz et al., 2008;Prsa and Thier, 2011). Therefore, timing sensitivity likely plays an important role in motor adaptation.

In this study, we recorded Purkinje cell discharge from rhesus monkeys using a robotic manipulandum to move a cursor between two targets in the presence of a novel assistive or resistive mechanical force perturbation. We hypothesized that the simple spike firing discharge from Purkinje cells should exhibit progressive changes with kinematic adaptation and these changes would be reflected in the encoding of kinematic parameters. We also hypothesized that the timing of the encoding would change, including the relative contributions of feedforward and feedback signals as adaptation progressed. Specifically, we predicted that feedback signals would be accentuated during the early phases of learning, while predictive signals would become more pronounced during late adaptation.

Methods

All animal experimentation was approved by the Institutional Animal Care and Use Committee of the University of Minnesota and conducted in accordance with the guidelines of the National Institutes of Health.

Behavioral paradigm

Two monkeys (N: female 6.5 kg; I: male 7.6 kg) were trained to use a 2 joint robotic manipulandum in the horizontal plane (InMotion2, Interactive Motion Inc., Watertown MA) to control a 0.5 x 0.5 cm black "+" style cursor on a vertical video screen mounted

at eye level 50 cm in front of the animal. The gain was set to unity so that 1 cm of hand movement resulted in 1 cm of cursor movement.

All tasks required fast (≤ 750 ms) reaching movements between two 1.5 cm diameter, circular targets spaced 10 cm apart (Figure 15). We elected to use this design as opposed to a center-out reach task to increase the distance requirement, effectively allowing more options for positioning the perturbations. As described below, perturbation parameters were changed each day. Also, requiring the monkey to move across the entire workspace maximized position variability and peak velocity, two variables that strongly modulate Purkinje cell simple spike firing (Hewitt et al., 2011;Pasalar et al., 2006;Roitman et al., 2005). Every trial began with the appearance of a yellow start target that required cursor placement within the target for a randomized initial hold period (0.75- 1 s). Trials ended with a 1.25 s final hold period in the end target. Monkeys were allowed 750 ms to intercept the end target and 200 ms time outside the targets to accommodate overshooting or straying beyond target borders during the hold periods. Animals received a juice reward on successful trials.

A complete recording session included four different reaching tasks completed in block fashion. The first "PD (preferred direction) reach" block of trials (Figure 15A) evaluated the cell's firing discharge across all 8 possible reach directions (0 to 315^{o}, spaced 45^{o} apart) with no active robot forces. These trials were used to estimate the cell's preferred direction, and all subsequent trials were performed along this trajectory. The second "baseline error clamp" block (Figure 15B) recorded baseline cell firing in an error clamp (Scheidt et al., 2000). The error clamp consisted of robot-generated virtual walls that required the animal to move along a highly defined channel towards the target, minimizing small tangential kinematic errors that might mask learning effects. The error clamp was used to restrict tangential deviations that might otherwise produce large error signals in the simple spike firing (Popa et al., 2012). The error clamp channel also included a "funnel" at the start target to direct the hand into the 1.0 mm diameter channel. A second inverted "funnel" at the end target position smoothly transitioned movements

from the channel to the full 1.5 cm diameter of the end target. Error clamp wall forces scaled for the monkeys included an elastic spring force (-1000 N/m) and viscous damping (Vx: -30 N*s/m; Vy: -5 N*s/m). Use of these wall forces were well tolerated by the monkeys and clamped mean maximum tangential hand deviation to ±0.33 cm from a straight line between the start target and the end target for all error clamp trials.

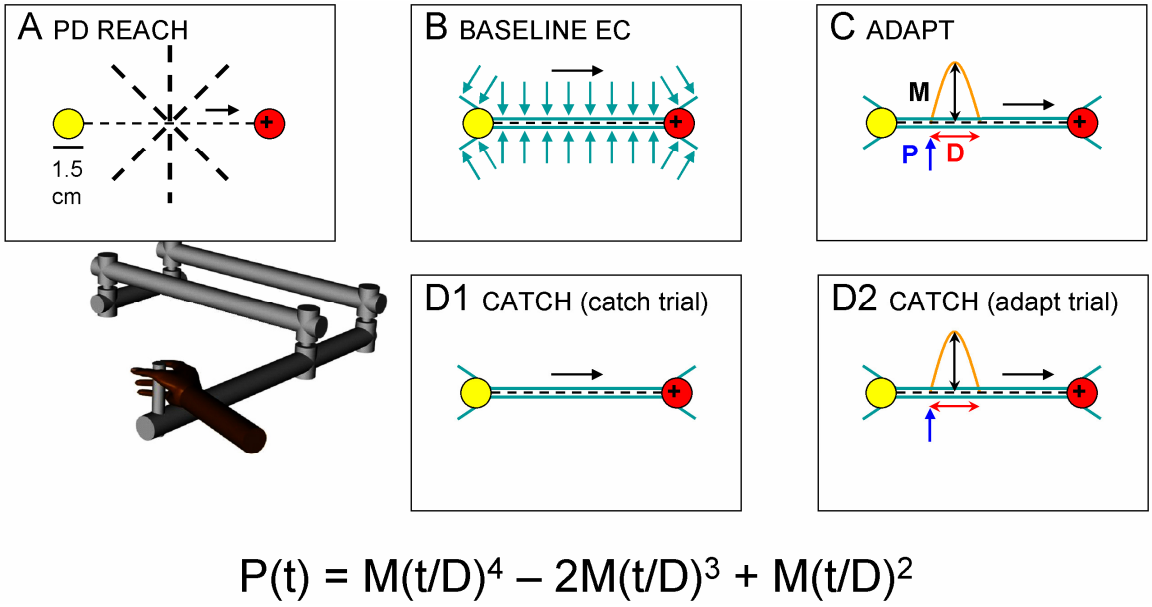

Figure 16: *Perturbation task*. Rhesus monkeys used a robotic manipulandum to control a "+" style cursor and make four types of very fast reaching movements between a yellow start and red end cue target displayed on a computer monitor. A) PD REACH epoch: Movements made across 8 directions with no robot forces identified a Purkinje cell's preferred direction (PD). All subsequent reaching movements during a recording session were along this direction. B) BASELINE EC epoch: Error clamp (EC) trials used robot-generated virtual walls (blue arrows) to restrict tangential movement to an hourglass-shaped area (blue). C) ADAPT epoch: The equation below describes a predictable, bell-shaped perturbation force (P(t), orange) that either assisted or resisted movements inside the error clamp. Colored arrows illustrate perturbation components that were randomized between recording sessions: black= Magnitude (M), red= Duration (D), blue= Start Position (P). D) CATCH epoch: The same adapt parameters were repeated (D2) with the addition of randomly occurring catch trials (D1). Catch trial parameters matched baseline EC. In all panels, black dashed lines illustrate actual channel width and black arrows movement direction.

The third "adapt" block introduced a force perturbation along the monkey's movement path to investigate how Purkinje cells adapt to external environmental changes. The

perturbation occurred within the error clamp, parallel to the direction of movement (Figure 15C). The bell-shaped perturbation was defined as (Wagner and Smith, 2008):

Eqn. (1) $$P(t)= M(t/D)^4 - 2M(t/D)^3 + M(t/D)^2$$

Time **t** and the subsequent perturbation force **P(t)** began once hand position passed a pre-determined start position, making the perturbation both position and time dependent. Perturbation parameters were randomized between recording sessions to induce "new" learning each day. Varying start position (20, 35, or 50% of 10 cm path), magnitude **M** (± 6, 7, 8, 9, or 10 N)(Richardson et al., 2008), and duration **D** (100, 150, or 200 ms) provided 90 different unique perturbation combinations. Positive magnitudes resulted in assistive perturbations that pushed the hand towards, and often beyond, the end target. In contrast, negative resistive perturbations opposed movement towards the end target. The fourth "catch" block continued adaptation to the perturbation (Figure 15D-1), but also included catch trials (randomized at 10-15%, Figure 15D-2), during which the perturbation was unexpectedly absent. All attempted catch trials were rewarded, regardless of whether the monkey successfully reached the end target. Finally, if the neuronal recording was stable and the animals were willing, a second block of error clamp baseline trials were recorded to assess whether kinematics and simple spike firing returned to the original baseline levels. For each recording session, a monkey typically executed 80 PD reach (~10 each direction), 40 baseline error clamp, 110 adapt, and 110 catch trials (of which 11-17 were randomized true catch trials).

Surgical procedures

Head restraint hardware, including a circular stainless steel halo attached to the skull with 4 stainless steel posts and screws, were placed on each monkey using aseptic surgical techniques and full anesthesia with isofluorane. In Monkey N, a recording chamber was placed over right parietal cortex, while Monkey I's chamber was placed over the left parietal cortex. Therefore, Monkey N used the right hand for all experiments while Monkey I used the left hand. Recording chambers were stereotaxically positioned (-0.6

cm anterior/posterior, +1.00 cm medial/lateral) over a 2.0 cm craniotomy in order to target lobules IV-VI of the intermediate/lateral zones where hand and arm related Purkinje cells have been described (Thach, 1968;Mano and Yamamoto, 1980;Fortier et al., 1989;Ojakangas and Ebner, 1992;Fu et al., 1997a;Roitman et al., 2005;Pasalar et al., 2006;Yamamoto et al., 2007;Hewitt et al., 2011). Previous results using these same two monkeys combined full head MRI and CT images in Monkey Cicerone to model recording chamber locations and electrode penetrations (Miocinovic et al., 2007). Models for both monkeys showed electrode recording positions mostly in lobules IV-V of the intermediate zone, anterior to the primary fissure (Hewitt et al., 2011).

Electrophysiological recordings & data collection

After full recovery from chamber implantation surgery, extracellular recordings were obtained using Pt-Ir electrodes with parylene C insulation (0.8-1.5 MΩ impedance, Alpha Omega Engineering, Nazareth, Israel) that were inserted just deep enough to penetrate the parietal dura using a 22 gauge guide tube. Electrodes were advanced to mean depths of 27.3 ± 4.4 mm using a hydraulic microdrive (Narishige Group, Japan). Purkinje cells were identified by the presence of complex spikes and discriminated online using the Multiple Spike Detector System (Alpha Omega Engineering, Nazareth, Israel) after conventional amplification and filtering (30 Hz-3kHz band pass, 60 Hz notch). Resulting spike trains were digitized and stored at 1 kHz. The raw electrophysiological data was also digitized and stored at 32 kHz. Spike trains were then transformed to a continuous firing rate using fractional intervals, downsampled to 100 Hz, and low pass filtered (4^{th} order Butterworth with a 5 Hz cut-off).

Optical encoders at each robot joint acquired hand position and were used to display cursor position in real-time on the computer screen. Forces applied to the manipulandum were also determined using a six-degrees-of-freedom transducer (model Gamma, ATI Industrial Automation, Apex, NC) mounted at the handle. Hand position (P), target position, and applied force were digitized and stored at 200 Hz. Movement direction, velocity (V), acceleration (A), and other kinematic variables were calculated from the

stored position data (Roitman et al., 2005;Pasalar et al., 2006). All analyses were performed using MATLAB software (MathWorks, Natick, MA).

Data from individual trials were aligned on movement onset (defined as velocity ≥ 5 cm/s) for analyses. All analyses used only the time interval -500 ms to 1500 ms, unless otherwise specified, which excluded portions of the initial and final hold periods. To compare between the eight possible movement directions, kinematic results were transformed to parallel or tangential coordinates. Movement in the parallel direction follows the shortest path between the start and end targets, while tangential movements are perpendicular to this path. Subscripts are used to denote parallel (p) vs. tangential (t) coordinates.

Quantifying kinematic adaptation

Successful trials from the adaptation block were divided into three learning stages: early (first 10 trials), middle (median 10 trials), and late (final 10 trials). For comparisons, trials were also sampled from the baseline error clamp (final 10 trials) and catch (all true catch trials) blocks. Catch trials randomly occurring <5 trials after the previous catch trial were eliminated from analyses, as the monkeys often exhibited some adaptation on closely paired catch trials. Mean traces were computed for each kinematic parameter and group of trials (Figures 17 and 18). For each recording session, mean baseline kinematic traces were subtracted from mean early or mean catch traces to evaluate how adaptation counteracted the effects of the perturbation. Correlation coefficients comparing the similarity of these difference traces were calculated using MATLAB.

Mean position (P_p, P_t), velocity (V_p, V_t), and acceleration (A_p, A_t) profiles were constructed by averaging the last 10 successful late adaptation trials (i.e. red traces in Figures 17 & 18). Root mean square deviation (RMSD) measures compared each trial of adaptation to the mean profiles, and the results were fit to logarithmic functions to model learning. Learning rates were approximated by calculating the standard time constant (τ) of exponential decay for all significant ($p \leq 0.05$) logarithmic fits. Each curve's lower

bound, or asymptote, was defined as the trial at which the change in slope was ≤ 0.0001. Identifying this point often required extrapolating the curve beyond the actual 110 adapt trials. The τ time constant is the trial number at which the curve reached 1/e or ~37% of its maximum range.

RMSD values were similarly calculated to compare mean profiles from the last 10 baseline and late adapt trials for each cell during the 700 ms following movement onset. This time period cut off the initial and final hold periods to isolate only the initial movement without corrections. The results for each parameter were then normalized by the range of recorded values and averaged across the population to measure the percent change in movement kinematics.

Analysis of simple spike firing

A two-step analysis was used to determine the number of Purkinje cells with significant changes in simple spike firing and the time course of those changes. For the first step, firing changes before and during adaptation were quantified by calculating mean simple spike firing rates from four task-related time windows for individual trials. Time windows were defined as 1) prior to movement onset, 2) prior to perturbation start, 3) duration of the perturbation, and 4) post perturbation end. All four window lengths matched the perturbation duration (e.g. 100, 150, or 200 ms) for each recording session. A 2-way ANOVA (treatment factors were epoch and time window, 10 repetitions from each category, $\alpha = 0.05$) was used to identify cells with significant firing changes between early and late adaptation in at least 1 of the 4 time windows. To identify significant predictive firing changes (i.e. prior to the perturbation), post-hoc Bonferroni-corrected Student t-tests evaluated mean firing in the first two time windows for cells with significant ANOVA results. For the second step, we applied the RMSD analysis outlined above for the kinematics to the simple spike firing. The RMSD of the simple spike firing profiles for individual trials were compared to the average profile from the last 10 adaptation trials and the RMSD values fitted to logarithmic functions to model learning and estimate the time course of the changes.

Simple spike firing data from single trials of a recording session were fit to linear regression models for movement kinematics. Previous eye and limb movement studies indicate that Purkinje cells in this region are significantly tuned to kinematic parameters such as position, velocity, and acceleration (Hewitt et al., 2011;Roitman et al., 2005;Coltz et al., 1999a;Fu et al., 1997a;Marple-Horvat and Stein, 1987;Medina and Lisberger, 2009;Shidara et al., 1993). As previously mentioned (see data collection), movement kinematics were transformed into parallel or tangential coordinates to easily compare between the eight possible movement directions. This provided 6 kinematic model parameters: position (P_p, P_t), velocity (V_p, V_t), and acceleration (A_p, A_t). As these parameters were often correlated for most recording sessions, we examined each parameter in isolation by regressing against the firing residuals (FR), which removed the firing variability associated with the other 5 parameters. The FR for a given kinematic parameter were obtained by regressing the actual instantaneous (i.e. non-averaged) firing (f) from individual trials against a multi-linear model containing the other 5 parameters. For example, equation 2 below was used to acquire the FR needed to evaluate Pp independently of P_t, V_p, V_t, A_p, and A_t.

Eqn. (2)
$$f(t)= \beta_o(\tau) + \beta_{Pt} P_t(t - \tau) + \beta_{Vp} V_p(t - \tau) + \beta_{Vt} V_t(t - \tau) + \beta_{Ap} A_p(t - \tau) + \beta_{At} A_t(t - \tau) + \varepsilon(t - \tau)$$

The error term ε is the firing residuals and represents the remaining variability in the simple spike discharge after everything but P_p is removed. We refer to the firing residuals as FR_{Pp}, in which the subscript denotes the kinematic parameter of interest. The model parameter τ, described below, was incorporated to estimate the time lead or lag between simple spike firing and the kinematics, and β_o denotes baseline firing. This approach was previously validated with control regressions to confirm that the firing residuals contained no information about the other parameters (Popa et al., 2012). Next, using the simple linear regression models in equations 3-8, the appropriate firing residuals were regressed to the individual kinematic parameters.

Eqn. (3) $$FR_{Pp}(t)= \beta_o(\tau) + \beta_{Pp} P_p(t - \tau) + \varepsilon(t - \tau)$$

Eqn. (4) $$FR_{Pt}(t)= \beta_o(\tau) + \beta_{Pt} P_t(t - \tau) + \varepsilon(t - \tau)$$

Eqn. (5) $$FR_{Vp}(t)= \beta_o(\tau) + \beta_{Vp} V_p(t - \tau) + \varepsilon(t - \tau)$$

Eqn. (6) $$FR_{Vt}(t)= \beta_o(\tau) + \beta_{Vt} V_t(t - \tau) + \varepsilon(t - \tau)$$

Eqn. (7) $$FR_{Ap}(t)= \beta_o(\tau) + \beta_{Ap} A_p(t - \tau) + \varepsilon(t - \tau)$$

Eqn. (8) $$FR_{At}(t)= \beta_o(\tau) + \beta_{At} A_t(t - \tau) + \varepsilon(t - \tau)$$

For each set of regressions, the value of the timing variable τ shifted in 20 ms bins from -500 to 500 ms (Pasalar et al., 2006;Hewitt et al., 2011;Popa et al., 2012) to assess the time lead or lag between neural firing and movement kinematics. Negative values (i.e. $\tau < 0$) indicate that firing leads, or predicts, movement kinematics in a feedforward manner, whereas positive values (i.e. $\tau \geq 0$) indicate the firing lags, or provides feedback, about movement kinematics. Therefore 51 individual regressions were performed, resulting in 51 different values of τ. Note that the same τ value associated with a simple linear regression result (eqns. 3-8) was used to calculate the associated firing residuals. As in other studies (Ashe and Georgopoulos, 1994;Gomi et al., 1998;Medina and Lisberger, 2009;Hewitt et al., 2011), τ does not add an additional degree of freedom to the model.

Temporal profiles were generated comparing the coefficients of determination (R^2 values) or regression coefficients (βs) to the 51 τ values. The τ value at which an R^2 profile was maximal was selected as the optimal τ, and the corresponding β values were used for analyses. For some analyses, both a feedforward and feedback τ value were selected as optimal if both results were significant. All regression analyses were based on single trials, not averaged data. Averaging firing across trials will inflate R^2 values because the natural variation across trial repetitions (i.e. noise) is effectively aggregated within the estimate of the variability caused by the signal (Kenney, 1979). Therefore, the R^2 values reported in this study may appear smaller than studies using average firing, but the R^2 values must be understood in the context that the analyses were based on single trial data.

Significance was tested at each τ using the F statistic with the degrees of freedom determined by the number of observations. Type 1 error rate was $\alpha = 0.05$. We imposed an additional threshold of $R^2 \geq 0.02$ for a significant fit (Popa et al., 2012).

Results

Behavioral kinematics and simple spike firing were successfully collected during the adapt block for 48 recording sessions in Monkey N and 90 recording sessions in Monkey I. For monkey I, 3 out of the 90 recording sessions yielded two Purkinje cells isolated on separate channels. Consequently, this data set provided 138 behavioral and 141 neuronal firing recordings. However, 16 recording sessions did not have usable baseline data. Therefore, analyses that include the baseline data only utilize the other 121 Purkinje cells with complete data.

Perturbations produce adaptive changes in behavior

Hand kinematics demonstrated adaptation to both the resistive and assistive perturbations. Hand position traces (X vs. Y, Figure 17A) display the error clamp's effectiveness in producing very repeatable movements that cross the entire parallel workspace, but utilize only a small portion of the tangential workspace. As desired, most kinematic variability occurs parallel to the direction of movement rather than tangentially (compare Figures 17 and 18, noting differences in y-axes). For a resistive recording session, the hand mostly overshoots the end target (red circle) during catch trials (blue). Conversely, for an assistive force, the monkey's hand barely reached the end target center when the resistive perturbation was unexpectedly removed.

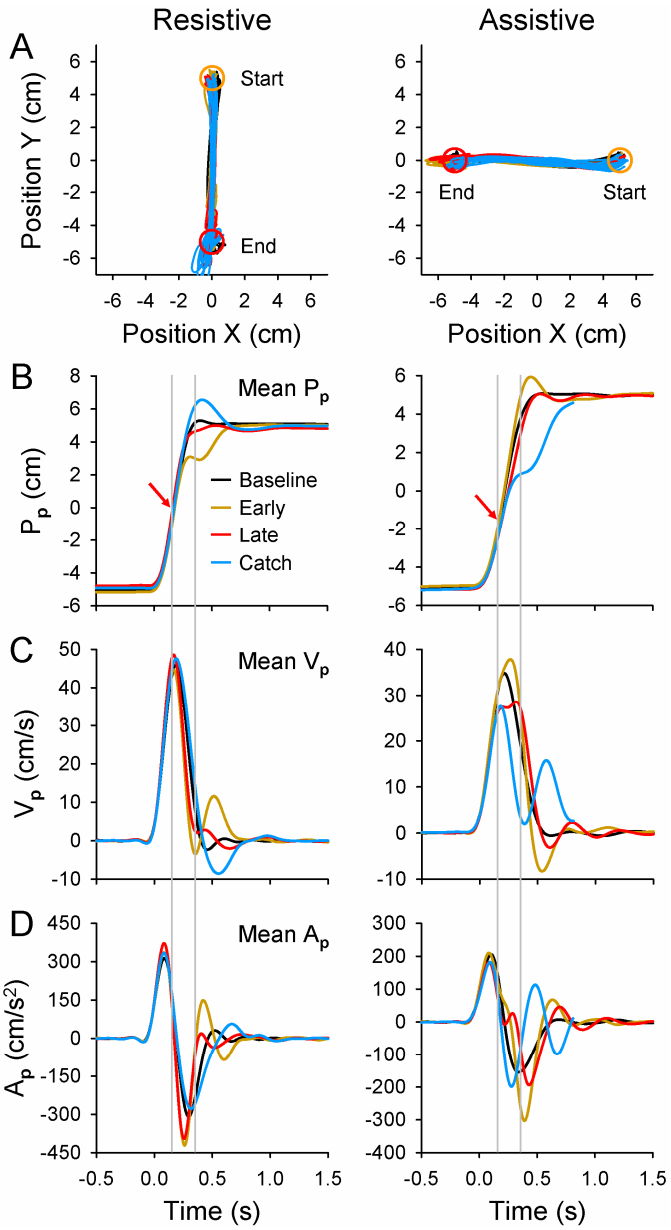

Figure 17: *Hand movement kinematics, parallel*. A) Shown are the actual hand position coordinates (X, Y) from baseline error clamp (black), early adapt (gold), late adapt (red), and catch trials (blue) for example resistive (Monkey I, left column) and assistive (Monkey N, right column) recording sessions. Note that 1.5 cm start (yellow circle) and end (red circle) targets centered at +5 and -5 cm produce a position workspace span of -5.75 to 5.75 cm. Position data covers the entire trial duration, including hold periods. B) Mean parallel hand position (P_p) trajectories were plotted vs. time for the same trials. Red arrows depict the perturbation start position. Grey dashed lines show approximate perturbation start and end times. C & D) Mean hand velocity (V_p) and acceleration (A_p) traces are shown. In all plots, data represent 10 trials from each condition except for catch trials (n= 7 resistive, n= 12 assistive). Perturbation parameters and preferred directions were: *resistive* M= -9 N, D= 200 ms, P= 0 cm (50%), 270^o; *assistive* M= +7 N, D= 200 ms, P= -1.5 cm (35%), 180^o.

Perturbation effects and learning are apparent in the plots of mean parallel position versus time (P_p, Figure 17B). Baseline error clamp trials (black) display smooth transitions from -5 cm to 5 cm for both examples. During early adapt trials (gold), the perturbation disrupts the baseline pattern. The perturbation is a bell-shaped pulse, resulting in a delay between the perturbation start (red arrows) and where the magnitude (and thus behavioral changes) is maximal. Resistive perturbations delay reaching the target (i.e. the hand "undershoots" the target), so that a quick catch-up movement is needed to intercept the target before time expires. The catch-up movement following the perturbation is evident in the early adapt velocity trace (V_p, Figure 17C). With learning, the mean late adapt traces (red) again closely resemble baseline conditions and target interception is efficient. Catch trial (blue) changes also confirm that adaptation occurred. The monkey clearly overshoots the target in catch P_p movements, and must move backwards into the target as illustrated by the negative portion of the catch V_p trace at ~400 ms. Comparisons of the early adapt and catch trial profiles at this point show that they are approximately equal in magnitude but oppositely signed. This demonstrates after-effects, which indicate that the monkey learned the specific perturbation parameters. Acceleration changes (A_p, Figure 17D) are also evident. In both early and late adapt, the resistive perturbation immediately produces a large negative acceleration. This requires the monkey to reverse towards positive accelerations more quickly than in the baseline trials. Catch trials, in contrast, remain at negative acceleration for a longer time interval than even the baseline trials.

In the assistive perturbation, adaptation is opposite that of the resistive perturbation, but has the same general properties. Parallel position traces (P_p, Figure 17B) show that, during early adapt, the perturbation causes the hand to overshoot the target. Adaptation leads to efficient target interception, and the late adapt trace closely resembles baseline. Catch trials expose the learning, in that the hand "undershoots" the target and must make a quick catch-up movement that is evident in the velocity trace at ~500 ms (V_p, Figure 17C). Comparing the early adapt and catch trials reveals opposite acceleration patterns

(A_p, Figure 17D) as the hand approaches the target. Therefore, after-effects due to adaptation can be identified in all of the kinematic profiles.

Tangential movement kinematics (Figure 18) occur on much smaller scales than their parallel counterparts. Like parallel kinematics, the perturbation causes the early adapt traces (gold) to deviate from baseline in all measures (P_t, V_t, and A_t) for both the resistive and assistive conditions. In contrast, however, learning does not result in the kinematics returning to their baseline profiles. Late adapt traces instead often resemble mean early adapt profiles. Catch trial responses are opposite that of late adapt in some cases (e.g. compare V_t from 250-500 ms), but the response is often not proportional in magnitude. In some sessions, including both examples shown here, the monkeys used the error clamp wall as a bumper to diminish the perturbation effects. For example, friction from the error clamp wall could be used to attenuate the effects of the assistive force. However, this strategy often arose late in the adaptation block. Therefore, the kinematic data suggest that movement adaptation in tangential directions played a less significant role than parallel directions in adapting to the perturbations, as confirmed below (see Figures 19 and 20).

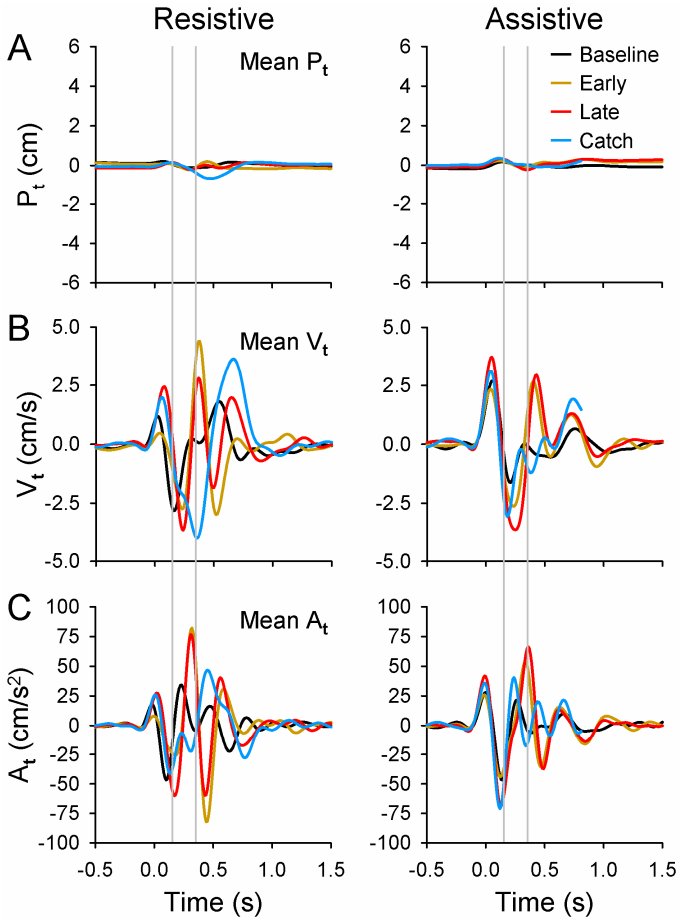

Figure 18: *Hand movement kinematics, tangential*. Mean hand kinematics from baseline error clamp (black), early adapt (gold), late adapt (red), and catch trials (blue) are plotted vs. time for the tangential components of A) position (P_t), B) velocity (V_t), and C) acceleration (A_t). Grey dashed lines show approximate perturbation start and end times. Data are from the same example trials of the resistive (left column) and assistive (right column) recording sessions shown in Figure 17.

Differences within a single recording session were quantified by calculating the RMSD between mean baseline and late adaptation profiles (n=10 trials) for all 6 kinematic parameters. The mean percent changes across the population were low for the parallel movements (P_p= 1.7%, V_p= 3.1%, A_p= 3.7%) compared to tangential movements (P_t= 22.3%, V_t= 8.1%, A_t= 6.8%), again confirming that movement adaptation primarily occurred in the parallel direction. Importantly, this analysis shows that the final adapted movement kinematics closely resemble the original movement.

To specifically address learning during the adapt epoch, we assessed how single trial kinematics progressed towards a final reaching pattern that efficiently intercepted the target despite the perturbation. This final pattern was represented by the mean position (P_p, P_t), velocity (V_p, V_t), and acceleration (A_p, A_t) traces of late adapt trials (i.e. red traces in Figures 17 and 18). RMSD measures compared each successful adapt trial (i.e. only trials where the target was intercepted) to the mean late adapt traces. Results from the example resistive recording session were fit to logarithmic functions (Figure 19A), and reveal that the monkey quickly adapted towards the final parallel kinematic patterns ($p < 0.001$ for parameters P_p, V_p, and A_p). Across all recording sessions, there were more instances of significant learning for the parallel parameters (n= 73 P_p, n= 90 V_p, and n= 84 A_p) than the tangential parameters (n= 42 P_t, n= 64 V_t, and n= 61 A_t). Significant adaptation ($p \leq 0.05$) occurred in 87.0% (120/138) of the sessions in at least one parameter. This left only 13.0% (18/138) of the recording sessions without evidence of significant learning using this one measure. The majority of non-adapting sessions used an assistive perturbation (11/18). Continuous adaptation without a plateau or late changes in reaching patterns occasionally produced RMSD results not well fit by a logarithmic function, and may explain why several sessions did not reach significance despite identifiable changes in the kinematics.

We further quantified the rate of learning by calculating the standard time constant τ of exponential decay (see Methods) for all parameters in a recording session with significant adaptation. The red arrows in Figure 19A indicate the trial number at which the time constant τ is reached for the example data (P_p= 20, V_p= 19, and A_p= 23). Across all sessions, mean τ values were much lower with smaller standard deviations for the parallel parameters (τ= 13.5 ± 2.9 P_p, τ= 12.6 ± 3.0 V_p, and τ= 17.6 ± 5.1 A_p, Figure 19B) compared to the tangential parameters (τ= 40.1 ± 7.2 P_t, τ= 24.8 ± 7.6 V_t, and τ= 25.8 ± 7.9 A_t, Figure 19C). All τ values from position, velocity, and acceleration were grouped by parallel vs. tangential movement direction for comparison. The τ distributions suggest that learning occurred more quickly in parallel movement directions ($t(389) = -18.87$, $p < 0.001$). Therefore, the majority of the adaptation took place along the parallel

movement direction and occurred at a faster rate. Progressive changes in tangential movements most likely served to refine the movements and perhaps increase the efficiency of target interception.

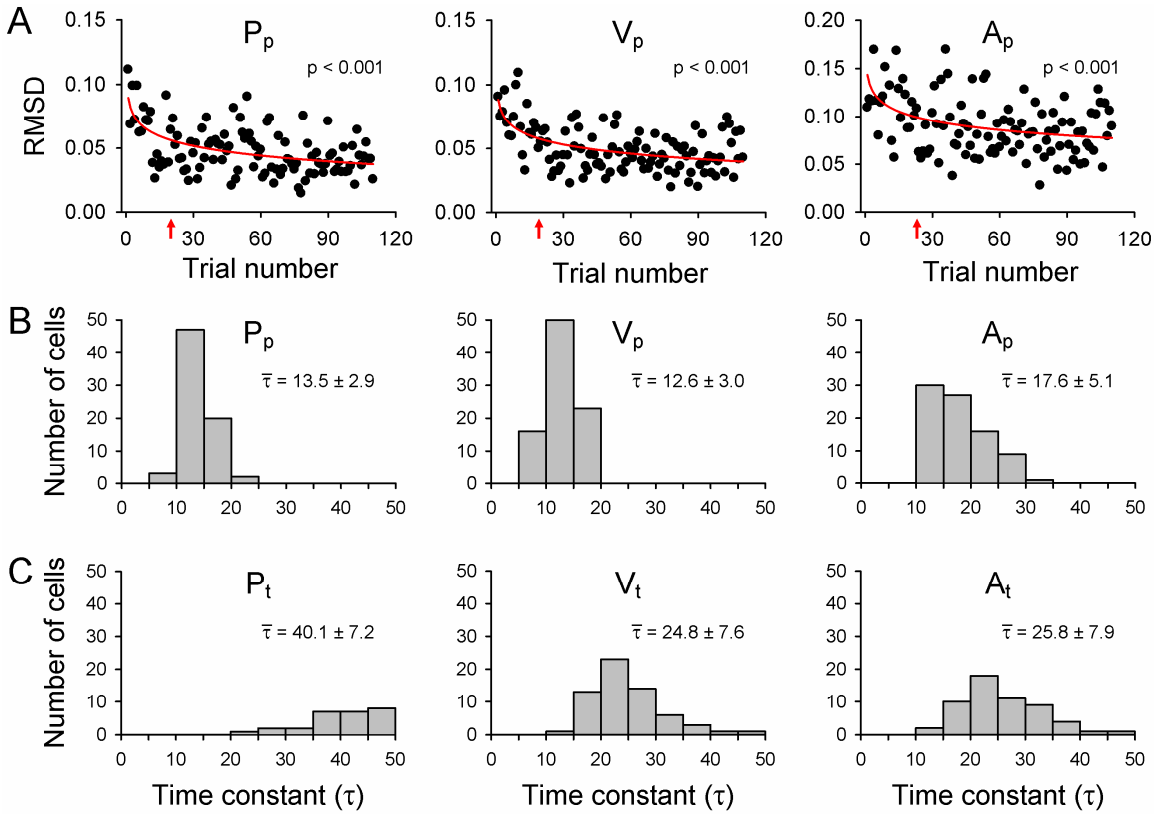

Figure 19: *Kinematic learning and adaptation rates*. A) RMSD measures compared individual adapt trial kinematics to the corresponding mean late adapt trace. RMSD by trial number are plotted for the parallel kinematic parameters position (P_p), velocity (V_p), and acceleration (A_p) of the example assistive recording session (Figures 17 & 18). Logarithmic fits (red lines) and p-values are provided. Red arrows indicate the trial number where the standard time constant of exponential decay (τ) was reached. Histograms show the distributions of τ values for the B) parallel or C) tangential components of position, velocity, and acceleration. Means ± SD of the time constants are shown for each histogram.

Finally, we evaluated adaptation after-effects by contrasting early adapt and catch trial kinematics. We reasoned that learning should effectively remove the effects of the early perturbation on the movement kinematics by counterbalancing the perturbation. The catch trials should reveal the contribution of adaptation to the kinematics. For each recording session, mean baseline kinematic traces (e.g. Figures 17 and 18) were

subtracted from mean early or mean catch traces to construct mean difference traces. These difference traces emphasize how early adapt (grey) or catch (black) kinematics differ from baseline. The example data from a resistive session show that difference traces for the parallel kinematic parameters (Figure 20A) are nearly equal and opposite in magnitude over time, while the tangential difference traces (Figure 20C) are less correlated. Correlation coefficients quantify these observations, with mean ρs less than -0.6 for the parallel parameters P_p, V_p, and A_p (Figure 20B). In contrast, tangential correlation coefficients P_t, V_t, and A_t are all approximately zero (Figure 20D). Correlation coefficients from all the parameters were grouped by movement direction. A t-test comparing the parallel versus tangential correlation coefficients confirmed the means were significantly different ($t(586)= -19.73$, $p< 0.001$). Repeating the correlation coefficient analyses with time shifts between the two difference traces did not significantly alter the outcomes (data not shown). Again, these results imply that the majority of learning was in the parallel direction of movement and that adaptation involved precisely matching the effects of the perturbation on arm kinematics.

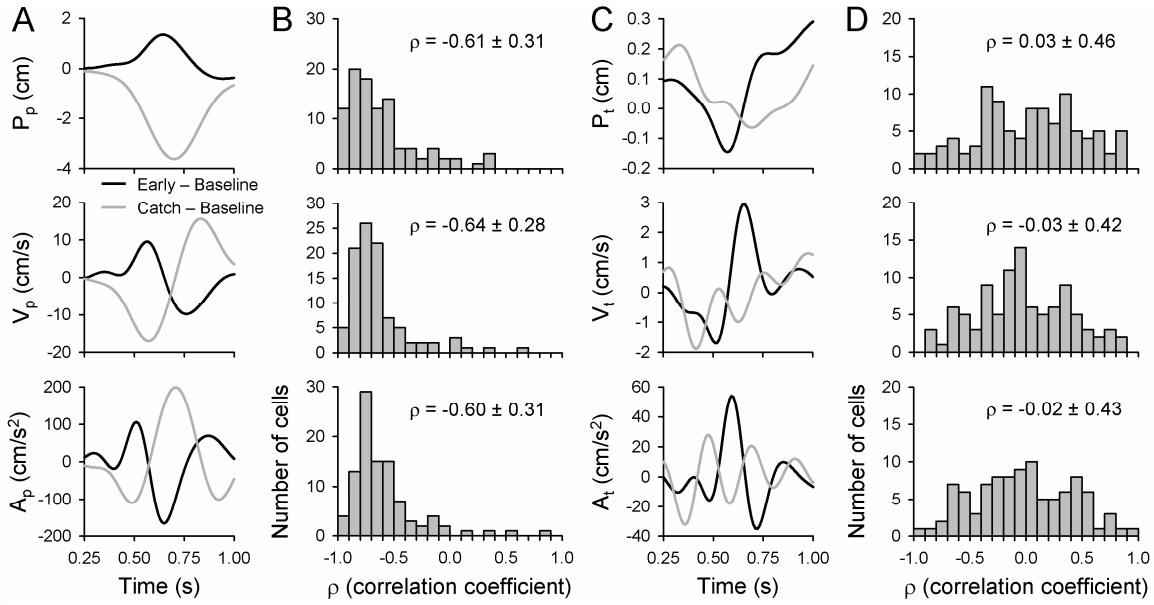

Figure 20: *Kinematics precisely adapt to perturbations*. Mean baseline kinematic traces were subtracted from mean early (black) or catch (light grey) traces to emphasize kinematic changes due to the perturbations. A) Resultant difference traces for parallel kinematic parameters position (P_p), velocity (V_p), or acceleration (A_p) are plotted versus time for the example assistive Purkinje cell recording shown in Figures 17 & 18. The shortened time interval (0 – 0.75 s) primarily covers the reaching period. B) Histograms show correlation coefficients resulting from comparison of the two difference traces. All sessions with successfully recorded baseline, adaptation, and catch trials were included (n= 98). C & D) Similar difference traces and correlation coefficient histograms (n= 98) are included for the tangential kinematic parameters position (P_t), velocity (V_t), and acceleration (A_t). For each histogram, the means ± SD of the correlation coefficients are shown.

Perturbations produce adaptive changes in simple spike firing

Each of the 141 Purkinje cells recorded during this task exhibited distinct firing modulation. To illustrate this, simple spike firing responses from four different Purkinje cells (1 assistive and 1 resistive perturbation from each monkey) are plotted for consecutive baseline and adaptation trials versus time (Figure 21). Qualitative analyses of the firing discharge show that each Purkinje cell is highly tuned to movement, with marked increases or decreases in firing activity at movement onset (left vertical line). After the perturbation is introduced, progressive changes in Purkinje cell firing rates occur that remain through late adaptation. The four cells chosen illustrate the diversity of firing and adaptation observed across Purkinje cells.

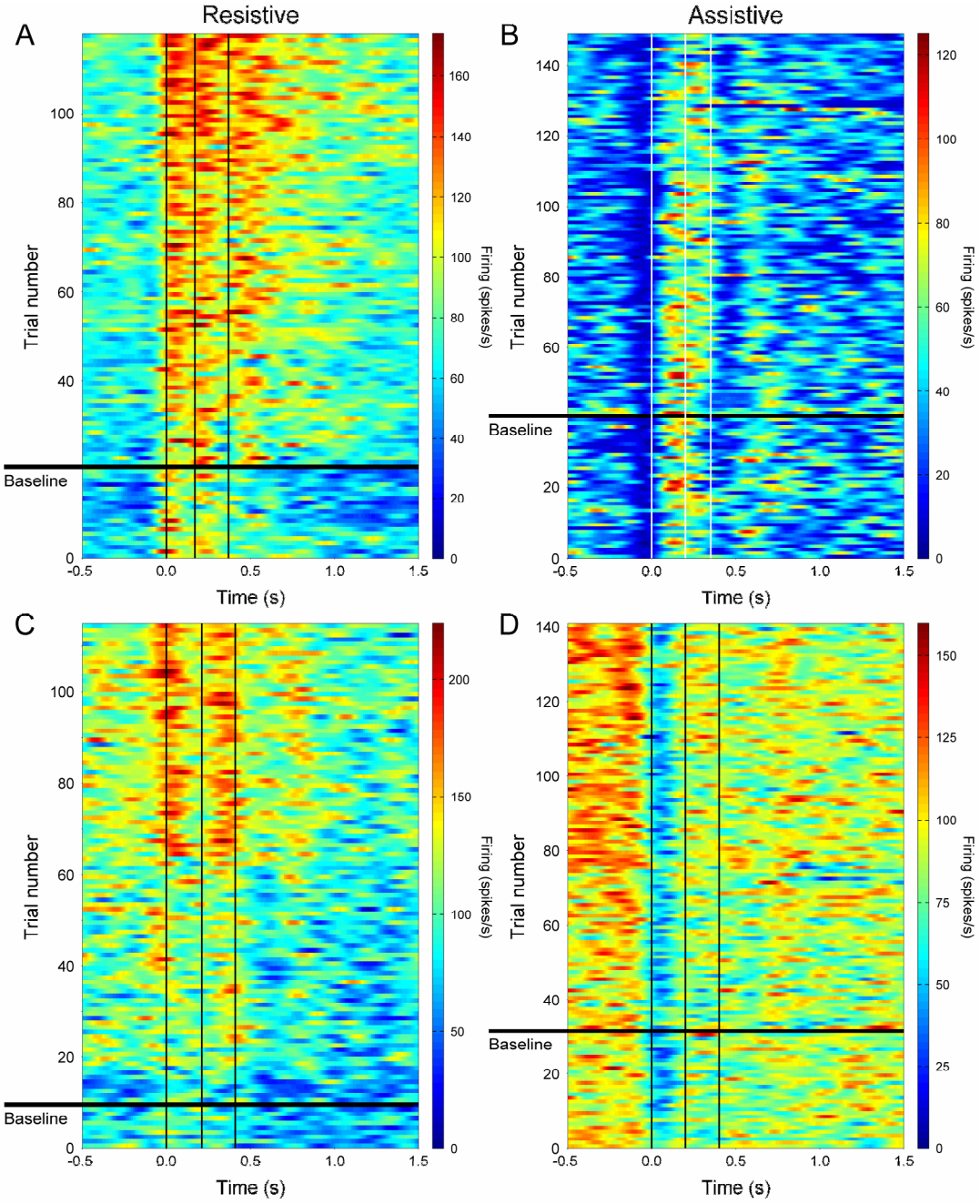

Figure 21: *Simple spike firing responses*. Recorded simple spikes were converted to instantaneous firing rates, aligned on movement onset (t= 0), and plotted versus time for 4 example Purkinje cells. Rows below the horizontal black line depict baseline data, while rows above chronologically show firing from all successful adaptation trials. Vertical lines depict movement onset (left), mean perturbation start (middle), and mean perturbation end (right). Perturbation parameters and preferred directions were *Monkey I:* A) M= -9 N, D= 200 ms, P= 0 cm (50%), 270°; B) M= +9 N, D= 150 ms, P= -1.5 cm (35%), 225°; *Monkey N:* C) M= -9 N, D= 200 ms, P= 0 cm (50%), 135°; D) M= +7 N, D= 200 ms, P= -1.5 cm (35%), 180°.

The first Purkinje cell (Figure 21A) demonstrates distinct increased firing across all key movement time periods during adaptation to a resistive perturbation. Firing prior to movement onset (left vertical line, t= 0 s) increases quickly, from little to no firing in the baseline epoch to tonic firing around 60 Hz during the adapt epoch. In the baseline epoch, there are only two "bands" of increased firing occurring after movement onset and what will be the perturbation start time (middle vertical line). After exposure to the perturbation, overall firing rates in these two bands also increase. In the first trial of early adapt, a third band of peak firing appears after the perturbation ends (right vertical line) and continues to increase with adaptation.

In contrast, a second Purkinje cell (Figure 21B) decreases its overall mean firing with adaptation to an assistive perturbation. With adaptation, the decrease in firing just prior to movement onset widens and another period of decreased firing after the perturbation ends (right vertical line) becomes more pronounced. Perturbation exposure also delays this cell's peak firing by ~150 ms, shifting the timing from just after movement onset in the baseline trials to during the perturbation in late adapt trials.

A third Purkinje cell (Figure 21C) shows only weak modulation during the baseline trials. Throughout the adaptation, firing increases in three bands. The first band is centered on movement onset, the second corresponds with the start of the perturbation, and the third band occurs at about 750 ms post perturbation when the target is intercepted. The changes begin in the early adapt epoch, shortly after the perturbation is first experienced. Similar to the first cell (Figure 21A), this cell also demonstrates increased background firing prior to movement onset.

Simple spike firing for a fourth Purkinje cell (Figure 21D) exhibits the most changes prior to movement onset. The background firing steadily increases after initial exposure to the perturbation and remains elevated in the late adaptation trials. Closer inspection of early versus late adapt trials reveals the period of decreased firing following movement onset shortens with adaptation, so that the blue "band" narrows slightly.

RMSD calculations comparing baseline mean firing profiles to that of late adaptation across the entire movement period confirm sizable changes in the simple spikes, showing that the firing profile changed an average of 25.3% ± 11.8% for all 141 Purkinje cells. However, as mentioned above, movement kinematics in parallel position, velocity, or acceleration only changed by 1.7%, 3.1%, or 3.7% respectively, suggesting that to adapt to a transient perturbation large changes in the simple spike firing across the population are required. Therefore, any changes in the sensitivity to the kinematic parameters truly reflect changes in the Purkinje cells and not simply an alteration in the movements.

Within individual cells, the firing analyses first tested for significant simple spike firing change with adaptation. We divided the simple spike firing into four task-related time windows: 1) prior to movement onset (left vertical line), 2) prior to perturbation start (middle vertical line), 3) duration of the perturbation, and 4) post perturbation end (right vertical line). The duration of each window matched the perturbation duration (e.g. 100, 150, or 200 ms) for the specific recording session. The first window provided a measure of the background firing and the other three windows focused on the firing in relation to the perturbation. The mean simple spike firing from each time window was compared across 10 trials each of early versus late adaptation (two-factor ANOVA with repeated measures, α=0.05). All four example Purkinje cells (Figure 21) showed significant changes in the mean firing rates between early and late adaptation (Purkinje cells A, B, and D $p < 0.0001$, C $p = 0.016$). Across the population, 56.0% (79/141) of Purkinje cells demonstrated significant firing changes between the early and late adapt epochs. For these Purkinje cells, post-hoc Student t-tests (Bonferroni corrected) found that the simple spike firing of 58.2% (46/79) cells specifically showed predictive changes in response to the perturbation (i.e. changes occurred prior to the perturbation in window 1, window 2, or both windows 1 and 2). This corresponded to 36.7% (29/79) neurons significant for changes prior to movement onset (window 1) and 40.5% (32/79) prior to the perturbation start (window 2). All subsequent simple spike firing analyses were restricted to the 79 significant Purkinje cells.

To compare rates of firing adaptation with those of kinematic adaptation, we similarly calculated the RMSD between each trial of adaptation and a final firing pattern that was modeled as the mean of the final 10 late adapt trials. Results for the four example Purkinje cells were modeled by logarithmic functions ($p < 0.001$ for all 4 neurons), and demonstrate that the firing activity also exhibits progressive changes with learning in the same manner as the kinematics (Figure 22). This type of adaptation was found to be significant ($p < 0.05$) in 53.2% (42/79) of Purkinje cells with significant firing changes. Again, continuous adaptation without a plateau or late changes in the firing patterns produced RMSD results were not well fit by a logarithmic function and explain why the firing adaptation in many neurons did not reach significance.

We further quantified the rate of firing adaptation by calculating the standard time constant (τ) of exponential decay (see Methods) for all recording sessions with significant firing adaptation as measured by the RMSD. The red arrows in Figure 22A-D indicate the trial number at which the time constant τ is reached for the example data (A= 29, B= 30, C= 17, and D= 51). The distribution of τ values for all Purkinje cells with significant RMSD logarithmic fits is provided (Figure 22E). The mean τ value of 29.7±10.6 is much greater than mean τ values for the kinematics (Figure 19), suggesting that firing adaptation occurs more slowly and follows kinematic adaptation.

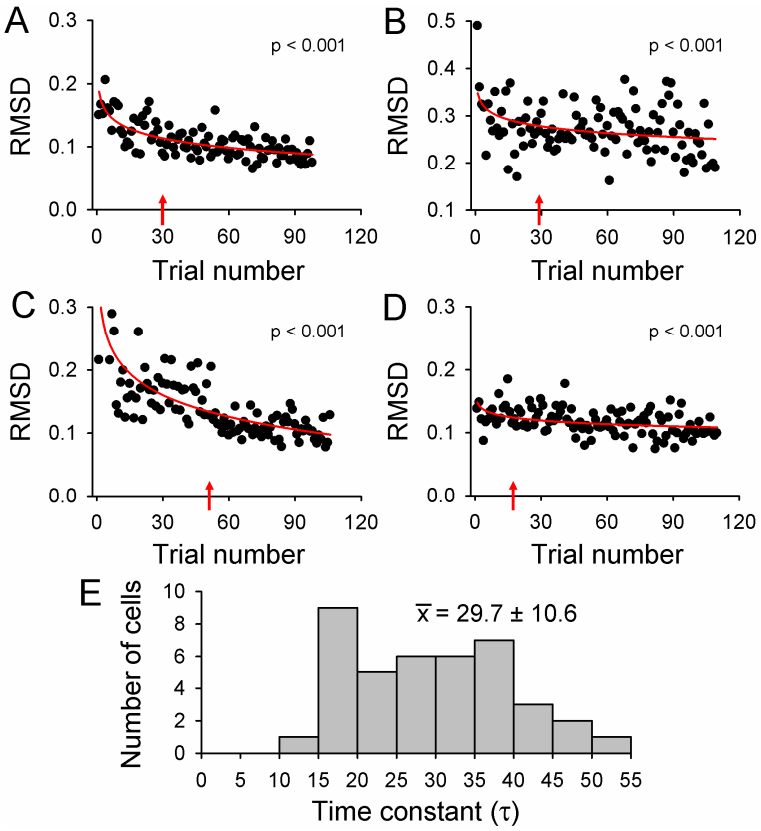

Figure 22: *Simple spike firing learning and adaptation rates*. RMSD measures compared individual adapt trial firing to the corresponding mean late adapt trace. **A-D)** RMSD by trial number are plotted for the 4 example Purkinje cells from Figure 21. Logarithmic fits (red lines) and p-values are provided. Red arrows indicate the trial number where the standard time constant of exponential decay (τ) was reached. **E)** The distribution of firing time constants (τ) is shown for Purkinje cells with significant logarithmic fits (n=42), along with the mean ± SD.

Simple spike firing modulates with movement kinematics

All firing analyses up to this point were performed on the instantaneous firing from individual trials without fitting the data to a model. We evaluated firing modulation by fitting the simple spike firing from individual trials of a recording session to linear regression models for movement kinematics. As movement kinematics were often correlated, we examined the six kinematic parameters (P_p, P_t, V_p, V_t, A_p, and A_t) in isolation by regressing against the firing residuals (FR) after removing the firing variability associated with the 5 other parameters (see Methods). The models (equations 3-8) included a timing variable τ that shifted in 20 ms bins from -500 to 500 ms and estimated the time lead or lag between neural firing and kinematics. Positive values (i.e.

$\tau \geq 0$) indicate that the firing lags, or provides feedback, about movement kinematics. Negative values (i.e. $\tau < 0$) indicate the firing leads movement kinematics in a feedforward manner. Temporal profiles were generated to compare the coefficients of determination (R^2 values) to the τ values.

Individual plots of τ versus R^2 across parameters and epochs suggest that firing adaptation might occur by two mechanisms. First, the sensitivity to a parameter increases or decreases as measured by the R^2 value. An example Purkinje cell recorded during adaptation to an assistive perturbation shows significant simple spike modulation to all parameters except P_t (Figure 23). However, the largest R^2 values are for P_p and V_p, indicating that the simple spike encoding is best tuned to these parameters. Significant feedback peaks for P_p (column 1) are indicated by the black stars. In going down the column from baseline trials through early, middle, and late adaptation, the associated R^2 values for P_p increase from 0.18 to 0.29, suggesting that the Purkinje cell's sensitivity to P_p increases with adaptation. The timing of the significant peak changes little (500 ms to 440 ms). Similarly, significant feedback peaks for V_p (column 3) change very little in time with adaptation (40 ms to 80 ms). However, the R^2 values increase from 0.21 to 0.26. Initial exposure to the perturbation in early adaptation causes the R^2 values for both P_p and V_p to decrease (0.11 and 0.20 respectively), and a second feedforward peak (red star) emerges for V_p at -340 ms. The R^2 values for this peak increase from 0.06 to 0.10, suggesting that the Purkinje cell begins to make predictions about V_p during the adaptation task. However, this feedforward peak also shifts in time from -340 ms to -160 ms. This second mechanism of firing adaptation alters the timing sensitivity, or degree to which the neuron provides feedforward or feedback information about a parameter. In this case, the timing of the maximal R^2 value shifts.

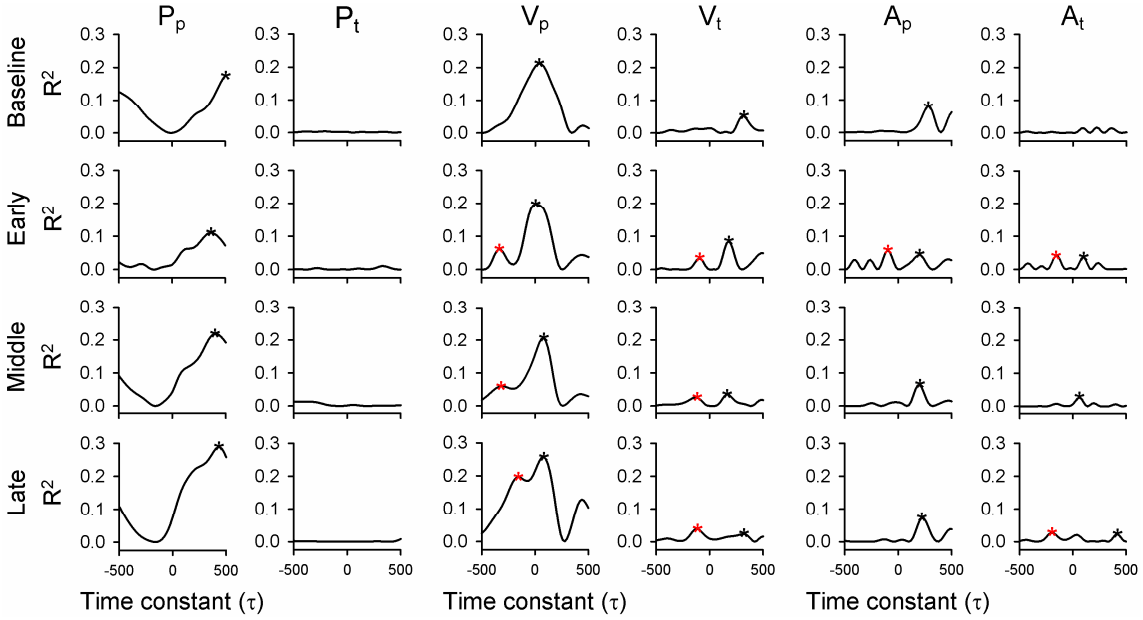

Figure 23: *Example temporal profile, Monkey I.* Temporal profiles compared the coefficients of determination (R^2 values) to the 51 time constant values (τ) used in the regression analyses. Profiles were generated for all 6 model parameters (columns) across the task epochs of baseline, early, middle, and late adaptation (rows). Stars indicate the significant feedforward (red) or feedback (black) τ peaks. Note this is the same Purkinje cell shown in Figure 21A.

Another example Purkinje cell, also recorded during an assistive perturbation, demonstrates pronounced timing shifts in the maximal R^2 values (Figure 24). Again, neural firing is best tuned to P_p (column 1) and V_p (column 3). During baseline movements, the maximal P_p R^2 value of 0.13 occurs at -320 ms. With adaptation, the maximal R^2 shifts feedforward to -480 ms and increases to 0.21. Feedback signals for V_p (black stars) also shift the timing of the maximal R^2 with exposure to the perturbation (240 ms baseline to 140 ms early adapt). However, in late adapt, the maximal R^2 at 220 ms shifts back towards the baseline value. Feedback sensitivity to V_p more than doubles, as the R^2 increases from 0.06 in baseline to 0.17. Importantly, a second feedforward peak for V_p (red star) emerges during early adapt at -220 ms. Although the R^2 value is initially low at 0.04, the peak shifts to 0.11 at -140 ms in middle adapt. This value is slightly greater than the feedback peak, so that the firing during middle adapt encodes both predictive (i.e. feedforward) and feedback information about movement velocity. Dual encoding of feedforward and feedback velocity signals persists through late adaptation,

with a feedforward R^2 of 0.14 at -160 ms and a feedback R^2 of 0.17 at 220 ms. Across the population, simultaneous significant feedforward and feedback signals within a single cell were found in all 6 kinematic parameters (data not shown). This dual encoding of both feedforward and feedback signals occurred most commonly for V_p as in the firing of the two example Purkinje cells (Figures 23 and 24).

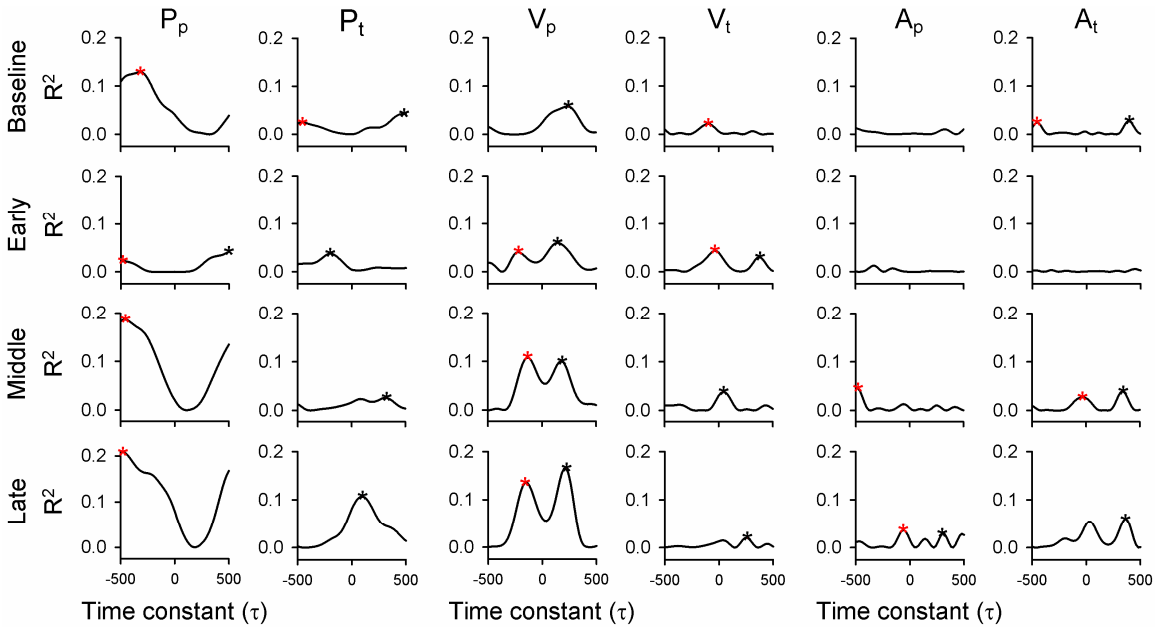

Figure 24: *Example temporal profile, Monkey N*. Temporal profiles compared the coefficients of determination (R^2 values) to the 51 time constant values (τ) used in the regression analyses. Profiles were generated for all 6 model parameters (columns) across the task epochs of baseline, early, middle, and late adaptation (rows). Stars indicate the significant feedforward (red) or feedback (black) τ peaks. Note this is the same Purkinje cell shown in Figure 21C.

Parameter sensitivity

The simple spike firing of many Purkinje cells was tuned to multiple parameters, but typically one or two parameters dominated the modulation (see Figures 23-24). Again, the method of regressing against the firing residuals ensures that any firing variability related to the other parameters is removed, so that significant regression fits reflect the sensitivity to a parameter isolated from the other parameters. To assess sensitivity to the 6 model parameters, we plotted distributions of the coefficients of determination (R^2 value) from all significant regression results across baseline, early, middle, and late adaptation epochs. Parallel parameter P_p, V_p, and A_p results are shown in Figure 25, while tangential parameters P_t, V_t, and A_t follow in Figure 26. Means and standard

deviations of all the R^2 values were calculated across all four epochs for each parameter. The mean R^2 values, shown at the top of each column in Figures 25 and 26, indicate that the population of Purkinje cells is most sensitive to the model parameters P_p and V_p (P_p= 0.094 ± 0.073, V_p= 0.090 ± 0.071). Parallel acceleration explains much less of the firing variability (A_p= 0.045 ± 0.032). Fewer cells modulated significantly with the tangential parameters P_t, V_t, and A_t so that resulting R^2 values from these models are much smaller. The shapes of the distributions are roughly equivalent for both feedforward (white bars) and feedback (grey bars) regression results. However, the number of Purkinje cells with significant fits (numbers in parentheses) is always greater for the feedback than the feedforward timing across all parameters and epochs. The result is more Purkinje cell firing with large R^2 values for feedback signals.

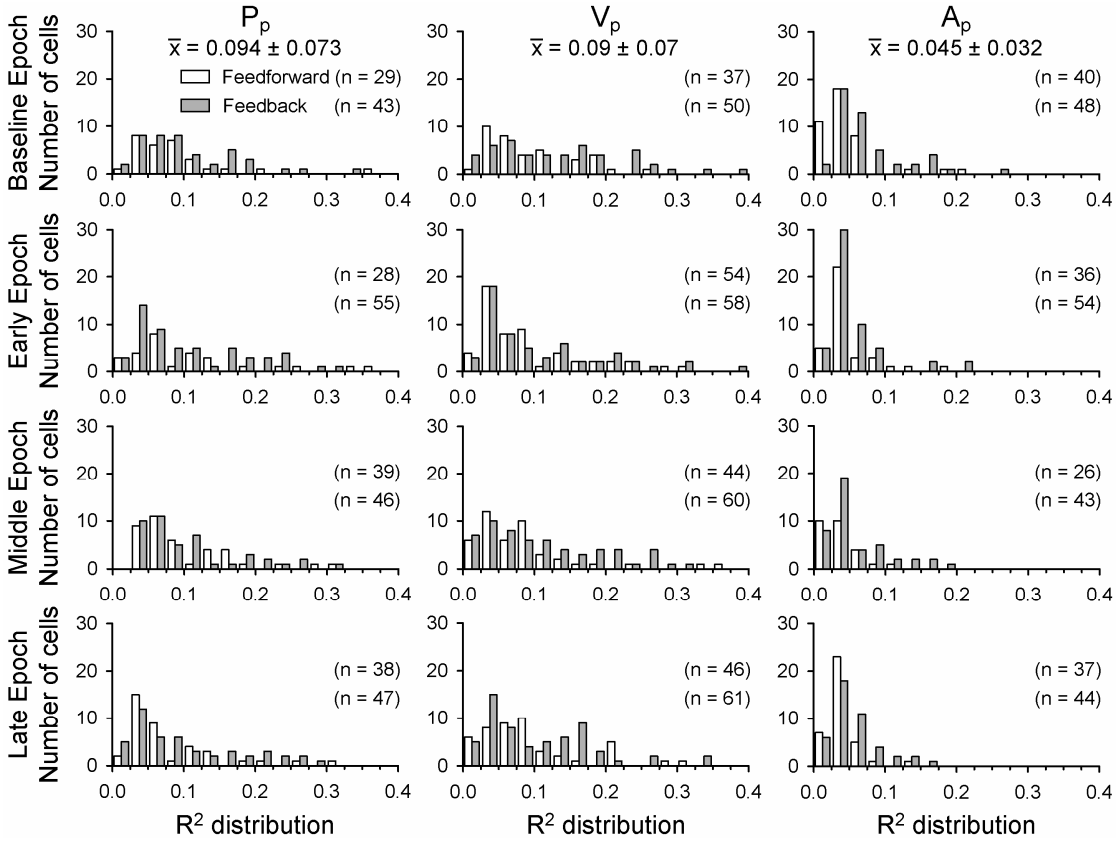

Figure 25: *Distribution of R^2 values, parallel*. Regression analyses R^2 values associated with feedforward (white) or feedback (grey) peak τs were binned for the parallel kinematic model parameters P_p, V_p, and A_p (columns) across task epochs of baseline, early, middle, and late adaptation (rows). Values in parentheses indicate numbers of Purkinje cells with significant feedforward (top) or feedback (bottom) peaks.

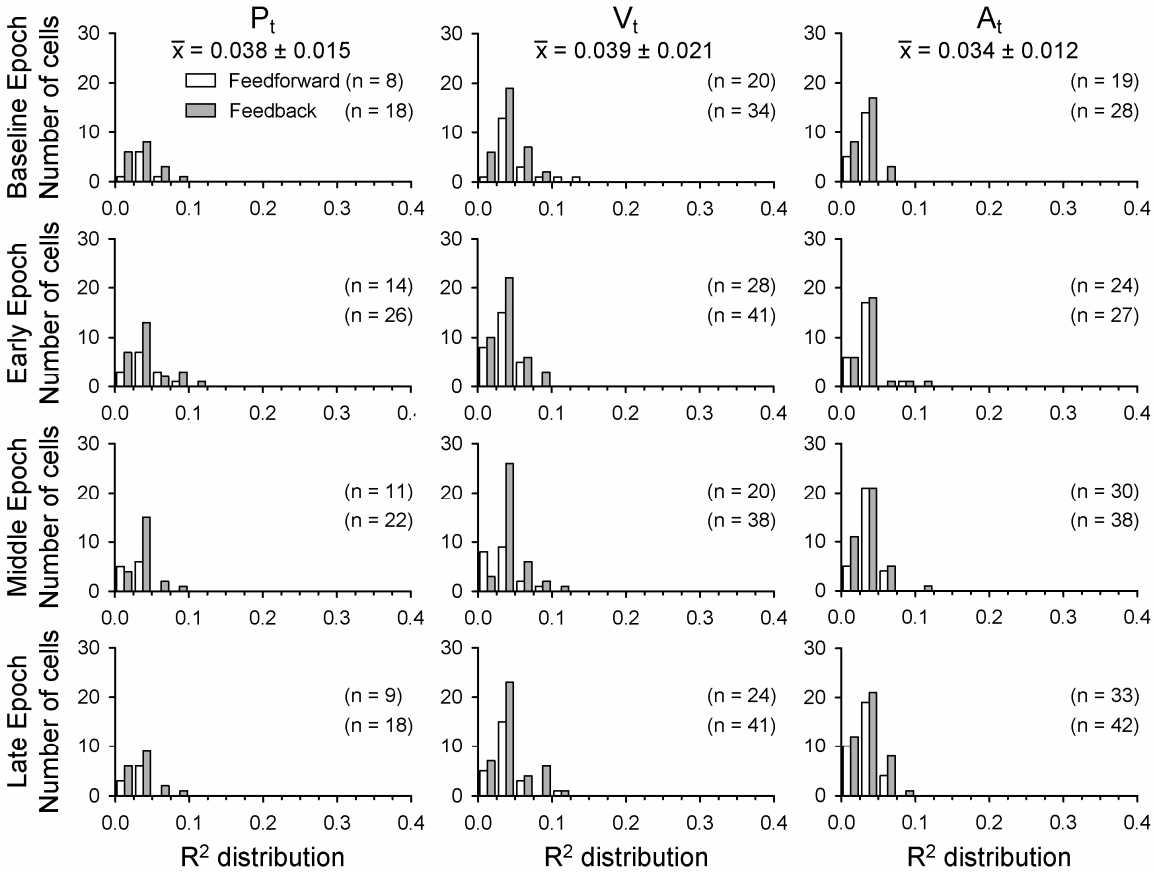

Figure 26: *Distribution of R^2 values, tangential*. Regression analyses R^2 values associated with feedforward (white) or feedback (grey) peak τs were binned for the tangential kinematic model parameters P_t, V_t, and A_t (columns) across task epochs of baseline, early, middle, and late adaptation (rows). Values in parentheses indicate numbers of Purkinje cells with significant feedforward (top) or feedback (bottom) peaks.

To evaluate changes in parameter tuning, the kinematic parameter describing the most firing variability (i.e. parameter with largest R^2 value for each Purkinje cell) was identified for each phase of adaptation (Figure 27). Results were binned by the dominant parameter. During baseline conditions (column 1), sensitivity to V_p dominates the simple spike discharge from half (n= 40) of all Purkinje cells. However, when exposed to the perturbation in early adaptation (column 2), sensitivity to P_p significantly increases ($X^2(2, N= 88) = 17.63$, $p< 0.001$) and V_p signals subsequently decrease slightly ($X^2(2, N= 121) = 4.00$, N.S.). Recall that the perturbation start position is randomly changed each recording session and is one of the perturbation features that the animals must learn. As adaptation continues (columns 3-4), V_p encoding remains steady, suggesting that velocity

sensitivity is critical to the movement. Again, the tangential kinematics rarely are the dominant parameter encoded in the simple spike discharge (also shown in Figures 23-26). Therefore, we focus the remaining analyses of changes in simple spike sensitivity and timing on evaluation of the parallel kinematics.

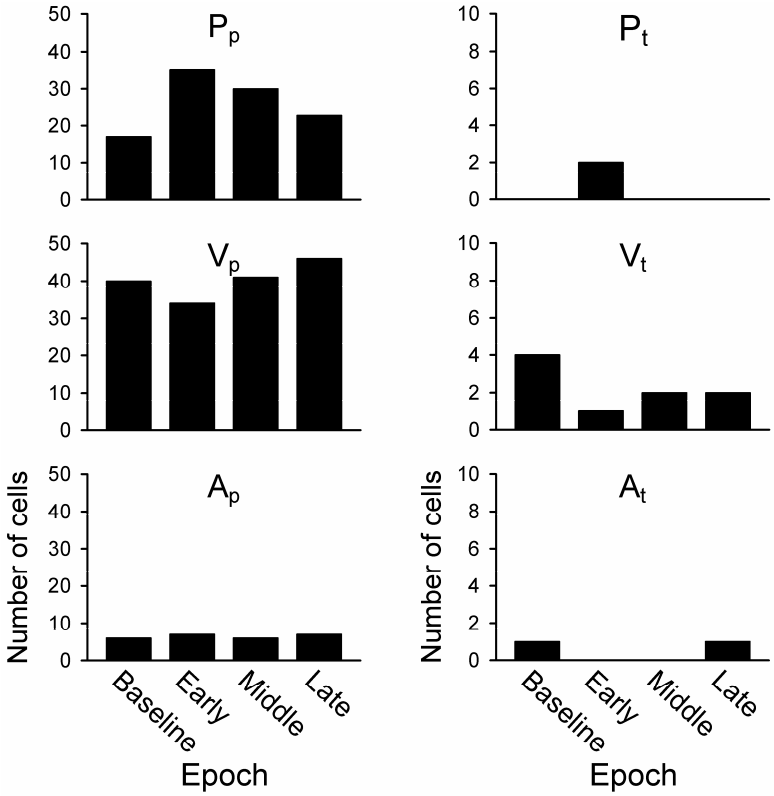

Figure 27: *Dominant parameter, all τ peaks*. The kinematic parameter describing the most firing variability (i.e. greatest R^2 value) was identified for each Purkinje cell across all 6 kinematic parameters P_p, P_t, V_p, V_t, A_p, and A_t during adaptation to the perturbation. Results were binned across the task epochs of baseline, early, middle, and late adaptation.

We expected that adaptive changes in parameter sensitivity should alter the values of the β regression coefficients, so we examined the distributions of β values for all significant peak R^2s. For all three kinematic parameters P_p, V_p, and A_p, the distributions (Figure 28) appear normally distributed, with the exception of almost no β values near zero. This occurs because the plots were limited to only include significant regression results (see Methods). In both the early and late P_p distributions, feedforward βs (white) tend towards more negative values than feedback βs (grey), while the values for parameters V_p and A_p are more equal. A multi-ANOVA was used to test for differences in the β

distributions with parameter (P_p, V_p, A_p), epoch (baseline, late), and timing (feedforward, feedback) as the main factors. Distributions differ significantly by the main effects of parameter ($F(2,508)= 5.87$, $p= 0.003$) and feedforward vs. feedback timing ($F(1,508)= 31.16$, $p< 0.001$). However, there are no significant changes between the baseline and late adapt epochs ($F(1,508)= 0$, N.S.) indicating that learning did not cause a global shift in the β values. Tukey-Kramer post-hoc comparisons of the 6 groups confirmed that the feedforward versus feedback βs differed for P_p (M= -1.81, 95% CI, [-2.33, -1.29]), but not V_p or A_p.

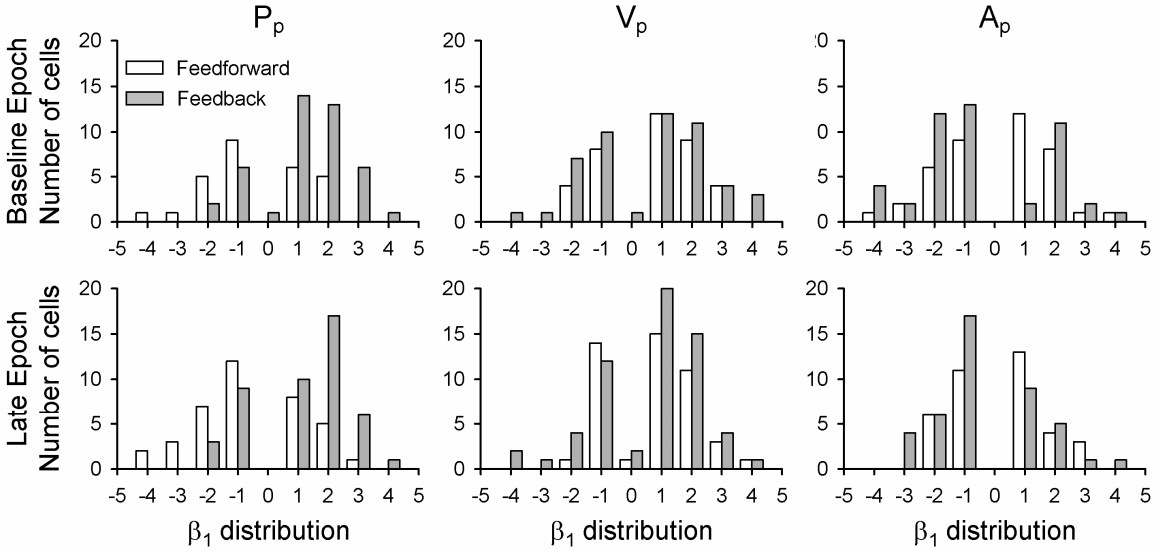

Figure 28: *Distribution of β values*. Histograms show the distribution of β values resulting from regression analyses. Values are grouped by feedforward (white) or feedback (grey) peak τs and the model parameters P_p, V_p, and A_p (columns). Results are shown for the task epochs of baseline and late adaptation (rows).

Although adaptation produced no overall change in β values at the population level, β coefficients within many individual Purkinje cells changed progressively with learning. To identify changes, we compared regression results from individual Purkinje cells. To be considered "tuned" to a parameter, a Purkinje cell needed a significant peak at all 4 epochs of the adaptation period—baseline, early, middle, and late adapt. From the population of 79 cells with significant firing changes, 87.3% (69/79) met this requirement for at least one parameter, testifying to the robust parameter representation. If the β confidence intervals from the baseline and late adapt epochs overlapped, we determined

there was no change in β values with adaptation. Otherwise, β values for that Purkinje cell and parameter were grouped as increasing or decreasing. Figure 29 shows the changes in β values across the 4 epochs for 9 example cells that were grouped as increasing ("inc", column 1), no change ("nc", column 2), or decreasing ("dec", column 3). The table in Figure 29D gives the number of cells with these three profiles for each of the parallel kinematic parameters. Consistent with previous findings, a majority of Purkinje cells were tuned to the parameters P_p or V_p, with 37 Purkinje cells having a change in sensitivity (increase or decrease) to P_p with learning and 44 Purkinje cells having a change in sensitivity to V_p. These two parameters account for most of the cells categorized in the table (Figure 29). As the P_p examples illustrate, an increase or decrease in the β values could result in a sign change (e.g. P_p inc, negative to positive) or simply a magnitude change (e.g. P_p dec). Changes in β magnitude tended to be greater when the β changed sign. Sign changes were found in 20% (4/20) P_p inc, 11.8% (2/17) P_p dec, 36.8% (7/19) V_p inc, 28.0% (7/25) V_p dec, 100% (8/8) A_p inc, and 53% (7/13) of the A_p dec grouped Purkinje cells. The change in the sign of the β for a parameter shows that the nature of the encoding can switch with adaptation. Overall, this analysis of the changes in simple spike sensitivity for specific parameters demonstrates that there is a substantial reassignment of kinematic encoding occurring in a large fraction of individual Purkinje cells, even though the population net sensitivity does not change.

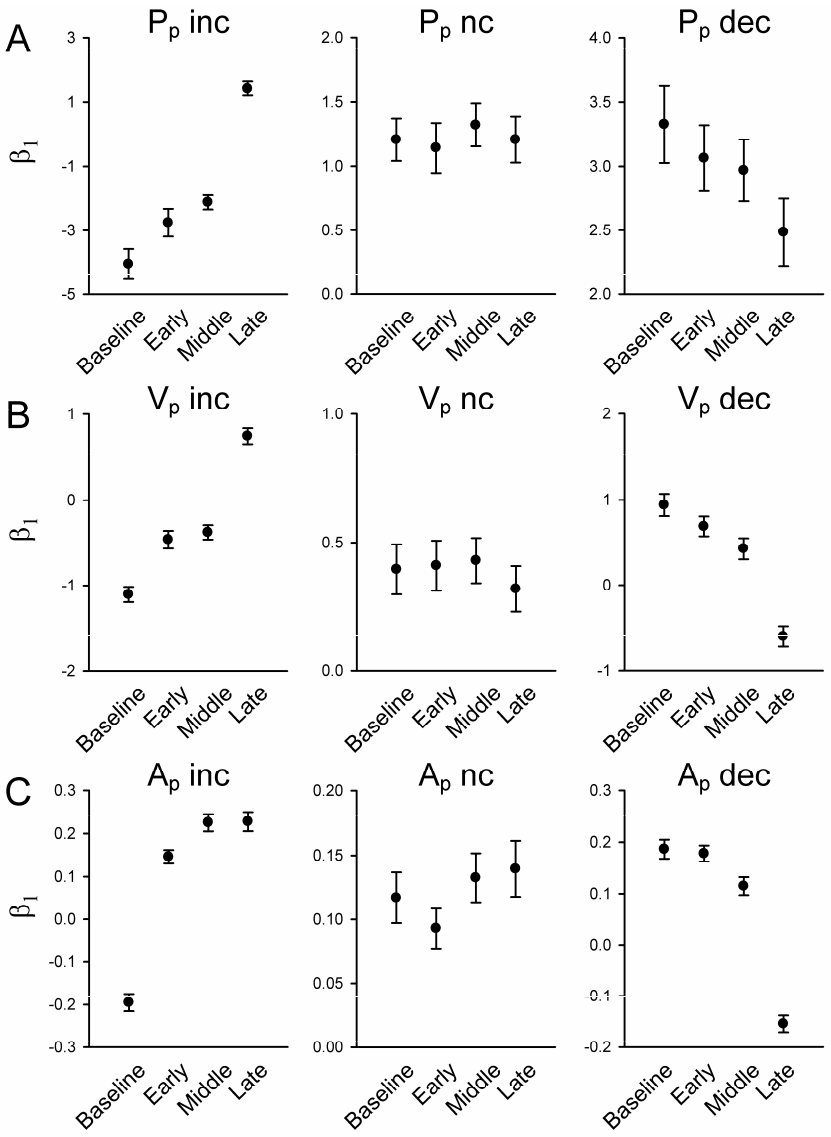

D

	inc	nc	dec
P_p	20	16	17
V_p	19	17	25
A_p	8	13	13

Figure 29: *Parameter sensitivity*. Regression analyses β values from all Purkinje cells with significant firing changes (n= 79) were grouped as increasing (inc), no change (nc), or decreasing (dec) using the β confidence intervals from baseline and late adaptation trials. Example β coefficients from different Purkinje cells illustrate adaptive changes in parameter sensitivity for A) parallel position P_p, B) parallel velocity V_p, and C) parallel acceleration A_p. D) The table indicates the number of Purkinje cells allocated to each group.

Timing sensitivity

The means and SDs of all τ values producing significant fits to the regression models were calculated across all 6 model parameters (Figure 30). Results are grouped by feedforward (white) and feedback (grey) τs, and shown for the task epochs of baseline (Figure 30A) and late adaptation (Figure 30B). Two-factor ANOVA tests (α= 0.025, Bonferroni corrected) assessed differences in both the feedforward and feedback τ values. Although the means vary by parameter (Feedforward: $F(5,328)= 5.87$, $p<0.001$, Feedback: $F(5,462)= 3.38$, $p=0.005$), there is no significant difference between the baseline and late adapt epochs (Feedforward: $F(1,328)= 1.03$, N.S., Feedback: $F(1,462)= 0$, N.S.). As with simple spike sensitivity to the kinematic parameters, there is no net population change in the timing of the simple spike encoding.

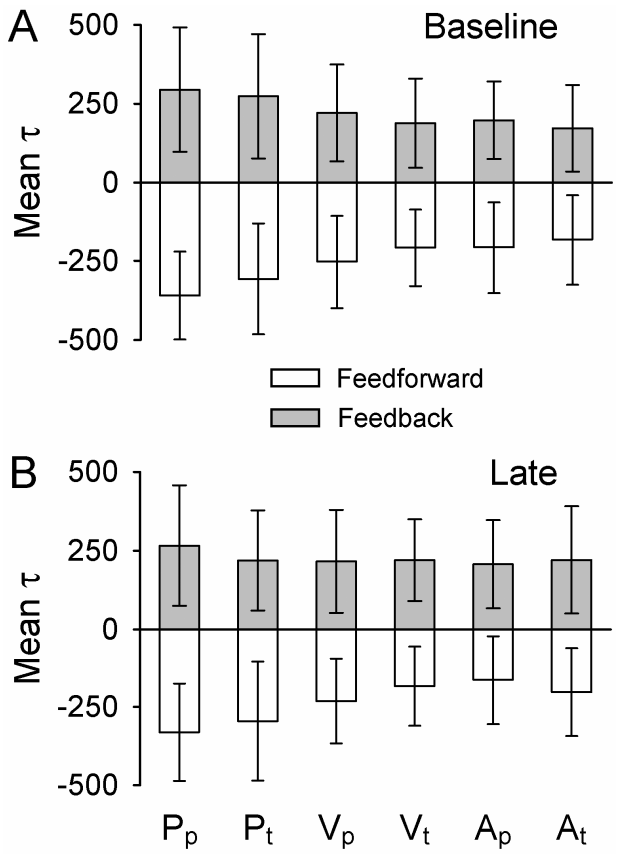

Figure 30: *Mean τ values*. Significant feedforward (white) or feedback (grey) τ values resulting from regression analyses were averaged across all 6 model parameters and plotted for the task epochs of baseline and late adaptation. Bars indicate SDs.

Although adaptation produced little global change in the population of τ values, plots of the R^2 vs. τ temporal profiles for individual cells reveal significant time changes (Figures 23-24). In some instances, the τ value associated with the maximal R^2 even transitions from a feedback value that lags the neural signals, to a feedforward value that leads the neural firing (e.g. see V_p, Figure 24). When parameter sensitivity is examined with the grouping of feedforward versus feedback timing, significant changes appear with adaptation. We again identified the kinematic parameter describing the most firing variability (i.e. parameter with largest R^2 value for each Purkinje cell, see Figure 27), but included both feedback and feedforward maximal R^2 values if the neural signals for a parameter showed two significant peaks. In the feedback group (Figure 31, column 2), perturbation exposure in early adapt brings about a significant increase in the P_p representations ($X^2(2, N= 87) = 8.52$, $p= 0.014$) and V_p signals subsequently decrease ($X^2(2, N = 95)= 6.35$, $p = 0.042$). This agrees with the combined results (Figure 27). However, in the feedforward population (Figure 31, column 1), there is no change in P_p representations until middle adapt ($X^2(2, N= 65) = 5.65$, $p = 0.059$). A subsequent decrease in V_p again results, but the change is not significant ($X^2(2, N= 74) = 1.73$, N.S.) It is interesting that the feedforward changes in P_p and V_p representations occur in the middle adapt epoch, following similar feedback changes that occur more immediately in early adapt. A_p representations appear to play less of a role. Dominant representations of A_p are minimal for both the feedforward and feedback groups, with no significant changes taking place during adaptation.

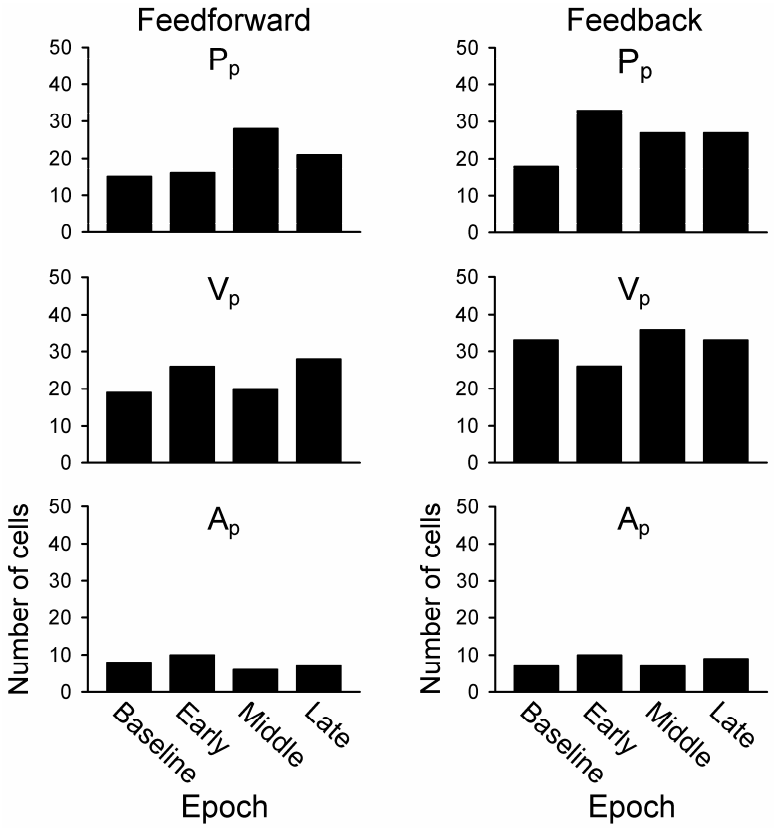

Figure 31: *Dominant parameter, feedforward vs. feedback τ peaks*. The kinematic parameter describing the most firing variability (i.e. greatest R^2 value) was identified for each Purkinje cell at significant feedforward and feedback time constants (τ) for all 6 kinematic parameters P_p, P_t, V_p, V_t, A_p, and A_t. Results were binned across the task epochs of baseline, early, middle, and late adaptation.

Three examples illustrate the types of timing sensitivity changes observed in the simple spike firing (Figure 32A-C). In an example Purkinje cell tuned to P_p, the maximal R^2 is at a feedforward (red star) τ value of -80 ms during the baseline epoch (Figure 32A). At the same time, a second significant peak occurs at the feedback (black star) τ value of 280 ms. With adaptation, the feedforward peak remains at -60 ms but begins to diminish, while the feedback peak holds steady at 260 ms. By late adapt, the feedforward peak no longer exists and the neural firing encodes only a feedback signal at 340 ms. This example illustrates a substantial change in timing sensitivity, moving from feedforward to feedback encoding of a parameter. This means the firing discharge no longer leads hand position, but instead lags the actual hand movements.

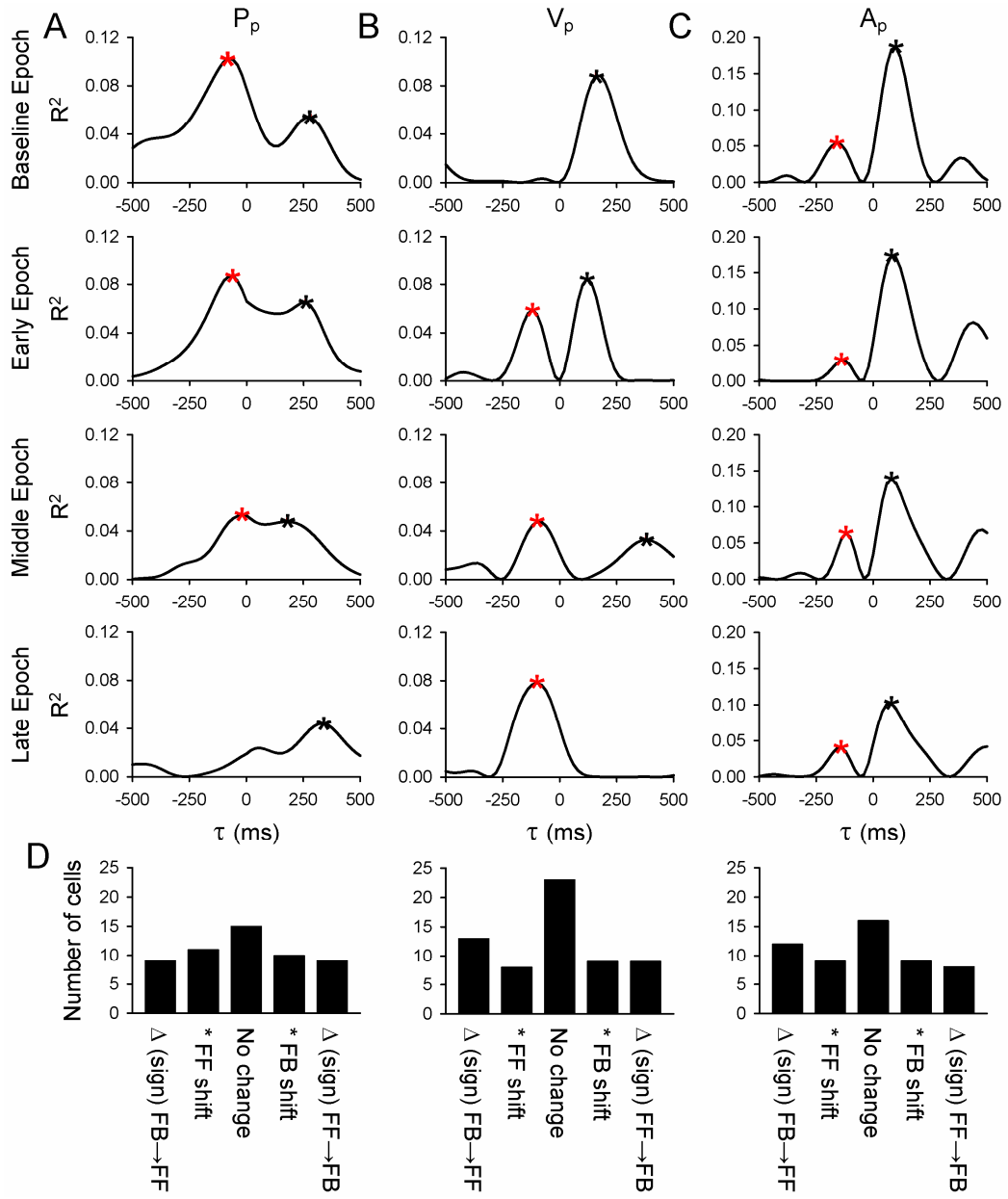

Figure 32: *Timing sensitivity*. Temporal profiles compared the coefficients of determination (R^2 values) to the time constant values (τ) used in the regression analyses. Profiles demonstrating time shifts from A) feedforward to feedback, B) feedback to feedforward, or C) no change were generated for 3 different example Purkinje cells significantly tuned to P_p, V_p, and A_p respectively. Rows depict the task epochs baseline, early, middle, and late adaptation. Stars indicate significant feedforward (red) or feedback (black) τ peaks. D) The time change (in ms) between baseline and late adapt optimal τ values (i.e. producing largest R^2 value) was calculated for all significant Purkinje cells (n= 79). Results were binned by 5 groups according to the time shift (left to right) 1) change sign from feedback→ feedforward, 2) significant feedforward shift, 3) no significant change, 4) significant feedback shift, 5) change sign from feedforward to feedback. A significant shift indicated a change of at least 100 ms.

A second example cell tuned to V_p undergoes the opposite transformation (Figure 32B). In this Purkinje cell, only a feedback peak exists at a τ value of 100 ms during baseline trials. This feedback peak remains at 120 ms in early adapt, but a second feedforward peak additionally appears at -120 ms. Both feedforward and feedback peaks remain in middle adapt, but the feedback peak shifts to 380 ms and has a much lower R^2 value. At the end of adaptation, only a feedforward peak remains at a τ value of 100 ms. In this example, Purkinje cell timing sensitivity changes sign, going from feedback to feedforward tuning. The firing discharge goes from lagging, or providing feedback about hand movement velocity, to leading the actual hand movements.

Simple spike firing from a third example Purkinje cell is tuned to the parameter A_p (Figure 32C). The dominant feedback peak appears at a τ value of 180 ms during baseline trials, and continues to steadily dominate all 3 epochs of early, middle, and late adaptation at a τ value of 80 ms. The second feedforward peak occurs at -160 ms in baseline trials. Adaptation causes very little shift in the feedforward peak timing, with τ values of -140, -120, and -140 ms for the epochs of early, middle, and late adaptation. Therefore, Purkinje cell timing sensitivity can also show very little change with adaptation and remain constant even for the long time period required to record approximately 150 combined baseline and adaptation trials.

To quantify changes in the timing sensitivity from individual cells, we computed the differences between baseline and late adapt optimal τ values (i.e. τ producing the maximal R^2 peak). A "significant" shift in the τ value was defined as 100 ms. The differences were then tallied by kinematic parameter into 5 groups: 1) sign change from feedback (FB) to feedforward (FF), 2) significant feedforward shift, 3) no significant change, 4) significant feedback shift, or 5) sign change from feedforward to feedback (Figure 32D). Across all 3 kinematic parameters, at least 1/3 of the Purkinje cell τ values demonstrates a substantial shift that changes sign over the course of the adaptation trials (P_p= 33.0% (18/54), V_p= 35.5% (22/62), A_p= 37.0% (20/54). Changes towards

feedforward and feedback τ values are similar for P_p (FF= 37.0% (20/54), FB= 35.2% (19/54), but more Purkinje cells shift or change sign towards predictive feedforward τ values for V_p and A_p (V_p: FF= 33.9% (21/62), FB= 29.0% (18/62), A_p: FF= 38.9% (21/54), FB= 31.5% (17/54)). Therefore, shifts in the timing of the parameter encoding are common.

Discussion

Advantages of mechanical perturbation task

Most electrophysiology studies of motor learning and adaptation in the cerebellar cortex have examined eye movements, including the vestibulo-ocular reflex (VOR), saccades, and smooth pursuit (Catz et al., 2005;Catz et al., 2008;Medina and Lisberger, 2009;Medina and Lisberger, 2008;Dash et al., 2010;Dash et al., 2013;Watanabe, 1984;Miles et al., 1980;Lisberger et al., 1994). While these studies have provided important insights regarding how Purkinje cell firing adapts to novel constraints, the learning paradigms utilized typically manipulate the eye movements by changing target position or direction. Therefore, the final adapted movement differs from the original baseline conditions. For example, in saccadic learning, monkeys were trained to make saccades to shifting target positions on a visual display. Once a saccade was initiated, the target moved, requiring an adjustment in saccade amplitude that the monkeys quickly learned (Catz et al., 2005;Catz et al., 2008;Kojima et al., 2010). In smooth pursuit learning, paradigms typically require monkeys to track a target that suddenly changes direction, again changing the original movement (Medina and Lisberger, 2008;Medina and Lisberger, 2009). In VOR adaptation, monkeys wear prism glasses or sit on a spinning platform in order to increase or decrease motion of the visual world with head movement. Adaptation requires learning new gains to correctly stabilize the eyes on a target during rapid head movements (Raymond and Lisberger, 1997;Lisberger and Fuchs, 1978;Lisberger et al., 1994;Miles et al., 1980).

In the present study, the monkeys exhibited remarkable abilities to quickly adapt to an assistive or resistive mechanical perturbation. Late adaptation kinematic profiles are

smooth and continuous, without any overt evidence of the mechanical perturbation. This is true for all combinations of perturbation magnitude, sign (assistive or resistive), duration, and start position. RMSD analyses confirm that the late learning kinematics change very little from the baseline movements, despite the noticeable deviations in early learning. Finally, catch trials clearly demonstrate that the monkeys have learned the dynamics and timing of the perturbations. Catch trial kinematics display after-effects in which the mean catch traces for P_p, V_p, or A_p during the time period when the perturbation should occur are nearly identical but opposite in sign (i.e. mirror-images) to the early adapt trials. Quantification of the after-effects show that the early adaptation and catch trials are strongly anti-correlated for the parallel parameters of P_p, V_p, and A_p (Figure 20B). The after-effects provide strong evidence that the monkeys anticipate the perturbations, and are not simply improving their reaction time to the perturbation onset. Instead, the motor system is generating feedforward commands that effectively counteract the perturbation as found in other grip force (Dugas and Smith, 1992;Nowak et al., 2007;Flanagan and Wing, 1997), force field (Richter et al., 2004;Scheidt et al., 2000;Shadmehr and Mussa-Ivaldi, 1994), and visuomotor adaptation (Krakauer et al., 2000) studies.

Studying limb movements may provide insights about cerebellar learning that differ from the results of eye movement studies. Although the simplicity of eye movements is advantageous, the associated adaptation paradigms only require adjusting a single parameter such as the gain of the VOR, amplitude of a saccade, or direction of smooth pursuit. Because of the low mass of the eye, eye movements are typically described in purely kinematic terms. More complex tasks may be necessary to unlock the full complement of plasticity mechanisms that the cerebellum possesses, as reviewed in Chapter 1. Very few other studies have recorded activity from cerebellar neurons during adaptation in limb movements. A classical study by Gilbert and Thach mechanically perturbed wrist flexion/extension movements with a torque motor (Gilbert and Thach, 1977). Although animals adapted to the perturbations, there was little analysis of the behavior. The other key limb movement learning study used a visuomotor

transformation in which the "gain" of a reaching movement increased or decreased by altering the relationship between hand movements and a cursor projected onto a screen (Ojakangas and Ebner, 1990;Ojakangas and Ebner, 1990;Ojakangas and Ebner, 1990). These experiments also introduced catch trials to document learned behavior from a simple strategy change or improved reflex response. To our knowledge, no other Purkinje cell electrophysiology studies have used mechanical perturbations.

The adaptation produced by this learning paradigm provides several advantages over the methods used in previous studies. First, the kinematics before and after learning are highly similar, particularly along the parallel direction. For smooth pursuit learning used by Medina and Lisberger, learned trajectory is not identical to baseline controls (Medina and Lisberger, 2009;Medina and Lisberger, 2008). Therefore comparisons of the simple spike activity in the learned versus control conditions are complicated. In one comparison, the simple spike firing during normal pursuit in the direction of the maximal Purkinje cell response (on-direction) was compared with the movements along the learned direction that included initiation of pursuit along the orthogonal direction (off-direction) and then movement ~45^{o} between the on- and off- directions. In another analysis, the movements in the pre-direction consisted of smooth pursuit along 45^{o}. Therefore the analysis of the simple spike firing properties were referenced to kinematics that differed (irrespective of the learning aspects) prior to and after learning. In a series of studies, Thier and colleagues examined the changes in Purkinje cell simple spike activity during saccade adaptation resulting in a change in the amplitude of the saccade (Catz et al., 2005;Catz et al., 2008). A smooth pursuit adaptation paradigm used by these authors also produces eye movement kinematics that differed in the baseline versus adapted state (Dash et al., 2010;Dash et al., 2013). Similarly, visuomotor adaptation to reaching movements also results in movements of different amplitudes (Medina and Lisberger, 2009;Ojakangas and Ebner, 1991). In VOR adaptation studies, both the amplitude and velocity of the eye movements are changed (Lisberger et al., 1994;Watanabe, 1984;Watanabe, 1984). Therefore, in these previous studies the comparisons in simple spike discharge before and after learning are in relation to

movements with different kinematics, adding a confound in the interpretation of the changes in firing. Second, the position and time-based mechanical perturbation requires specific, precise adaptation to the particular perturbation parameters. The perturbations varied between recording sessions in timing, direction, amplitude, and whether assistive or resistive. Adapting to these mechanical perturbations likely requires integrating feedback about the perturbation into a predictive, coordinated response that includes timing, kinematic and dynamic components. Although complex, the mechanical perturbation may be more representative of the motor adaptation that occurs under normal conditions.

Parallel vs. tangential kinematic adaptation

To facilitate comparisons between all 8 potential reach directions, movement kinematics were transformed into parallel or tangential coordinates. Behavioral results verify that the largest kinematic changes occur parallel to the direction of the reach, with much smaller changes in the tangential directions. While this partly results from the error clamp, more adaptation along the direction of movement is expected because the mechanical perturbation acts solely in the parallel direction. Matching the perturbation magnitude, sign, and duration requires more extensive changes in parallel movements. Again, RMSD measures show only small differences between late adapt and baseline kinematics for the parallel parameters, whereas the tangential counterparts are much larger. Additionally, parallel and tangential kinematic adaptation rates differ, with tangential adaptation considerably slower. This suggests two different adaptation processes occur for the parallel and tangential components of the movements.

The functional implications of the tangential adaptation are more difficult to understand. After exposure to a new perturbation, monkeys tend to exert force against the error clamp walls. This may help stabilize movements against the perturbation. However, the marked differences in adaptation times (Figure 19A) and simple spike firing parameter sensitivity (compare Figures 25 and 26) show that the increased wall force is not a major determinant of the overall kinematic adaptation.

Rates of adaptation

The time course of adaptation along the direction of the movement is quite fast, with mean exponential time constants of decay (τ) around 13 trials for the parallel kinematic parameters P_p and V_p and 17 trials for A_p (Figure 19B). This is considerably faster than reported for saccade adaptation using the McLaughlin paradigm, either in nonhuman primates or human subjects (Prsa and Thier, 2011). In monkeys, the number of trials to increase saccade amplitude is ~200-400 and to decrease saccade amplitude is ~30-60. The marked difference in adaptation rates may lie in the nature of the paradigms. In saccade adaptation, subjects adapt to a change in target location following saccade initiation. The only feedback available is the visual errors from the images presented on the screen. The mechanical perturbation stimulates numerous somatosensory receptors, so that subjects have access both to visual and proprioceptive feedback. These multiple sources of feedback information likely contribute to the more rapid rates of adaptation. Combining sensory modalities improves motor control and facilitates optimal adaptation.

Firing adaptation occurs more slowly, with exponential time constants of decay (τ) around 30 trials. This is much greater than the mean time constants for parallel kinematic adaptation. It also lags tangential velocity and acceleration adaptation. Differential time courses, with simple spike changes occurring over a more prolonged time course than kinematics, have also been observed for visuomotor adaptation (Ojakangas and Ebner, 1991). Most other cerebellar studies have not directly compared the behavioral and simple spike firing adaptation rates (Medina and Lisberger, 2009;Catz et al., 2005;Dash et al., 2010). At the population level, these findings imply that kinematic adaptation occurs first via a separate process, and Purkinje cell simple spike adaptation follows. A corollary interpretation is that these Purkinje cells are not the output of an inverse dynamics internal model—that is, they do not encode the motor command. This supports previous findings that Purkinje cells in this region of the cerebellum do not encode loads and/or muscle activity (Dash et al., 2013;Roitman et al., 2005;Pasalar et al., 2006). One possible explanation is that Purkinje cells in this region act as a forward internal model to

predict future hand movement kinematics (Wolpert et al., 1998;Kawato and Wolpert, 1998). In early adaptation, kinematic predictions from the forward internal model are compromised until the inverse dynamics model, located elsewhere in the CNS, first solves the problem of how to adapt to the mechanical perturbation. The later changes in simple spike activity could reflect updating of the forward internal model after the inverse dynamics model output has stabilized (Krakauer et al., 1999;Wolpert and Kawato, 1998;Wolpert et al., 1998).

Simple spike changes to parameter sensitivity

Regression models fitting the simple spike firing to the six kinematic model parameters confirm that Purkinje cells in this area of the cerebellum (lobules IV-VI of the intermediate zone) are highly sensitive to movement kinematics. Of the cells demonstrating significant firing changes with adaptation, 87.3% (69/79) produce a significant R^2 peak across all 4 task epochs for at least one kinematic parameter. This demonstrates that parameter representations in the neural signals are robust and consistent even though analyses were performed on individual trials without averaging.

Across the population, P_p and V_p were the kinematic parameters with the most explanatory power (Figures 25 and 26), and velocity and position encoding tended to dominate the firing of individual cells. Individual β regression coefficients displayed progressive changes with learning (Figure 29). The number of cells increasing and decreasing their sensitivity to P_p or V_p were approximately equal. This was not unexpected, since adaptation to the mechanical perturbations requires both position and velocity changes. Numerous other studies of reaching movements also show that Purkinje cells in this area modulate with position and velocity (Coltz et al., 1999a;Roitman et al., 2005;Fu et al., 1997a;Marple-Horvat and Stein, 1987;Fortier et al., 1989). However, the β values for P_p and V_p do not act exactly alike. Feedforward P_p representations skew towards negative β values, while feedback representations tend towards positive β values. The β values for V_p show no significant difference for feedback versus feedforward signals. During adaptation, the β values for V_p are more

likely to change sign than β values for P_p when increasing (36.8% vs. 20.0%) or decreasing (28.0% vs. 11.8%) in sensitivity. Therefore, the position and velocity representations have intrinsic differences that need to be investigated more fully.

An interesting result is that acceleration has the least explanatory power of the kinematic parameters. Across all cells and task epochs, the mean A_p R^2 is 0.04 compared to 0.09 for both P_p and V_p (Figure 25). Fewer cells are significantly tuned to acceleration across all 4 epochs (Figure 25), and therefore fewer cells demonstrate increases or decreases in A_p β values. Since acceleration would be strongly coupled to the inertial forces of the limb, this is consistent with other limb movement studies finding little or no correlation with forces or limb EMG in Purkinje cell simple spike discharge (Coltz et al., 1999a;Roitman et al., 2005;Pasalar et al., 2006). In contrast, acceleration parameters are often used to successfully model the simple spike discharge in relation to eye movements (Shidara et al., 1993;Gomi et al., 1998;Medina and Lisberger, 2009;Dash et al., 2012). The question remains whether the differential explanatory encoding of acceleration in the simple spike firing reflects differences in the tuning sensitivity in the floccular complex/oculomotor vermis versus intermediate zone, or if it simply arises from the task. In baseline conditions, the number of Purkinje cells tuned to A_p is greater than P_p and roughly equal to V_p (Figure 25). The number of Purkinje cells tuned to P_p and V_p increase with adaptation, but Purkinje cells tuned to A_p decrease to totals that are slightly below baseline. Further, monkeys adapted to A_p kinematics more slowly than P_p or V_p kinematics (Figure 19). Whatever the underlying mechanism, acceleration encoding in Purkinje cells is less than that reported for eye movement tasks.

The changes in simple spike sensitivity to kinematic parameters are consistent with prior findings in smooth pursuit adaptation studies(Medina and Lisberger, 2009). However, our approach to quantifying the adaptation differs. In the smooth pursuit studies, the change in simple spike firing was calculated by subtracting the mean eye velocity and firing rate for pre-learning trials from the mean responses for late learning. The resulting differences were the “learned” components, and regression coefficients were calculated

for this select subset of the data. We performed our regression analyses across the entire trial and included all of the simple spike modulation. In our opinion, this provides a better comparison of parameter sensitivity before and after learning, because the β and R^2 values encompass the full range of simple spike variability. It also allows for comparison across early, middle, and late adaptation rather than limiting it to baseline versus late learning. This is important, as the R^2, β, and τ values from many individual Purkinje cells change progressively during the adaptation trials. The number of cells tuned to position and velocity kinematics increases incrementally with adaptation (Figure 25), and population sensitivity to P_p and V_p change in early and middle adapt. Clearly, the encoding capacity of individual Purkinje cells is very dynamic, and cells likely change their parameter tuning as needed to adjust to new constraints in the environment.

Simple spike changes to timing sensitivity

Timing sensitivity is critical to investigate, as many Purkinje cells demonstrate firing changes prior to the perturbation start or even movement onset. Some of the firing changes also occur in time windows after the perturbation ends. Together, these observations imply that learning-related encoding may manifest as feedforward and/or feedback signals. Across all parameters and epochs, feedforward and feedback signals provide roughly equivalent R^2 values (Figures 25 and 26). However, there are more Purkinje cells with significant tuning at the feedback τ values. This differs from a prior study of random tracking, where the population was skewed towards negative values and the mean population τ was -35.1 ± 192.8 ms (Hewitt et al., 2011). It is surprising that this perturbation task invokes a larger feedback response, since it is more predictable than random tracking. The difference may arise because we allowed individual feedforward and feedback τ values for each parameter, whereas the random tracking study calculated a single global τ value from a multi-linear regression model. The results suggest that Purkinje cells encode multiple signals simultaneously, with both feedback and feedforward representations in individual cells. Evaluating timing sensitivity with a single τ value may not provide an optimal representation of all the signals that are present.

Additionally, individual Purkinje cells show dramatic changes in timing sensitivity. Across all 3 kinematic parameters, at least 1/3 of the Purkinje cell τ values demonstrate a substantial shift that changes sign over the course of the adaptation trials (Figure 32). Changes towards feedforward and feedback τ values are similar for the parameter P_p, but more Purkinje cells shift or change sign towards predictive feedforward τ values for V_p and A_p. Other Purkinje cells show no timing sensitivity changes with adaptation, and remain significantly tuned and stable for the duration of the experiments. When we identified the kinematic parameter describing the most firing variability for each Purkinje cell (i.e. parameter with the largest R^2 value) at both feedforward and feedback τ values, we found significant changes in the representations of P_p and V_p. Importantly, changes in feedforward representations of P_p and V_p appear to complement changes in the feedback representations that occur one epoch earlier (Figure 31).

These dynamic changes imply that the cerebellar cortex's contribution to adaptation is more complex than the timing model put forth by Thier and colleagues for saccade adaptation of Purkinje cell firing in the oculomotor vermis (Catz et al., 2005;Dash et al., 2013). These researchers argue that while timing adaptation is the primary change in the simple spike firing, it can only be modeled and understood at the population level. Timing adaptation occurs by adding and removing Purkinje cells with different response times, so that the neural signals converging onto the deep cerebellar nuclei are altered. Adding late-responding simple spike modulation increases the saccade amplitude, while early-responding simple spike modulation decreases it. However, the present results demonstrate that changes in timing sensitivity occur at the single cell level. In our view limiting Purkinje cell timing sensitivity to only a population-based response does not provide the complexity needed to produce the highly specific adaptation profiles required for more complex limb movements.

Comparison to previous studies

Only one previous study directly examined changes in the sensitivity of Purkinje cell simple spike firing during motor learning. Using a smooth pursuit tracking task in which the monkeys adapted to a change in target motion direction after the initiation of pursuit, Medina and Lisberger found that the simple spike velocity sensitivity of the "learned" component of the response changed widely for a large number of Purkinje cells (Medina and Lisberger, 2009). The authors argued that if the adaptive changes occurred outside the cerebellum, they would not expect to see changes in parameter sensitivity (increases and decreases in the β regression coefficients) during the learned component of the movement. Similar to our results, they found distributed changes in the simple spike sensitivity to velocity. However, acceleration was a strong component of the eye movements, and the authors concluded that the position model parameter should be excluded. Several aspects of this previous study's analyses complicate the interpretation. As described above, comparisons of pre- and post- learning in the smooth pursuit task were of different movements. In our study, the reaching movements in the baseline condition are very similar to those in late learning, even though the movement was mechanically perturbed. The importance of the relatively constant kinematics along the direction of adaptation is that the observed changes in simple spike firing are clearly dissociated from the movement properties. Therefore, the changes in the position, velocity, and acceleration sensitivities truly reflect changes in the Purkinje cells and not simply an alteration in the movements.

Compatibility with a forward internal model

The present findings strongly suggest that the nature of the kinematic encoding of individual Purkinje cells is altered during learning. These alterations can affect sensitivity both to specific kinematic parameters and timing components. We interpret these results as support for the hypothesis that Purkinje cells in this area of the cerebellum are the output of a forward internal model. Importantly, the simple spike discharge of individual Purkinje cells carries both predictive and feedback signals about individual kinematic parameters. Having both classes of signals represented in the same

cell may facilitate the required comparisons between predictions and feedback that is needed to update and fine tune the model's predictions.

CHAPTER 4: ADDITIONAL DISCUSSION AND NEXT STEPS

Random tracking task

The random tracking study in Chapter 2 argued that the paradigm provided for assessment of motor signals present in the discharge of neurons, including Purkinje cells. The paradigm afforded greater coverage of the workspace kinematics, including the full range of position, direction, speed, and velocity signals that were minimally correlated during the behavior. This afforded several advantages over previous tasks. First, the task was completely unpredictable (Figures 5 and 6) and not confounded by cyclical or repetitive kinematics, so that timing sensitivity in the Purkinje cell discharge could be accurately evaluated. The power of uncorrelated parameters allowed us to make unambiguous statements about relationships between firing and kinematics, including insight into predictions encoded in the simple spike firing. Secondly, the complete workspace coverage provided a data set that greatly increased the variability in the data, and therefore the information about the relationships between simple spikes and kinematics could be more accurately assessed. It also covered the range of kinematics used in other tasks like circular tracking or center-out reach. Therefore, the model results better reflected the full capacity of the encoded signals and could generalize to other tasks like circular tracking or center-out reach with minimal bias.

Another important methods outcome from this study was demonstrating that regression coefficients obtained from single trial data without averaging provides useful information regarding the simple spike firing. Although resultant R^2 values were much lower than those attained when the same data was averaged, the model's physiological relevance was demonstrated by successfully using the regression coefficients to estimate the simple spike firing on circular tracking and center-out reach tasks. It is well established that averaging artificially reduces the inherent variability of the data set (Zar, 1999;Kenny, 1979), so that the model does not reflect the expected levels of noise in the data and may not generalize to other movements and tasks. Validating this analysis provided the means

for studying the progressive changes in parameter and timing sensitivity of the Purkinje cell firing discharge in Chapter 3.

The advantages of the random tracking paradigm have already been realized. An additional analysis of the same data set reveals that the monkeys utilize several visuomotor performance errors to accurately track the moving target (Popa et al., 2012). These error signals include the position between the cursor and target center (XE and YE), the radial distance between the cursor and target center (RE), and a directional error (PDE). Behavioral analyses similar to those for the kinematic variables (Figure 5) again illustrate that the monkeys strive to keep the cursor in the center of the target. Importantly, these error parameters are uncorrelated with the kinematic parameters. Using a firing residual analyses, the error encoding was demonstrated to be independent of the kinematic encoding established in Chapter 2. Such a decoupling among the model parameters would not be possible in reaching movements used previously (Fu et al., 1997a;Marple-Horvat and Stein, 1987) or in Chapter 3. For example, distance to the target would be identical to the distance error and anti-correlated with parallel position P_p. Achieving this level of independence amongst the parameters is highly desirable. Therefore, the utility of the random tracking paradigm has already had an important impact beyond this thesis.

Mechanical perturbation task

As discussed in Chapter 3, the mechanical perturbation used in the learning paradigm provides several advantages over the tasks used in previous studies. Unlike other force perturbation studies (Wagner and Smith, 2008;Scheidt et al., 2000;Maschke et al., 2004), learning occurs in the direction of movement (i.e. parallel direction) rather than tangential to the movement. Constraining learning to the direction of movement was essential for studying Purkinje cell simple spike firing, as further analyses of the random tracking data showed that the simple spike discharge is highly tuned to kinematic errors (Popa et al., 2012). We also used an error clamp to limit kinematic errors, so that the learning results could not be confounded with neural firing changes due to tangential errors. Another

advantage of this task design is that movement kinematics before and after learning are highly similar, particularly along the parallel direction. In contrast to other studies (Medina and Lisberger, 2009;Catz et al., 2005;Kojima et al., 2010;Medina and Lisberger, 2008;Raymond and Lisberger, 1997;Lisberger and Fuchs, 1978), there are almost no kinematic differences pre- and post- learning, so that changes in the firing discharge can be clearly isolated. Additionally, the position and time-based mechanical perturbation requires specific, very stereotyped adaptation to the particular perturbation parameters. This reduces behavioral variability between animals (e.g. reaction time), requires integration of multiple sensory feedback mechanisms (e.g. visual and proprioceptive), and produces measurable after-effects, where movement kinematics during catch trials are opposite in sign (like a mirror image) those produced during early learning (Figure 20). After-effects confirm that the learned behavior is not simply an improvement in reaction time or a reflex response. Yet, the resulting adaptive response can easily be altered each day by changing the perturbation parameters. For these reasons, this paradigm would adapt well to studying adaptation in many other areas of the CNS, including timing and parameter sensitivity in the deep cerebellar nuclei.

The perturbation task has provided a rich data set with possibilities for many more insights into cerebellar function beyond the learning that was examined in Chapter 3. First, evaluating simple spike firing during the catch trials is critical to understanding the physiological relevance of the feedforward and feedback signals encoded, and specifically if the feedforward signals represent the types of kinematic predictions anticipated from a forward internal model. Differences in mean position, velocity, and acceleration kinematic traces from early and catch trials show marked after-effects. A next step in the analyses is to identify differences in the simple spike firing between late adapt and catch trials. One approach might be to use regression model coefficients and τ values to estimate catch trial firing for two conditions: the actual kinematics for the catch trial versus the expected kinematics for a correctly perturbed trial. Then, similar to the random tracking analyses, the estimated firing could be compared to the actual firing to determine if Purkinje cells incorrectly predict kinematics on the catch trials. Presumably,

the simple spike firing would be similar to that observed in the adapted state for at least 100-200 ms until the feedback introduced an error correction. Another testable hypothesis is that Purkinje cells with strong feedforward components would more closely match the expected firing, while feedback Purkinje cells might accurately depict the catch trial kinematics. This analysis would help confirm that the Purkinje cells adapted consistent with the output from a forward internal model.

Rich error signals should also be present in the mechanical perturbation data set. As mentioned, caution is needed to ensure the error signals and kinematics are not correlated. This may require defining new errors that are specific to this task. The perturbation introduces large errors in the kinematics that diminish with adaptation. In addition to altering the movement kinematics, assistive perturbations result in overshooting the target while resistive perturbations cause the monkeys to undershoot it. Therefore, evaluating error signal encoding during this task and how it compares to the error signals during random tracking is essential for better understanding learning and adaptation in the Purkinje cell simple spike firing.

An additional benefit of this data set is that complex spikes were reliably recorded for the entire adaptation epoch in at least 1/3 of the Purkinje cells, which should provide at least 50 cells (25 from each monkey) to analyze. The nature of complex spike encoding is highly debated. One predominant hypothesis of cerebellar learning is that the complex spike signals errors (Oscarsson, 1980;Ito, 2000). Other studies suggest that it encodes kinematics or some aspect of the task (Kitazawa et al., 1998;Fu et al., 1997b). Still other studies postulate that the complex spikes are responsible for timing information (Welsh et al., 1995;Braitenberg and Atwood, 1958;Keele and Ivry, 1990;O'Reilly et al., 2008;Liu et al., 2008;Wu et al., 2011). Analyzing the complex spike discharge in the perturbation task could be used to test these hypotheses, providing the opportunity to answer several highly debated questions in the field.

Implications for a forward internal model

Both the random tracking and mechanical perturbation experiments were designed to answer questions about the nature of kinematic encoding from Purkinje cells in lobules IV-VI of the intermediate zone. The hypothesis is that Purkinje cell simple spike firing represents the output from a forward internal model. With regard to hand movements, a forward internal model would use the motor command and information about the current state of the arm and hand in order to predict the future state of the hand (Wolpert et al., 1998;Kawato and Wolpert, 1998). These predictions might be in terms of kinematic variables, such as position or velocity (Miall and Wolpert, 1996;Ebner et al., 2011;Ebner and Pasalar, 2008). These kinematic predictions could have multiple uses, including coordinating movements between multiple limbs or joints, anticipating errors, and facilitating learning by comparing expected feedback to the actual feedback.

Robust kinematic representations

A forward internal model of the hand would be expected to predict the future state of the hand, likely in terms of kinematic variables. Both the mechanical perturbation and random tracking tasks confirmed that kinematics were robustly represented in the Purkinje cell simple spike firing, as extensively reported in prior studies (Coltz et al., 1999a;Mano and Yamamoto, 1980;Roitman et al., 2005;Fu et al., 1997a;Shidara et al., 1993;Medina and Lisberger, 2009;Stone and Lisberger, 1990). In both tasks, velocity representations explained most of the firing variability across the population, with position also contributing extensively. Contrary to other studies, especially in eye movements (Shidara et al., 1993;Medina and Lisberger, 2009;Stone and Lisberger, 1990), acceleration was not highly represented in the population simple spike discharge. One factor may be that the eye movement circuitry is less complex, with only a few synapses separating the flocculus from the cranial nerves controlling the eye muscles. The flocculus might be hard-wired for sensitivity to force parameters, like acceleration, to provide useful signals to the eye movement controller. Previous limb movement studies in this region of the cerebellum also found no correlations with force or EMG signals (Coltz et al., 1999a), even when the force magnitude required to track a target was

specifically manipulated (Pasalar et al., 2006). Once a trial began, the force magnitude was constant, so that this study (Pasalar et al., 2006) did not require any learning. In contrast, a learning study examining single joint movements at the wrist reported firing changes that modulated with load, or force, production (Gilbert and Thach, 1977). It has also been shown that acceleration plays a minor role in intercepting and tracking targets, while velocity is a key control parameter (Roitman et al., 2004;Engel and Soechting, 2000). Therefore, the lack of acceleration sensitivity may be task-dependent, as acceleration encoding did dominate the simple spike firing of a small number of Purkinje cells (Figure 27). Some cells also showed significant R^2 values for the acceleration parameter approaching 0.2 (Figure 25). Future studies are needed to definitively conclude if acceleration sensitivity is truly represented in the cerebellar cortex, or if the lack of acceleration sensitivity is just an artifact of the task. One possible experiment might involve modifying the mechanical perturbation to introduce an acceleration dependent adaptation.

Invariant encoding across tasks

Central to the forward internal model theory is whether one model exists for encoding kinematic parameters that can generalize to other tasks or if multiple models exist for different actions (Wolpert and Kawato, 1998;Kawato and Wolpert, 1998;Wolpert et al., 1998). One fMRI study showed that after learning to use two different novel "tools" activation areas for the two different movements were in distinct areas of the lateral and posterior cerebellum with almost no overlap (Imamizu et al., 2003), providing evidence for multiple models. However, one might argue that a single model that can be quickly modified when learning new movements is a more efficient strategy. Many limb movements can be broken into submovements that are similar across a wide range of tasks (Roitman et al., 2004;Pasalar et al., 2005;Miall et al., 1986). Therefore, we hypothesized that kinematic parameter encoding from individual Purkinje cells is by and large invariant across tasks, with modest changes occurring in the parameter and timing sensitivity for different tasks. Regression coefficients generated from the random tracking data set were used to estimate firing for the center-out reach and circular

tracking tasks. For both tests, correlation coefficients comparing the estimated firing to the actual recorded firing indicate that most cells encode hand kinematics invariantly. However, a number of cells provide poor estimates of the firing, with several cells from the circular tracking task even having negative anti-correlated coefficients. Although the anti-correlated results may seem to contradict the hypothesis, results from the mechanical perturbation study show that the simple spike firing from individual Purkinje cells can dramatically change with learning, showing large changes in the gains for individual parameter encoding (βs) and timing sensitivity (τs). These results infer that kinematic encoding from the cerebellar cortex uses a model that can generalize between tasks, but is also highly plastic and adaptable.

Timing sensitivity: feedforward, feedback, or both?

One of the most interesting outcomes of this work that has not been directly addressed by others is the timing sensitivity of the simple spike encoding. Timing sensitivity is critical to the forward internal model hypothesis. The model is hypothesized to output predictions about future limb kinematics, but must overcome delays in the feedback signals used to construct the predictions and update the model. Although timing relationships between the firing discharge and movement kinematics have been reported, the studies have always been confounded by task constraints (Coltz et al., 1999a;Fu et al., 1997a;Marple-Horvat and Stein, 1987). This is especially problematic in tasks like circular tracking, where the cyclic movements can co-vary with the firing discharge at multiple points in time (Roitman et al., 2005;Pasalar et al., 2006). The random tracking study was the first to quantify time constants across the cell population in an unpredictable task, and showed that both feedforward and feedback signaling is represented in the population. However, the mean τ value of -35.1 ± 192.8 ms provides strong evidence for feedforward encoding that is compatible with acting as the predictive signals from a forward internal model. In the perturbation task, Purkinje cell firing responses also demonstrated strong predictive encoding (Figure 30), but regression results showed more significant peaks at feedback τ values than feedforward (Figure 25). It may be interesting to reassess the timing signals in the random tracking task, as the

original analyses even on single parameters limited the results to a single τ at the maximal R^2 value. If two significant τ peaks are allowed in the model, more feedback signals may become apparent as in the mechanical perturbation task. One might hypothesize that strong feedback tuning to multiple parameters is needed in error-based learning, in order to validate the predictions and update the model. This is especially true if comparisons of the expected kinematics (i.e. the predictions) and actual kinematics occur in individual cells. Therefore, Purkinje cells from the random tracking task with strong feedforward predictions might also be expected to have feedback signals that were missed in our original analysis.

Many cells exhibited feedforward and feedback representations for a given parameter that were equally strong (e.g. Figure 24 V_p representations in late adapt). The cerebellum can certainly support both feedforward and feedback control, as it possesses numerous bi-directional connections with the motor cortex (Kelly and Strick, 2003;Ito, 1984) and extensive sensory inputs (Bloedel and Courville, 1981). The physiological relevance of the dual feedforward and feedback signals remains undetermined. A forward internal model by definition would require feedfoward and predictive control (Bastian, 2006;Ebner and Pasalar, 2008). Feedback representations could have multiple uses. Most simply, the feedback signals could convey delayed information about the current state. The forward model would then have to compensate for the delay when determining the current state of the hand or limb. Modeling the "current state" could perhaps account for the large number of τs around times of 0 ms for most model parameters (Figure 15). Several other theories suggest that the feedback signals are used to compute sensory prediction errors, by comparing the predicted and actual sensory feedback for a given motor command (Miall and Wolpert, 1996;Wolpert and Ghahramani, 2000). The sensory prediction errors would be used to assess the accuracy of the forward internal model predictions and make adjustments as needed. Although the errors could be calculated from the kinematic variables examined in this thesis, the error signals found in the additional analyses of the random tracking data (Popa et al., 2012) also provide strong evidence for this theory. These timing sensitivity findings provide strong agreement with

the hypothesis that Purkinje cells in this area of the cerebellum are the output of a forward internal model, with information conveyed by the feedback signals used to update and fine tune the model's feedforward predictions of movement kinematics.

Factors influencing the timing relationships of the signals remain unknown. The task itself appears to have little effect, as the range of τ values are similar between single joint wrist flexion/extension (Mano and Yamamoto, 1980), center-out reach (Marple-Horvat and Stein, 1987;Fu et al., 1997a), manual tracking (Roitman et al., 2005), and reach-to-grasp (Dugas and Smith, 1992). While conclusions from the earlier random tracking study speculated that the timing sensitivity might be hard-wired, results from the mechanical perturbation task confirm that this is not the case, with approximately 2/3 of the Purkinje cells showing significant timing changes in the encoded signals (Figure 32D). Therefore, timing sensitivity also contributes to the encoding plasticity, providing Purkinje cells with additional flexibility for changing their simple spike firing with learning.

Interactions between timing and parameter sensitivity

Position encoding results from the perturbation study provoke some interesting questions about how timing information can affect parameter sensitivity in the simple spike firing discharge. Both data sets showed that the positional time constants (τs) cluster at ±500 ms, whereas velocity and acceleration τ values are normally distributed (Figure 15 and Chapter 3). Additionally, histograms of the P_p and P_t β values reveal a significant difference between the feedforward and feedback representations (Figure 28). The regression coefficients for feedforward position representations are significantly skewed towards negative β values, while feedback representations tend towards positive β values (P_p: M= -1.81, 95% CI, [-2.33, -1.29]). Again, this trend was not present in the velocity or acceleration signals (V_p: M= 0.11, 95% CI, [-0.36, 0.57], A_p: M= 0.02, 95% CI, [-0.47, 0.52]). Additionally, when identifying the dominant parameter encoded in individual Purkinje cells, segregating the analysis into feedforward and feedback representations revealed that a majority of the Pp signal increase with adaptation first appears in the

feedback population in early adapt. Increases in feedforward representations follow soon after in middle adapt (Figure 31). Clearly, timing sensitivity and parameter sensitivity show some dependence, at least in the position signals. However, during learning, the β values for V_p are more likely to change sign than P_p β values when increasing (36.8% vs. 20.0%) or decreasing (28.0% vs. 11.8%) in sensitivity (Chapter 3). In contrast, Purkinje cell timing sensitivity for all 3 parameters changed almost equally, with about 1/3 of the τ values demonstrating a substantial time shift that reversed sign during the course of adaptation. Therefore, it is likely possible to have dramatic changes in timing without affecting parameter sensitivity and vice versa. Interactions between parameter and timing sensitivity must be explored more fully. It is also necessary to readdress the random tracking data to see if the β values distribute differently for the feedforward and feedback representations of the position signals.

Learning and adaptation

A forward internal model must learn to anticipate changes in the external environment, such as the perturbation, so that it can modify its predictions accordingly. Adaptation to the perturbation invoked shifts in the sensitivity of all parameters, with V_p and P_p most demonstrating progressive changes in the β values (Figure 29). At the population level, the time course of the firing adaptation (Figure 22) occurs more slowly than the kinematic adaptation rates (Figure 19). This implies that kinematic adaptation occurs first, via a separate process, and Purkinje cell simple spike adaptation follows. One possible explanation is that in early adaptation, kinematic predictions from the forward internal model are compromised until the inverse dynamics model, located elsewhere in the CNS, first solves the problem of how to adapt to the mechanical perturbation. The later changes in simple spike activity could reflect updating of the forward internal model after the inverse dynamics model has stabilized (Krakauer et al., 1999;Wolpert and Kawato, 1998;Wolpert et al., 1998).

Further support that the simple spike feedback signals are used to update model predictions are shown in the dominant parameter analyses. Across the population,

position signals show significant increases when first exposed to the perturbation in early adaptation (Figure 27). It is striking that the position signals increase at this time, because one of the perturbation parameters that changed daily was the perturbation start position. Closer inspection reveals that feedback P_p signals cause the increase in early adaptation, but feedforward P_p signals change later and increase in middle adapt (Figure 31). Velocity representations follow a similar pattern. Feedback V_p signals decrease in early adaptation while feedforward V_p signals decrease in middle adapt (Figure 31). Again, these changes might be interpreted as the model relying upon feedback representations to identify prediction errors and initiate changes in the parameter sensitivity. This information conveyed by the feedback signals is then used to update and fine tune the model's feedforward predictions of movement kinematics.

To explore this concept further would require manipulating the feedback representations in the task design. If feedback signals are used to update the feedforward predictions, then removing or degrading the feedback could be used to test this hypothesis. For example, the cursor that provides visual feedback could be displayed at the start and end of the movement but removed during the actual movement. Another approach to degrade the quality of the cursor feedback would be would be to provide a cloud of dots for the cursor, as used in studies to introduce uncertainty into the feedback (Berniker and Kording, 2008). One would predict an overall reduction in the feedback signals in the simple spike discharge. Of more interest, this hypothesis suggests that the feedforward signals would change more slowly during adaptation and that the quality of the feedback signals would decrease. A decoding analysis could be used to test the feedforward signals (Popa et al., 2012) with the expectation that these signals are less robust if the feedback during learning is noisy or lacking entirely.

Conclusions

The results from this work provide evidence that Purkinje cells in the intermediate cerebellar cortex act as the output of a forward internal model. The findings show that many of the theorized model components are present. Simple spikes encode both

feedforward and feedback information about kinematics, with position and velocity signals dominating in both tasks. This supplies the predictive signals used downstream and the feedback information potentially used locally to construct predictions, calculate errors, and update the model. Many cells exhibit dual encoding for individual kinematic parameters, so that these separate feedforward and feedback mechanisms may take place within individual cells. For most cells, model coefficients estimated from the random tracking data accurately estimate firing in both the circular tracking or center-out reach tasks. This suggests a global model that can generalize to many tasks with modest changes in the parameter weightings, rather than multiple discrete models for different movements. Adaptation to a novel force perturbation produces steady, progressive changes in both parameter and timing sensitivity. Often, the β value for a parameter changes sign from negative to positive with learning. The time constant τ can also undergo dramatic plasticity, with ~2/3 of the cells exhibiting significant time shifts. Interactions between the parameter and timing sensitivity must be further evaluated, but population analyses suggest that large changes in parameter sensitivity first occur in the feedback signals, then transfer to the feedforward representations. This may reflect use of the feedback signals to update and fine tune model predictions.

However, more evidence is needed to determine that Purkinje cell simple spike firing is truly the output of a forward internal model. Future work will continue evaluating how the simple spike firing changes with adaptation. It is especially key to consider how complex spikes contribute to adaptation, if changes in the feedback signals alter model predictions, and how individual cells utilize the dual feedforward and feedback representations. Importantly, the cerebellum must be studied as a whole system. Future experiments must also address how the signals are used downstream by recording from the deep cerebellar nuclei.

References

Abend W, Bizzi E, Morasso P (1982) Human arm trajectory formation. Brain 105:331-348.

Aizenman CD, Linden DJ (2000) Rapid, synaptically driven increases in the intrinsic excitability of cerebellar deep nuclear neurons. Nat Neurosci 3:109-111.

Akhtar S, Shamotienko O, Papakosta M, Ali F, Dolly JO (2002) Characteristics of brain Kv1 channels tailored to mimic native counterparts by tandem linkage of alpha subunits: implications for K^+ channelopathies. J Biol Chem 277:16376-16382.

Albus JS (1971) A theory of cerebellar function. Math Biosci 10:25-61.

Ariff G, Donchin O, Nanayakkara T, Shadmehr R (2002) A real-time state predictor in motor control: study of saccadic eye movements during unseen reaching movements. J Neurosci 22:7721-7729.

Armano S, Rossi P, Taglietti V, D'Angelo E (2000) Long-term potentiation of intrinsic excitability at the mossy fiber-granule cell synapse of rat cerebellum. J Neurosci 20:5208-5216.

Ashe J, Georgopoulos AP (1994) Movement parameters and neural activity in motor cortex and area 5. Cereb Cortex 4:590-600.

Atkeson CG, Hollerbach JM (1985) Kinematic features of unrestrained vertical arm movements. J Neurosci 5:2318-2330.

Bao S, Chen L, Kim JJ, Thompson RF (2002) Cerebellar cortical inhibition and classical eyeblink conditioning. Proc Natl Acad Sci U S A 99:1592-1597.

Barash S, Melikyan A, Sivakov A, Zhang M, Glickstein M, Thier P (1999) Saccadic dysmetria and adaptation after lesions of the cerebellar cortex. J Neurosci 19:10931-10939.

Barbour B (1993) Synaptic currents evoked in Purkinje cells by stimulating individual granule cells. Neuron 11:759-769.

Barmack NH, Shojaku H (1995) Vestibular and visual climbing fiber signals evoked in the uvula-nodulus of the rabbit cerebellum by natural stimulation. J Neurophysiol 74:2573-2589.

Bastian AJ (2006) Learning to predict the future: the cerebellum adapts feedforward movement control. Curr Opin Neurobiol 16:645-649.

Bastian AJ, Martin TA, Keating JG, Thach WT (1996) Cerebellar ataxia: abnormal control of interaction torques across multiple joints. J Neurophysiol 76:492-509.

Beaubaton D, Grangetto A, Paillard J (1978) Contribution of positional and movement cues to visuomotor reaching in split-brain monkey. In: Structure and function of cerebral commissures (Russell I, van Hoff MW, Berlucchi G, eds), pp 371-384. Boston: University Park Press.

Bell CC (2002) Evolution of cerebellum-like structures. Brain Behav Evol 59:312-326.

Bell CC, Han V, Sawtell NB (2008) Cerebellum-like structures and their implications for cerebellar function. Annu Rev Neurosci 31:1-24.

Belmeguenai A, Hosy E, Bengtsson F, Pedroarena CM, Piochon C, Teuling E, He Q, Ohtsuki G, De Jeu MT, Elgersma Y, De Zeeuw CI, Jorntell H, Hansel C (2010) Intrinsic plasticity complements long-term potentiation in parallel fiber input gain control in cerebellar Purkinje cells. J Neurosci 30:13630-13643.

Belsley DA, Kuh E, Welsch RE (1980) Detecting and Assessing Collinearity. In: Regression Diagnostics: Identifying Influential Data and Sources of Collinearity pp 85-190.

Bengtsson F, Jorntell H (2009) Sensory transmission in cerebellar granule cells relies on similarly coded mossy fiber inputs. Proc Natl Acad Sci USA 106:2389-2394.

Berniker M, Kording K (2008) Estimating the sources of motor errors for adaptation and generalization. Nat Neurosci 11:1454-1461.

Bhushan N, Shadmehr R (1999) Computational nature of human adaptive control during learning of reaching movements in force fields. Biol Cybern 81:39-60.

Bloedel JR, Courville J (1981) A review of cerebellar afferent systems. In: Handbook of Physiology, Sect. 1, The Nervous System, Vol. II. Motor Control, Part 2 (Brooks VB, Geiger SR, eds), pp 735-830. Baltimore: Williams and Wilkins.

Bloedel JR, Roberts WJ (1971) Action of climbing fibers in cerebellar cortex of the cat. J Neurophysiol 34:17-31.

Bosco G, Poppele RE (1997) Representation of multiple kinematic parameters of the cat hindlimb in spinocerebellar activity. J Neurophysiol 78:1421-1432.

Bosco G, Rankin A, Poppele R (1996) Representation of passive hindlimb postures in cat spinocerebellar activity. J Neurophysiol 76:715-726.

Boyd LA, Winstein CJ (2004) Cerebellar stroke impairs temporal but not spatial accuracy during implicit motor learning. Neurorehabil Neural Repair 18:134-143.

Braitenberg V, Atwood RP (1958) Morphological observations on the cerebellar cortex. J Comp Neurol 109:1-33.

Catz N, Dicke PW, Thier P (2008) Cerebellar-dependent motor learning is based on pruning a Purkinje cell population response. Proc Natl Acad Sci U S A 105:7309-7314.

Catz N, Dicke PW, Thier P (2005) Cerebellar complex spike firing is suitable to induce as well as to stabilize motor learning. Curr Biol 15:2179-2189.

Coesmans M, Weber JT, De Zeeuw CI, Hansel C (2004) Bidirectional parallel fiber plasticity in the cerebellum under climbing fiber control. Neuron 44:691-700.

Coltz JD, Johnson MT, Ebner TJ (1999a) Cerebellar Purkinje cell simple spike discharge encodes movement velocity in primates during visuomotor arm tracking. J Neurosci 19:1782-1803.

Coltz JD, Johnson MTV, Ebner TJ (1999b) A neuronal population code for movement velocity in the simple spike discharge of cerebellar Purkinje cells. (Submitted).

Conquet F, Bashir ZI, Davies CH, Daniel H, Ferraguti F, Bordi F, Franz-Bacon K, Reggiani A, Matarese V, Conde F, Collingridge GL, Crepel F (1994) Motor deficit and impairment of synaptic plasticity in mice lacking mGluR1. Nature 372:237-243.

Crepel F, Krupa M (1988) Activation of protein kinase C induces a long-term depression of glutamate sensitivity of cerebellar Purkinje cells. An *in vitro* study. Brain Res 458:397-401.

D'Angelo E, Rossi P, Armano S, Taglietti V (1999) Evidence for NMDA and mGlu receptor-dependent long-term potentiation of mossy fiber-granule cell transmission in rat cerebellum. J Neurophysiol 81:277-287.

Dash S, Catz N, Dicke PW, Thier P (2012) Encoding of smooth-pursuit eye movement initiation by a population of vermal Purkinje cells. Cereb Cortex 22:877-891.

Dash S, Catz N, Dicke PW, Thier P (2010) Specific vermal complex spike responses build up during the course of smooth-pursuit adaptation, paralleling the decrease of performance error. Exp Brain Res 205:41-55.

Dash S, Dicke PW, Thier P (2013) A vermal Purkinje cell simple spike population response encodes the changes in eye movement kinematics due to smooth pursuit adaptation. Front Syst Neurosci 7:3.

De Zeeuw CI, Hansel C, Bian F, Koekkoek SK, van Alphen AM, Linden DJ, Oberdick J (1998) Expression of a protein kinase C inhibitor in Purkinje cells blocks cerebellar LTD and adaptation of the vestibulo-ocular reflex. Neuron 20:495-508.

Desmurget M, Grafton S (2000) Forward modeling allows feedback control for fast reaching movements. Trends Cogn Sci 4:423-431.

Diedrichsen J, Hashambhoy Y, Rane T, Shadmehr R (2005) Neural correlates of reach errors. J Neurosci 25:9919-9931.

Dugas C, Smith AM (1992) Responses of cerebellar Purkinje cells to slip of a hand-held object. J Neurophysiol 67:483-495.

Ebner TJ, Hewitt A, Popa L (2011) What features of movements are encoded in the discharge of cerebellar neurons during limb movements? Cerebellum 10:683-693.

Ebner TJ, Pasalar S (2008) Cerebellum predicts the future motor state. Cerebellum 7:583-588.

Eccles JC, Ito M, Szentagothai J (1967) The Cerebellum as a Neuronal Machine. Berlin: Springer-Verlag.

Ekerot CF, Kano M (1989) Stimulation parameters influencing climbing fibre induced long-term depression of parallel fibre synapses. Neurosci Res 6:264-268.

Ekerot CF, Kano M (1985) Long-term depression of parallel fibre synapses following stimulation of climbing fibers. Brain Res 342:357-360.

Engel KC, Soechting JF (2000) Manual tracking in two dimensions. J Neurophysiol 83:3483-3496.

Flament D, Ellermann JM, Kim S-G, Ugurbil K, Ebner TJ (1996) Functional magnetic resonance imaging of cerebellar activation during the learning of a visuomotor dissociation task. Hum Brain Map 4:210-226.

Flanagan JR, Wing AM (1997) The role of internal models in motion planning and control: evidence from grip force adjustments during movements of hand-held loads. J Neurosci 17:1519-1528.

Fortier PA, Kalaska JF, Smith AM (1989) Cerebellar neuronal activity related to whole-arm reaching movements in the monkey. J Neurophysiol 62:198-211.

Freund RJ (1971) Some Observations on Regressions with Grouped Data. The American Statistician 25:29-30.

Freund RJ, Littel RC (2000) SAS System for Regression. John Wiley & Sons, Inc.

Frysinger RC, Bourbonnais D, Kalaska JF, Smith AM (1984) Cerebellar cortical activity during antagonist cocontraction and reciprocal inhibition of forearm muscles. J Neurophysiol 51:32-49.

Fu QG, Flament D, Coltz JD, Ebner TJ (1997a) Relationship of cerebellar Purkinje cell simple spike discharge to movement kinematics in the monkey. J Neurophysiol 78:478-491.

Fu QG, Mason CR, Flament D, Coltz JD, Ebner TJ (1997b) Movement kinematics encoded in complex spike discharge of primate cerebellar Purkinje cells. NeuroReport 8:523-529.

Gao W, Dunbar RL, Chen G, Reinert KC, Oberdick J, Ebner TJ (2003) Optical imaging of long-term depression in the mouse cerebellar cortex *in vivo*. J Neurosci 23:1859-1866.

Garifoli A, Caserta C, Bosco G, Lombardo SA, Casabona A, Perciavalle V (2002) Kinematic features of passive forelimb movements and rat cuneate neuron discharges. NeuroReport 13:267-271.

Georgopoulos AP, Kalaska JF, Caminiti R, Massey JT (1982) On the relations between the direction of two-dimensional arm movements and cell discharge in primate motor cortex. J Neurosci 2:1527-1537.

Georgopoulos AP, Kalaska JF, Massey JT (1981) Spatial trajectories and reaction times of aimed movements: effects of practice, uncertainty, and change in target location. J Neurophysiol 46:725-743.

Giaquinta G, Casabona A, Valle MS, Bosco G, Perciavalle V (1999) On the relation of rat's external cuneate activity to global parameters of forelimb posture. NeuroReport 10:3075-3080.

Giaquinta G, Valle MS, Caserta C, Casabona A, Bosco G, Perciavalle V (2000) Sensory representation of passive movement kinematics by rat's spinocerebellar Purkinje cells. Neurosci Lett 285:41-44.

Gilbert PF, Thach WT (1977) Purkinje cell activity during motor learning. Brain Res 128:309-328.

Golla H, Tziridis K, Haarmeier T, Catz N, Barash S, Thier P (2008) Reduced saccadic resilience and impaired saccadic adaptation due to cerebellar disease. Eur J Neurosci 27:132-144.

Gomi H, Shidara M, Takemura A, Inoue Y, Kawano K, Kawato M (1998) Temporal firing patterns of Purkinje cells in the cerebellar ventral paraflocculus during ocular following responses in monkeys I. Simple spikes. J Neurophysiol 80:818-831.

Graf W, Simpson JI, Leonard CS (1988) Spatial organization of visual messages of the rabbit's cerebellar flocculus. II. Complex and simple spike responses of Purkinje cells. J Neurophysiol 60:2091-2121.

Grafton ST, Schmitt P, Van HJ, Diedrichsen J (2008) Neural substrates of visuomotor learning based on improved feedback control and prediction. Neuroimage 39:1383-1395.

Gray C, Perciavalle V, Poppele R (1993) Sensory responses to passive hindlimb joint rotation in the cerebellar cortex of the cat. Brain Res 622:280-284.

Hansel C, Linden DJ, D'Angelo E (2001) Beyond parallel fiber LTD: the diversity of synaptic and non-synaptic plasticity in the cerebellum. Nat Neurosci 4:467-475.

Harvey RJ, Porter R, Rawson JA (1977) The natural discharges of Purkinje cells in paravermal regions of lobules V and VI of the monkey's cerebellum. J Physiol 271:515-536.

Hewitt A, Popa L, Pasalar S, Hendrix CM, Ebner TJ (2011) Representation of limb kinematics in Purkinje cell simple spike discharge is conserved across multiple tasks. J Neurophysiol 106:2232-2247.

Hillman DE (1969) Morphological organization of frog cerebellar cortex: a light and electron microscopic study. J Neurophysiol 32:818-846.

Hirano T (1991) Differential pre- and postsynaptic mechanisms for synaptic potentiation and depression between a granule cell and a Purkinje cell in rat cerebellar culture. Synapse 7:321-323.

Holdefer RN, Miller LE (2009) Dynamic correspondence between Purkinje cell discharge and forelimb muscle activity during reaching. Brain Res 1295:67-75.

Hwang EJ, Smith MA, Shadmehr R (2006) Adaptation and generalization in acceleration-dependent force fields. Exp Brain Res 169:496-506.

Ichise T, Kano M, Hashimoto K, Yanagihara D, Nakao K, Shigemoto R, Katsuki M, Aiba A (2000) mGluR1 in cerebellar Purkinje cells essential for long-term depression, synapse elimination, and motor coordination. Science 288:1832-1835.

Imamizu H, Kawato M (2008) Neural correlates of predictive and postdictive switching mechanisms for internal models. J Neurosci 28:10751-10765.

Imamizu H, Kuroda T, Miyauchi S, Yoshioka T, Kawato M (2003) Modular organization of internal models of tools in the human cerebellum. Proc Natl Acad Sci 100:5461-5466.

Imamizu H, Miyauchi S, Tamada T, Sasaki Y, Takino R, Putz B, Yoshioka T, Kawato M (2000) Human cerebellar activity reflecting an acquired internal model of a new tool. Nature 403:192-195.

Isope P, Barbour B (2002) Properties of unitary granule cell-->Purkinje cell synapses in adult rat cerebellar slices. J Neurosci 22:9668-9678.

Ito M (1989) Long-term depression. Annu Rev Neurosci 12:85-102.

Ito M (2002) Historical review of the significance of the cerebellum and the role of Purkinje cells in motor learning. Ann NY Acad Sci 978:273-288.

Ito M (2000) Mechanisms of motor learning in the cerebellum. Brain Res 886:237-245.

Ito M (1984) The Cerebellum and Neural Control. New York: Raven Press.

Ito M (1982) Cerebellar control of the vestibulo-ocular reflex--around the flocculus hypothesis. Annu Rev Neurosci 5:275-296.

Ito M (2001) Cerebellar long-term depression: characterization, signal transduction, and functional roles. Physiol Rev 81:1143-1195.

Ito M, Kano M (1982) Long-lasting depression of parallel fiber-Purkinje cell transmission induced by conjunctive stimulation of parallel fibers and climbing fibers in the cerebellar cortex. Neurosci Lett 33:253-258.

Jorntell H, Hansel C (2006) Synaptic memories upside down: bidirectional plasticity at cerebellar parallel fiber-Purkinje cell synapses. Neuron 52:227-238.

Kalaska JF, Cohen DA, Hyde ML, Prud'homme M (1989) A comparison of movement direction-related versus load direction-related activity in primate motor cortex, using a two-dimensional reaching task. J Neurosci 9:2080-2102.

Kano M, Rexhausen U, Dreessen J, Konnerth A (1992) Synaptic excitation produces a long-lasting rebound potentiation of inhibitory synaptic signals in cerebellar Purkinje cells. Nature 356:601-604.

Kawato M (1999) Internal models for motor control and trajectory planning. Curr Opin Neurobiol 9:718-727.

Kawato M, Kuroda T, Imamizu H, Nakano E, Miyauchi S, Yoshioka T (2003) Internal forward models in the cerebellum: fMRI study on grip force and load force coupling. Prog Brain Res 142:171-188.

Kawato M, Wolpert D (1998) Internal models for motor control. Novartis Found Symp 218:291-304.

Keele SW, Ivry R (1990) Does the cerebellum provide a common computation for diverse tasks? A timing hypothesis. Ann NY Acad Sci 608:179-207.

Keele SW, Posner MI (1968) Processing of visual feedback in rapid movements. J Exp Psychol 77:155-158.

Kelly RM, Strick PL (2003) Cerebellar loops with motor cortex and prefrontal cortex of a nonhuman primate. J Neurosci 23:8432-8444.

Kelly TM, Zuo CC, Bloedel JR (1990) Classical conditioning of the eyeblink reflex in the decerebrate-decerebellate rabbit. Behav Brain Res 38:7-18.

Kenney DA (1979) Correlation and Causality. New York, Wiley.

Kenny DA (1979) Loose Ends. In: Correlation and Causality New York: John Wiley & Sons.

Khaliq ZM, Raman IM (2005) Axonal propagation of simple and complex spikes in cerebellar Purkinje neurons. J Neurosci 25:454-463.

Kitazawa S, Kimura T, Yin PB (1998) Cerebellar complex spikes encode both destinations and errors in arm movements. Nature 392:494-497.

Kobayashi Y, Kawano K, Takemura A, Inoue Y, Kitama T, Gomi H, Kawato M (1998) Temporal firing patterns of Purkinje cells in the cerebellar ventral paraflocculus during ocular following responses in monkeys II. Complex spikes. J Neurophysiol 80:832-848.

Koekkoek SK, Hulscher HC, Dortland BR, Hensbroek RA, Elgersma Y, Ruigrok TJ, De Zeeuw CI (2003) Cerebellar LTD and learning-dependent timing of conditioned eyelid responses. Science 301:1736-1739.

Kojima Y, Soetedjo R, Fuchs AF (2010) Changes in simple spike activity of some Purkinje cells in the oculomotor vermis during saccade adaptation are appropriate to participate in motor learning. J Neurosci 30:3715-3727.

Kolb FP, Rubia FJ, Bauswein E (1987) Cerebellar unit responses of the mossy fibre system to passive movements in the decerebrate cat. I. Responses to static parameters. Exp Brain Res 68:234-248.

Krakauer JW, Ghilardi MF, Ghez C (1999) Independent learning of internal models for kinematic and dynamic control of reaching. Nat Neurosci 2:1026-1031.

Krakauer JW, Pine ZM, Ghilardi MF, Ghez C (2000) Learning of visuomotor transformations for vectorial planning of reaching trajectories. J Neurosci 20:8916-8924.

Lacquaniti F, Soechting JF, Terzuolo SA (1986) Path constraints on point-to-point arm movements in three-dimensional space. Neuroscience 17:313-324.

Lacquaniti F, Terzuolo C, Viviani P (1983) The law relating the kinematic and figural aspects of drawing movements. Acta Psychol (Amst) 54:115-130.

Li CS, Padoa-Schioppa C, Bizzi E (2001) Neuronal correlates of motor performance and motor learning in the primary motor cortex of monkeys adapting to an external force field. Neuron 30:593-607.

Li JX, Medina JF, Frank LM, Lisberger SG (2011) Acquisition of neural learning in cerebellum and cerebral cortex for smooth pursuit eye movements. J Neurosci 31:12716-12726.

Linden DJ (1998) Synaptically evoked glutamate transport currents may be used to detect the expression of long-term potentiation in cerebellar culture. J Neurophysiol 79:3151-3156.

Linden DJ, Ahn S (1999) Activation of presynaptic cAMP-dependent protein kinase is required for induction of cerebellar long-term potentiation. J Neurosci 19:10221-10227.

Linden DJ, Connor JA (1991) Participation of postsynaptic PKC in cerebellar long-term depression in culture. Science 254:1656-1659.

Lisberger SG (2009) Internal models of eye movement in the floccular complex of the monkey cerebellum. Neuroscience 162:763-776.

Lisberger SG, Fuchs AF (1978) Role of primate flocculus during rapid behavioral modification of vestibuloocular reflex. I. Purkinje cell activity during visually guided horizontal smooth-pursuit eye movements and passive head rotation. J Neurophysiol 41:733-763.

Lisberger SG, Pavelko TA, Bronte-Stewart HM, Stone LS (1994) Neural basis for motor learning in the vestibuloocular reflex of primates. II. Changes in the responses of horizontal gaze velocity Purkinje cells in the cerebellar flocculus and ventral paraflocculus. J Neurophysiol 72:954-973.

Liu T, Xu D, Ashe J, Bushara K (2008) Specificity of inferior olive response to stimulus timing. J Neurophysiol 100:1557-1561.

Llinas R, Welsh JP (1993) On the cerebellum and motor learning. Curr Opin Neurobiol 3:958-965.

Mano N, Yamamoto K (1980) Simple-spike activity of cerebellar Purkinje cells related to visually guided wrist tracking movement in the monkey. J Neurophysiol 43:713-728.

Marple-Horvat DE, Stein JF (1987) Cerebellar neuronal activity related to arm movements in trained rhesus monkeys. J Physiol 394:351-366.

Marr D (1969) A theory of cerebellar cortex. J Physiol 202:437-470.

Martin TA, Keating JG, Goodkin HP, Bastian AJ, Thach WT (1996) Throwing while looking through prisms. I. Focal olivocerebellar lesions impair adaptation. Brain 119:1183-1198.

Maschke M, Gomez CM, Ebner TJ, Konczak J (2004) Hereditary cerebellar ataxia progressively impairs force adaptation during goal-directed arm movements. J Neurophysiol 91:230-238.

Mason CR, Hendrix CM, Ebner TJ (2006) Purkinje cells signal hand shape and grasp force during reach-to-grasp in the monkey. J Neurophysiol 95:144-158.

Mauk MD (1997) Roles of cerebellar cortex and nuclei in motor learning: contradictions or clues? Neuron 18:343-346.

McCormick DA, Thompson RF (1984) Cerebellum: essential involvement in the classically conditioned eyelid response. Science 223:296-299.

McDevitt CJ, Ebner TJ, Bloedel JR (1982) The changes in Purkinje cell simple spike activity following spontaneous climbing fiber inputs. Brain Res 237:484-491.

Medina JF, Lisberger SG (2009) Encoding and decoding of learned smooth pursuit eye movements in the floccular complex of the monkey cerebellum. J Neurophysiol 102:2039-2054.

Medina JF, Lisberger SG (2008) Links from complex spikes to local plasticity and motor learning in the cerebellum of awake-behaving monkeys. Nat Neurosci 11:1185-1192.

Miall RC, Christensen LO, Cain O, Stanley J (2007) Disruption of state estimation in the human lateral cerebellum. PLoS Biol 5:e316.

Miall RC, Imamizu H, Miyauchi S (2000) Activation of the cerebellum in co-ordinated eye and hand tracking movements: an fMRI study. Exp Brain Res 135:22-33.

Miall RC, Jenkinson EW (2005) Functional imaging of changes in cerebellar activity related to learning during a novel eye-hand tracking task. Exp Brain Res 166:170-183.

Miall RC, Weir DJ, Stein JF (1986) Manual tracking of visual targets by trained monkeys. Behav Brain Res 20:185-201.

Miall RC, Wolpert DM (1996) Forward models for physiological motor control. Neural Netw 9:1265-1279.

Miles FA, Braitman DJ, Dow BM (1980) Long-term adaptive changes in primate vestibuloocular reflex. IV. Electrophysiological observations in flocculus of adapted monkeys. J Neurophysiol 43:1477-1493.

Miller LE, Houk JC (1995) Motor co-ordinates in primate red nucleus: preferential relation to muscle activation versus kinematic variables. J Physiol 488 (Pt 2):533-548.

Miocinovic S, Zhang J, Xu W, Russo GS, Vitek JL, McIntyre CC (2007) Stereotactic neurosurgical planning, recording, and visualization for deep brain stimulation in non-human primates. J Neurosci Methods 162:32-41.

Monsivais P, Clark BA, Roth A, Hausser M (2005) Determinants of action potential propagation in cerebellar Purkinje cell axons. J Neurosci 25:464-472.

Monzee J, Drew T, Smith AM (2004) Effects of muscimol inactivation of the cerebellar nuclei on precision grip. J Neurophysiol 91:1240-1249.

Monzee J, Smith AM (2004) Responses of cerebellar interpositus neurons to predictable perturbations applied to an object held in a precision grip. J Neurophysiol 91:1230-1239.

Moran DW, Schwartz AB (1999) Motor cortical representation of speed and direction during reaching. J Neurophysiol 82:2676-2692.

Morton SM, Bastian AJ (2007) Mechanisms of cerebellar gait ataxia. Cerebellum 6:79-86.

Morton SM, Bastian AJ (2006) Cerebellar contributions to locomotor adaptations during splitbelt treadmill walking. J Neurosci 26:9107-9116.

Muller F, Dichgans J (1994) Dyscoordination of pinch and lift forces during grasp in patients with cerebellar lesions. Exp Brain Res 101:485-492.

Nanayakkara T, Shadmehr R (2003) Saccade adaptation in response to altered arm dynamics. J Neurophysiol 90:4016-4021.

Napper RM, Harvey RJ (1988) Number of parallel fiber synapses on an individual Purkinje cell in the cerebellum of the rat. J Comp Neurol 274:168-177.

Nezafat R, Shadmehr R, Holcomb HH (2001) Long-term adaptation to dynamics of reaching movements: a PET study. Exp Brain Res 140:66-76.

Nowak DA, Hermsdorfer J, Marquardt C, Fuchs HH (2002) Grip and load force coupling during discrete vertical arm movements with a grasped object in cerebellar atrophy. Exp Brain Res 145:28-39.

Nowak DA, Hermsdorfer J, Rost K, Timmann D, Topka H (2004) Predictive and reactive finger force control during catching in cerebellar degeneration. Cerebellum 3:227-235.

Nowak DA, Topka H, Timmann D, Boecker H, Hermsdorfer J (2007) The role of the cerebellum for predictive control of grasping. Cerebellum 6:7-17.

O'Grady KE (1982) Measures of Explained Variance: Cautions and Limitations. Psychol Bull 92:766-777.

O'Reilly JX, Mesulam MM, Nobre AC (2008) The cerebellum predicts the timing of perceptual events. J Neurosci 28:2252-2260.

Ojakangas CL, Ebner TJ (1991) Scaling of the metrics of visually-guided arm movements during motor learning in primates. Exp Brain Res 85:314-323.

Ojakangas CL, Ebner TJ (1992) Purkinje cell complex and simple spike changes during a voluntary arm movement learning task in the monkey. J Neurophysiol 68:2222-2236.

Ojakangas CL, Ebner TJ (1990) Purkinje cell complex spike modulation during voluntary motor learning in the primate. pp 638.

Oscarsson O (1980) Functional organization of olivary projection to the cerebellar anterior lobe. In: The Inferior Olivary Nucleus: Anatomy and Physiology (Courville J, ed), pp 279-290. New York: Raven.

Paninski L, Fellows MR, Hatsopoulos NG, Donoghue JP (2004a) Spatiotemporal tuning of motor cortical neurons for hand position and velocity. J Neurophysiol 91:515-532.

Paninski L, Shoham S, Fellows MR, Hatsopoulos NG, Donoghue JP (2004b) Superlinear population encoding of dynamic hand trajectory in primary motor cortex. J Neurosci 24:8551-8561.

Pasalar S, Roitman AV, Durfee WK, Ebner TJ (2006) Force field effects on cerebellar Purkinje cell discharge with implications for internal models. Nat Neurosci 9:1404-1411.

Pasalar S, Roitman AV, Ebner TJ (2005) Effects of speeds and force fields on submovements during circular manual tracking in humans. Exp Brain Res 163:214-225.

Paulin MG (2005) Evolution of the cerebellum as a neuronal machine for Bayesian state estimation. J Neural Eng 2:S219-S234.

Popa LS, Hewitt AL, Ebner TJ (2012) Predictive and feedback performance errors are signaled in the simple spike discharge of individual Purkinje cells. J Neurosci 32:15345-15358.

Prsa M, Thier P (2011) The role of the cerebellum in saccadic adaptation as a window into neural mechanisms of motor learning. Eur J Neurosci 33:2114-2128.

Rambold H, Churchland A, Selig Y, Jasmin L, Lisberger SG (2002) Partial ablations of the flocculus and ventral paraflocculus in monkeys cause linked deficits in smooth pursuit eye movements and adaptive modification of the VOR. J Neurophysiol 87:912-924.

Raymond JL, Lisberger SG (1997) Multiple subclasses of Purkinje cells in the primate floccular complex provide similar signals to guide learning in the vestibulo-ocular reflex. Learn Mem 3:503-518.

Raymond JL, Lisberger SG (1998) Neural learning rules for the vestibulo-ocular reflex. J Neurosci 18:9112-9129.

Richardson AG, Lassi-Tucci G, Padoa-Schioppa C, Bizzi E (2008) Neuronal activity in the cingulate motor areas during adaptation to a new dynamic environment. J Neurophysiol 99:1253-1266.

Richter S, Maschke M, Timmann D, Konczak J, Kalenscher T, Illenberger AR, Kalveram K (2004) Adaptive motor behavior of cerebellar patients during exposure to unfamiliar external forces. J Mot Behav 36:28-38.

Robinson DA (1976) Adaptive gain control of vestibuloocular reflex by the cerebellum. J Neurophysiol 39:954-969.

Roitman AV, Massaquoi SG, Takahashi K, Ebner TJ (2004) Kinematic analysis of manual tracking in monkeys: characterization of movement intermittencies during a circular tracking task. J Neurophysiol 91:901-911.

Roitman AV, Pasalar S, Ebner TJ (2009) Single trial coupling of Purkinje cell activity to speed and error signals during circular manual tracking. Exp Brain Res 192:241-251.

Roitman AV, Pasalar S, Johnson MT, Ebner TJ (2005) Position, direction of movement, and speed tuning of cerebellar Purkinje cells during circular manual tracking in monkey. J Neurosci 25:9244-9257.

Rost K, Nowak DA, Timmann D, Hermsdorfer J (2005) Preserved and impaired aspects of predictive grip force control in cerebellar patients. Clin Neurophysiol 116:1405-1414.

Rubia FJ, Kolb FP (1978) Responses of cerebellar units to a passive movement in the decerebrate cat. Exp Brain Res 31:387-401.

Sakurai M (1987) Synaptic modification of parallel fibre-Purkinje cell transmission in in vitro guinea-pig cerebellar slices. J Physiol 394:463-480.

Salin PA, Malenka RC, Nicoll RA (1996) Cyclic AMP mediates a presynaptic form of LTP at cerebellar parallel fiber synapses. Neuron 16:797-803.

Scheidt RA, Dingwell JB, Mussa-Ivaldi FA (2001) Learning to move amid uncertainty. J Neurophysiol 86:971-985.

Scheidt RA, Reinkensmeyer DJ, Conditt MA, Rymer WZ, Mussa-Ivaldi FA (2000) Persistence of motor adaptation during constrained, multi-joint, arm movements. J Neurophysiol 84:853-862.

Schonewille M, Gao Z, Boele HJ, Veloz MF, Amerika WE, Simek AA, De Jeu MT, Steinberg JP, Takamiya K, Hoebeek FE, Linden DJ, Huganir RL, De Zeeuw CI (2011) Reevaluating the role of LTD in cerebellar motor learning. Neuron 70:43-50.

Schwartz AB, Moran DW (1999) Motor cortical activity during drawing movements: population representation during lemniscate tracing. J Neurophysiol 82:2705-2718.

Schweighofer N, Arbib MA, Kawato M (1998) Role of the cerebellum in reaching movements in humans. I. Distributed inverse dynamics control. Eur J Neurosci 10:86-94.

Seidler RD, Purushotham A, Kim SG, Ugurbil K, Willingham D, Ashe J (2002) Cerebellum activation associated with performance change but not motor learning. Science 296:2043-2046.

Shadmehr R, Holcomb HH (1997) Neural correlates of motor memory consolidation. Science 277:821-825.

Shadmehr R, Mussa-Ivaldi FA (1994) Adaptive representation of dynamics during learning of a motor task. J Neurosci 14:3208-3224.

Shidara M, Kawano K, Gomi H, Kawato M (1993) Inverse-dynamics model eye movement control by Purkinje cells in the cerebellum. Nature 365:50-52.

Smith AM (1981) The coactivation of antagonist muscles. Can J Physiol Pharmacol 59:733-747.

Smith AM, Bourbonnais D (1981) Neuronal activity in cerebellar cortex related to control of prehensile force. J Neurophysiol 45:286-303.

Smith MA, Brandt J, Shadmehr R (2000) Motor disorder in Huntington's disease begins as a dysfunction in error feedback control. Nature 403:544-549.

Smith MA, Shadmehr R (2005) Intact ability to learn internal models of arm dynamics in Huntington's disease but not cerebellar degeneration. J Neurophysiol 93:2809-2821.

Soechting JF, Flanders M (1989) Errors in pointing are due to approximations in sensorimotor transformations. J Neurophysiol 62:595-608.

Soechting JF, Flanders M (2008) Extrapolation of visual motion for manual interception. J Neurophysiol 99:2956-2967.

Stein JF, Glickstein M (1992) Role of the cerebellum in visual guidance of movement. Physiol Rev 72:967-1017.

Stone LS, Lisberger SG (1990) Visual responses of Purkinje cells in the cerebellar flocculus during smooth-pursuit eye movements in monkeys. I. Simple spikes. J Neurophysiol 63:1241-1261.

Sturrock RR (1990) A comparison of quantitative histological changes in different regions of the ageing mouse cerebellum. J Hirnforsch 31:481-486.

Takagi M, Zee DS, Tamargo RJ (2000) Effects of lesions of the oculomotor cerebellar vermis on eye movements in primate: smooth pursuit. J Neurophysiol 83:2047-2062.

Takagi M, Zee DS, Tamargo RJ (1998) Effects of lesions of the oculomotor vermis on eye movements in primate: saccades. J Neurophysiol 80:1911-1931.

Thach WT (1968) Discharge of Purkinje and cerebellar nuclear neurons during rapidly alternating arm movements in the monkey. J Neurophysiol 31:785-797.

Thach WT (1970) Discharge of cerebellar neurons related to two maintained postures and two prompt movements. II. Purkinje cell output and input. J Neurophysiol 33:537-547.

Thompson RF, Krupa DJ (1994) Organization of memory traces in the mammalian brain. Annu Rev Neurosci 17:519-549.

Thoroughman KA, Shadmehr R (1999) Electromyographic correlates of learning an internal model of reaching movements. J Neurosci 19:8573-8588.

Tseng YW, Diedrichsen J, Krakauer JW, Shadmehr R, Bastian AJ (2007) Sensory prediction errors drive cerebellum-dependent adaptation of reaching. J Neurophysiol 98:54-62.

Valle MS, Bosco G, Poppele R (2000) Information processing in the spinocerebellar system. NeuroReport 11:4075-4079.

van Kan PL, Gibson AR, Houk JC (1993) Movement-related inputs to intermediate cerebellum of the monkey. J Neurophysiol 69:74-94.

Vercher JL, Lazzari S, Gauthier G (1997) Manuo-ocular coordination in target tracking. II. Comparing the model with human behavior. Biol Cybern 77:267-275.

Vercher JL, Sares F, Blouin J, Bourdin C, Gauthier G (2003) Role of sensory information in updating internal models of the effector during arm tracking. Prog Brain Res 142:203-222.

Vindras P, Viviani P (1998) Frames of reference and control parameters in visuomanual pointing. J Exp Psychol Hum Percept Perform 24:569-591.

Viviani P, Terzuolo C (1982) Trajectory determines movement dynamics. Neuroscience 7:431-437.

Wagner MJ, Smith MA (2008) Shared internal models for feedforward and feedback control. J Neurosci 28:10663-10673.

Wang YT, Linden DJ (2000) Expression of cerebellar long-term depression requires postsynaptic clathrin-mediated endocytosis. Neuron 25:635-647.

Watanabe E (1984) Neuronal events correlated with long-term adaptation of the horizontal vestibulo-ocular reflex in the primate flocculus. Brain Res 297:169-174.

Welsh JP, Lang EJ, Suglhara I, Llinas R (1995) Dynamic organization of motor control within the olivocerebellar system. Nature 374:453-457.

Wolpert DM, Ghahramani Z (2000) Computational principles of movement neuroscience. Nat Neurosci 3 Suppl:1212-1217.

Wolpert DM, Ghahramani Z, Jordan MI (1995) An internal model for sensorimotor integration. Science 269:1880-1882.

Wolpert DM, Kawato M (1998) Multiple paired forward and inverse models for motor control. Neural Netw 11:1317-1329.

Wolpert DM, Miall RC, Kawato M (1998) Internal models in the cerebellum. Trends in Cognitive Sciences 2:338-347.

Wu X, Ashe J, Bushara KO (2011) Role of olivocerebellar system in timing without awareness. Proc Natl Acad Sci U S A 108:13818-13822.

Xu-Wilson M, Chen-Harris H, Zee DS, Shadmehr R (2009) Cerebellar contributions to adaptive control of saccades in humans. J Neurosci 29:12930-12939.

Yamamoto K, Kawato M, Kotosaka S, Kitazawa S (2007) Encoding of movement dynamics by Purkinje cell simple spike activity during fast arm movements under resistive and assistive force fields. J Neurophysiol 97:1588-1599.

Yeo CH (1988) Cerebellum and classical conditioning. In: Cerebellum and Neural Plasticity (Glickstein M, Yeo CH, Stein J, eds), pp 321-338. New York: Plenum.

Yeo CH, Hardiman MJ, Glickstein M (1985a) Classical conditioning of the nictitating membrane response of the rabbit. III. Connections of cerebellar lobule HVI. Exp Brain Res 60:114-126.

Yeo CH, Hardiman MJ, Glickstein M (1985b) Classical conditioning of the nictitating membrane response of the rabbit. I. Lesions of the cerebellar nuclei. Exp Brain Res 60:87-98.

Zar JH (1999) Biostatistical Analysis. Upper Saddle River, NJ: Prentice Hall.